

Aus dem Adolf-Butenandt-Institut
Lehrstuhl Molekularbiologie
im Biomedizinischen Centrum
der Ludwig-Maximilians-Universität München
Vorstand: Prof. Dr. rer. nat. Peter B. Becker

Investigating the function of the H2A.Z-interactor PWWP2A



Dissertation

zum Erwerb des Doktorgrades der Naturwissenschaften

an der Medizinischen Fakultät der

Ludwig-Maximilians-Universität München

Stephanie Link

aus Erding

2019

Mit Genehmigung der Medizinischen Fakultät
der Universität München

Betreuerin: Prof. Dr. Sandra B. Hake

Zweitgutachter(in): Prof. Andreas Ladurner, PhD

Dekan: Prof. Dr. med. dent. Reinhard Hickel

Tag der mündlichen Prüfung: 24.07.2019

Eidesstattliche Versicherung

Ich erkläre hiermit an Eides statt, dass ich die vorliegende Dissertation mit dem Thema „Investigating the function of the H2A.Z-interactor PWWP2A“ selbständig verfasst, mich außer der angegebenen keiner weiteren Hilfsmittel bedient und alle Erkenntnisse, die ich aus dem Schrifttum ganz oder annähernd übernommen sind, als solche kenntlich gemacht und nach ihrer Herkunft unter Bezeichnung der Fundstelle einzeln nachgewiesen habe.

Ich erkläre des Weiteren, dass die hier vorgelegte Dissertation nicht in gleicher oder in ähnlicher Form bei einer anderen Stelle zur Erlangung eines akademischen Grades eingereicht wurde.

München, den 24.07.2019

Ort, Datum

Stephanie Link

TABLE OF CONTENTS

Summary.....	1
Zusammenfassung	2
1. INTRODUCTION	4
1.1 Chromatin structure and complexity	4
1.2 Posttranslational histone modifications	6
1.3 Nucleosome Remodeling.....	7
1.4 Core Histone Variants	8
1.5 Histone Variant H2A.Z	11
1.6 Functional genomic elements.....	16
1.7 PWWP2A	18
1.8 Objective.....	19
2. MATERIAL AND METHODS.....	21
2.1. Material	21
2.1.1 Technical devices	21
2.1.2 Consumables	22
2.1.3 Chemicals.....	22
2.1.4 Kits, enzymes and markers	24
2.1.5 Antibodies.....	24
2.1.6 Cell lines.....	25
2.1.7 Oligonucleotides	26
2.1.8 Plasmids.....	27
2.1.9 Buffers and solutions	27
2.2 Cell biological methods.....	29
2.2.1 Cultivation and manipulation of mammalian cells.....	29
2.2.2 Immunofluorescence Microscopy	30
2.2.3 Confocal Microscopy	31
2.2.4 Fluorescence Recovery After Photobleaching (FRAP) and live cell imaging.....	32

2.2.5 Fluorescence-Activated Cell Sorting (FACS)	32
2.3 Biochemical methods	33
2.3.1 SDS polyacrylamide gel electrophoresis (SDS-PAGE)	33
2.3.2 Immunoblotting.....	33
2.3.3 Preparation of cell lysates.....	33
2.3.4 Preparation of mononucleosomes	33
2.3.5 Native chromatin immunoprecipitation (nChIP).....	34
2.3.6 Native chromatin immunoprecipitation followed by quantitative label-free mass spectrometry (nChIP-MS)	35
2.3.7 Immunoprecipitation of MTA paralogues and MBD3 or recombinant PWWP2A.....	36
2.3.8 Acid extraction of histones	36
2.4 Molecular biological methods	37
2.4.1 RNA extraction.....	37
2.4.2 cDNA synthesis	37
2.4.3 Quantification of mRNA levels with quantitative PCR (qPCR).....	37
2.4.4 Preparation of libraries for nChIP-seq	38
2.4.5 Validation of nChIP-sequencing results with quantitative PCR (nChIP-qPCR).....	38
2.4.6 Assay for Transposase Accessible Chromatin with high-throughput sequencing (ATAC-seq)	38
2.5 Bioinformatics.....	40
2.5.1 nChIP-seq analysis	40
2.5.2 nChIP-MS analysis.....	41
2.5.3 ATAC-seq analysis	42
3. RESULTS	44
3.1 PWWP2A mediates mitosis progression.....	44
3.2 PWWP2A indirectly influences mitosis	47
3.3 H2A.Z's chromatin association is unimpeded by PWWP2A	50
3.4 PWWP2A binds weakly to H3K36me3-containing gene bodies and associates with regulatory regions.....	54
3.5 PWWP2A interacts with a MTA1-specific NuRD subcomplex	57

3.6 PWWP2A mediates changes in histone acetylation levels.....	60
4. DISCUSSION AND FUTURE PERSEPCTIVES.....	68
4.1 Towards understanding the role of PWWP2A in mitosis and <i>Xenopus</i> cranio-facial development	68
4.2 Probable functions of PWWP2A in NuRD recruitment and histone deacetylation.....	74
4.3 Multivalent chromatin binder PWWP2A localizes to different chromatin features genome-wide	82
4.4 Consensus and discrepancy between different PWWP2A studies	84
REFERENCES.....	86
ACKNOWLEDGMENTS	109
CURRICULUM VITAE	109

SUMMARY

Chromatin structure, complexity and hence function is conferred by a plethora of proteins mediating the transcriptional output of a cell and attributing to the cells' identity. These chromatin-based processes are to a great extent regulated by proteins that read and recognize histone modifications, histone variants as well as other chromatin related factors thereby determining downstream processes. The essential histone variant H2A.Z plays a pivotal role in a vast number of DNA-related processes such as transcriptional regulation, cell cycle control and DNA repair by to date poorly understood mechanisms and is primarily correlated with active gene transcription on a genome-wide basis. Previously, utilizing a mass spectrometry-based screen for H2A.Z-nucleosome interactors, our group identified PWWP2A as a novel binder of H2A.Z. PWWP2A binds to chromatin in a multivalent manner and is implicated in transcriptional regulation and cell cycle progression in human HeLa Kyoto cells as well as in craniofacial development in *Xenopus*. In this thesis, the function of PWWP2A in transcriptional regulation and mitosis was further investigated. Live-cell imaging revealed that the siRNA-mediated depletion of PWWP2A results in a severe defect in mitotic progression. This phenotype is supposedly not exerted by a structural role of PWWP2A but rather an indirect effect on the transcription of genes involved in tubulin- and actin-related processes. Accordingly, tubulin as well as actin fibers exhibited an aberrant morphology. PWWP2A was thoroughly characterized as strong H2A.Z-interactor, albeit the depletion of PWWP2A did not affect H2A.Z's chromatin association or occupancy. PWWP2A does not seem to contain any enzymatic activity, suggesting that PWWP2A's function depends on recruitment of chromatin modifying proteins. Using a mass spectrometry-based approach, specific interactors of PWWP2A were determined. Among the strongest PWWP2A-binders were members of the core NuRD complex, MTA1, HDAC1/2 and RBBP4/7, which we termed M1HR and which were previously also identified to precipitate with H2A.Z-nucleosomes. To assess whether loss of PWWP2A affects histone deacetylation executed by HDAC proteins, nChIP-seq of H3K27ac as well as H2A.Zac after PWWP2A depletion were performed. Interestingly, loss of PWWP2A led to an increase of acetylation levels of H3K27 and H2A.Z at some defined typically PWWP2A-bound intergenic loci. Analysis of the expression of nearby genes revealed that while some genes were upregulated upon PWWP2A depletion, others remained unchanged. Concordantly, we hypothesize that PWWP2A may balance histone acetylation via recruitment of M1HR and finetune transcriptional output. In summary, PWWP2A influences mitosis progression, craniofacial development and histone acetylation. However, whether the underlying mechanisms are interconnected remains to be elucidated.

ZUSAMMENFASSUNG

Chromatinstruktur, -komplexität und -funktion wird durch eine Vielzahl von Proteinen vermittelt, welche der Zelle ein spezifisches Transkriptionsmuster verleihen und somit die Identität einer Zelle bestimmen. Diese chromatinbasierten Prozesse werden weitgehend durch Proteine reguliert, die Histonmodifizierungen, Histonvarianten sowie andere chromatinbezogene Faktoren lesen und erkennen und damit nachgelagerte Prozesse beeinflussen. Die essenzielle Histonvariante H2A.Z spielt eine zentrale Rolle in einer Vielzahl DNA-bezogener Prozesse wie Transkriptionsregulation, Zellzykluskontrolle und DNA-Reparatur durch bisher wenig verstandene Mechanismen und korreliert genomweit hauptsächlich mit aktiver Gentranskription. In einer früheren Studie unserer Arbeitsgruppe wurde PWWP2A mithilfe eines Massenspektrometrie-basierenden Screenings für H2A.Z-Nukleosom-Interaktoren als neuartiger Bindepartner für H2A.Z identifiziert. PWWP2A bindet auf multivalente Weise an Chromatin und ist an Transkriptionsregulation und Zellzyklusprogression in menschlichen HeLa Zellen sowie an der kraniofazialen Entwicklung in *Xenopus* beteiligt. In dieser Arbeit wurde die Funktion von PWWP2A während der Mitose und in der transkriptionellen Regulation genauer untersucht. Lebendzell-Mikroskopie zeigte, dass die durch siRNA-vermittelte Depletion von PWWP2A zu einem schwerwiegenden Defekt der mitotischen Progression führt. Dieser Phänotyp wird vermutlich nicht durch eine strukturelle Rolle von PWWP2A ausgeübt, sondern eher durch einen indirekten Einfluss auf die Transkription von Genen, die an tubulin- und aktinverwandten Prozessen beteiligt sind. Dementsprechend wiesen sowohl Tubulin- als auch Aktinfasern eine abweichende Morphologie auf. PWWP2A wurde als starker H2A.Z-Interaktor charakterisiert, nichtsdestotrotz beeinträchtigt die Depletion von PWWP2A die Chromatinassoziation von H2A.Z nicht. PWWP2A scheint keine Domänen zu besitzen, die enzymatische Aktivität vermitteln, was nahelegt, dass die Funktion von PWWP2A von der Rekrutierung von chromatinmodifizierenden Proteinen abhängt. Unter Verwendung eines auf Massenspektrometrie basierenden Ansatzes wurden spezifische Interaktoren von PWWP2A bestimmt. Zu den stärksten PWWP2A-Bindern gehörten Mitglieder des NuRD-Komplexes, MTA1, HDAC1/2 und RBBP4/7, den wir M1HR nannten und der zuvor auch mit H2A.Z-Nukleosomen präzipitiert werden konnte. Um zu untersuchen, ob der Verlust von PWWP2A die Histon-Deacetylierung, welche von den HDAC-Proteinen ausgeführt wird, beeinflusst, wurden nChIP-seq Experimente von H3K27ac sowie H2A.Zac nach PWWP2A Depletion durchgeführt. Interessanterweise führte der Verlust von PWWP2A zu einer Zunahme der Acetylierung von H3K27 und H2A.Z an definierten, typischerweise PWWP2A-gebundenen intergenischen Loci. Die Expressionsanalyse benachbarter Gene zeigte, dass einige Gene nach Depletion von PWWP2A

ZUSAMMENFASSUNG

hochreguliert wurden, andere jedoch unverändert blieben. Möglicherweise beeinflusst PWWP2A die Histonacetylierung über die Rekrutierung von M1HR und passt dadurch die transkriptionelle Aktivität an. PWWP2A beeinflusst den Verlauf der Mitose, die kraniofaziale Entwicklung und die Histonacetylierung. Ob die zugrunde liegenden Mechanismen jedoch miteinander verbunden sind, bleibt abzuklären.

1. INTRODUCTION

1.1 Chromatin structure and complexity

To fit DNA into a nucleus of an eukaryotic cell, DNA is compacted and packaged with proteins to form a complex structure called chromatin [1]. Chromatin consists of a repeating nucleosome structure, with approximately 146 base pairs of DNA wrapped around an octameric histone core [2]. Histone octamers comprise a pairwise assembly of the canonical histone core proteins: H2A, H2B, H3 and H4 [2]. Further, N-terminal and C-terminal peptides protrude histone proteins, which are termed histone tails and are prone to posttranslational modifications [3, 4]. Linker DNA connects nucleosomes and linker histone H1 and non-histone proteins locate at such free DNA segments. Accordingly, linker histone H1 can be modified posttranslationally and regulates and stabilizes higher order chromatin structure [5]. Canonical histones are incorporated into chromatin in a replication-coupled, S-phase dependent manner. Histone chaperones orchestrate histone turnover and nucleosome assembly by aiding in synthesis, processing and site-specific delivery of histones [6]. Furthermore, chaperones sequester histones in conformations that are unrelated to nucleosomes to facilitate wrapping of DNA around histones [2]. Nucleosomes in actively transcribed genes and regulatory regions are prone to undergo fast turnover [7]. During the cell cycle as well as throughout developmental processes, chromatin undergoes versatile changes and levels of compaction. Those changes are not based on direct alterations of the underlying DNA sequence but spatial and temporal changes in dynamic chromatin marks. Chromatin architecture is thus shaped by a number of variables, including posttranslational modifications (PTMs) of histones, DNA methylation, non-coding RNAs (ncRNAs), usage of histone variants and activity of chromatin remodelers, which alter the position of or exchange nucleosomes [3, 8-10] (Figure 1.1). They ease transitions between different chromatin states thereby affecting chromatin organization ultimately regulating transcriptional output by RNA polymerase II (RNAPII). The level of chromatin compaction defines DNA accessibility and state of permission for transcription by RNAPII and hence transcriptional activity [11, 12]. Thus, regulation of chromatin structure represents a dynamic process with various factors involved. Moreover, the majority of chromatin-associated proteins contain domains that mediate binding to specific chromatin features. The above-mentioned factors do not execute their functions solely but rather accomplish their tasks in a complex and highly dynamic interplay, resulting in a defined chromatin signature of a cell.

1. INTRODUCTION

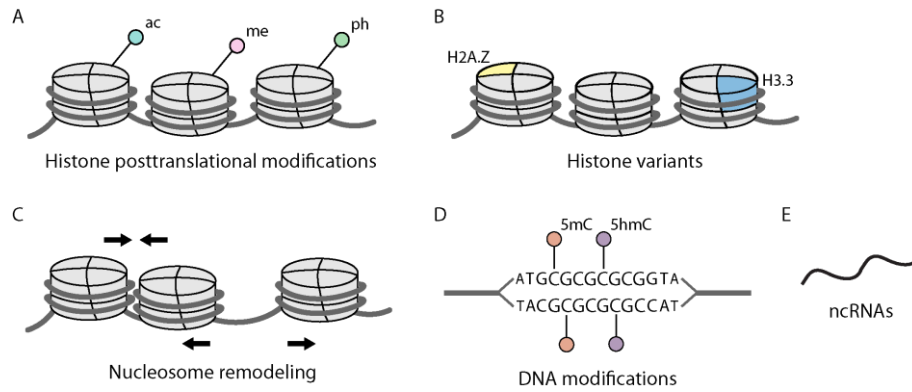


Figure 1.1: Modes of chromatin regulation. Chromatin structure and function is regulated by **A.** posttranslational histone modifications (such as acetylation (ac), methylation (me) and phosphorylation (ph)), **B.** exchange of canonical histones with histone variants (such H2A.Z or H3.3), **C.** nucleosome remodeling, **D.** DNA modifications (such as methylation (5mC) and hydroxymethylation (5hmC) and **E.** non-coding RNAs (ncRNAs). Further, crosstalk of these mechanisms contributes to the complexity of chromatin regulation.

In general, chromatin is categorized into euchromatin, which is less compacted and therefore transcriptionally active, and heterochromatin, which is tightly packed and accordingly transcriptionally repressive [13, 14]. Moreover, heterochromatic regions can be further subdivided into facultative and constitutive heterochromatin. While the distribution of facultative heterochromatin is cell type-specific and, for example, present at developmentally regulated regions such as the Barr body in differentiated female cells [15], constitutive heterochromatin features a high density of repetitive DNA elements at centromeres and telomeres [16]. The latter distinction into euchromatin and heterochromatin is being extended by the recent annotation of chromatin states which is further explained later in the text [17-19].

In mammals, DNA methylation and demethylation are important means to regulate gene expression [20, 21]. The *de novo* DNA methyltransferases DNMT3A, DNMT3B and DNMT3L establish new methylation patterns in embryonic development, differentiation and gametogenesis. During replication, DNA methylation patterns are propagated from the mother to the daughter strand by the maintenance DNA methyltransferase DNMT1 [8]. DNMT1 is tightly regulated by intra- as well as intermolecular interactions and its activity, stability and targeting is highly dependent on its cofactor UHRF1 [22-26]. The presence of a methylation mark (5mC) is a feature of silenced chromatin. Methylated cytosines can be further oxidized by the ten eleven translocation proteins (TET 1-3) to 5-hydroxymethylcytosine (5hmC), 5-formylcytosine (5fC) and 5-carboxycytosine (5caC) [27-29]. Contrary to 5mC, the oxidized derivatives are rather associated with transcriptional activity.

Another layer of chromatin regulation is added by ncRNAs that can vary in length from few to several thousand nucleotides and do not translate into proteins [30]. ncRNAs share some common features with protein-coding RNAs, such as being transcribed by RNAPII and containing polyA tails, but they

1. INTRODUCTION

are usually expressed at a lower level. ncRNAs are specifically expressed in certain tissues and developmental stages where they are thought to recruit chromatin remodeling complexes and transcription factors to sites of action.

As PTMs, nucleosome remodeling and histone variants are vital for this thesis, they are explained in greater detail below.

1.2 Posttranslational histone modifications

Almost two decades ago, a histone modification 'code' was postulated, proposing that PTMs on histones have a definite outcome and largely depend on reader proteins attracted by the PTMS itself or by the combinations of PTMS [3, 31]. Although the existence of the concept is a matter of debate, it still signifies a major landmark [32, 33]. In present times, the picture has become more complicated as histone PTMs exhibit a vast combinatorial complexity which is established through a dynamic interplay between histone PTM readers, writers and erasers. Most histone tail PTMs recruit chromatin-related proteins that recognize and read histone modifications via distinct domains, which in turn influence downstream processes such as transcription. The addition and removal of chemical modifications on amino acid side chains of histone tails as well as cores is executed by highly specialized enzymes termed writers and erasers, respectively [34]. Histone-modifying enzymes are recruited by transcriptional co-activators and/or -repressors, non-enzymatic chromatin binding proteins, RNAPII or adjacent histone modifications to their targets. While some histone PTMs are able to directly alter chromatin conformation, such as acetylation, other histone PTMs predominately function as recruiters [35]. To date, acetylation, methylation, phosphorylation and ubiquitination of histones represent the best-studied PTMs, nonetheless also ADP-ribosylation, butyrylation, crotonylation, deamination, formylation, glycosylation, propionylation and SUMOylation (small ubiquitin-like modifier) have been found on histones.

Methylation occurs in form of mono-, di- or trimethylation on lysine (K) residues or as mono- or dimethylation (symmetric or asymmetric) on arginine residues of histone proteins [36]. Lysine methyltransferases (KMTs) and lysine demethylases (KDMs) catalyze the addition or removal of methyl groups on K residues, respectively. Most KMT enzymes, like G9a or EZH2, contain a SET (Suppressor of Variegation, Enhancer of Zeste and Trithorax) domain, which is responsible for methylation of histone 3 lysine 9 (H3K9) or K27 (H3K27) [37, 38]. S-adenosyl-L-methionine (SAM) as a cofactor is utilized as methyl-group donor [39]. KDMs often belong to the Jumonji family, executing histone demethylation via hydroxylation [40]. Without altering the charge of the modified histone, K methylation can designate euchromatic as well as heterochromatic regions. While methylation on H3K4 is typically linked with a transcriptionally active chromatin state, trimethylation of H3K9 and

1. INTRODUCTION

H3K27 represent hallmarks of heterochromatin [41]. Moreover, in embryonic stem cells (ESCs) as well as during development, bivalent chromatin regions in which both activating and repressing modifications such as H3K4me3 and H3K27me3, respectively, are found colocalizing within the same nucleosome [42, 43]. Trimethylation of H3K36 (H3K36me3) is enriched at the bodies of active genes and regulates transcriptional elongation [44]. Consequently, proteins reading histone methylation contain methyl-lysine-binding motifs which exist in many flavors such as tudor, chromo, PHD or PWWP domains [45].

Similar to methylation, acetylation affects lysine residues and is regulated by histone acetyltransferases (HATs) that transfer an acetyl group from acetyl Coenzyme A [46, 47]. The addition of an acetyl group to a positively charged lysine induces charge neutralization. Due to a loss of electrostatic interactions between histones and DNA, acetylated sites are associated with transcriptionally active sites and thus an open euchromatic chromatin state [48]. Accordingly, acetylation of histones, such as H3K9ac, H3K14ac, H3K18ac, H3K23ac, H3K27ac and H3K36ac, generally correlates with active transcription, playing a central role in the regulation of gene expression [47]. Contrary to acetylation by HATs, deacetylation by histone deacetylases (HDACs) leads to transcriptional repression [49]. In general, proteins containing a bromodomain can recognize acetylated histone tails [50]. For example, H4K16ac controls chromatin structure and is enriched at transcriptional start sites of actively transcribed genes, supporting a positive role in gene transcription [48, 51]. Proteins containing a bromodomain can recognize acetylation marks and are involved in transcriptional regulation [52].

Histones are subject to phosphorylation at serine, threonine or tyrosine residues via a highly dynamic process, which results in a negative charge change at the affected residue [53]. The transfer of a phosphate group is catalyzed by protein kinases, which are either serine/threonine- or tyrosine-specific protein kinases while dephosphorylation is mediated by phosphatases. In addition to the cell cycle control system, Aurora B kinase catalyzes phosphorylation of H3S10, which is associated with chromosome condensation during mitosis [54]. Moreover, H3S10ph is crucial for transcriptional elongation in interphase cells [55]. Besides H3S10ph, also H2AT120ph, H3T3ph and H3S28ph represent marks of condensed mitotic chromatin [56, 57].

1.3 Nucleosome Remodeling

As mentioned above, the activity of chromatin remodelers contributes to chromatin structure changes. In general, nucleosome remodeling complexes as well as histone modifying enzymes modulate chromatin to influence DNA accessibility [58]. Chromatin remodeling complexes are usually macromolecular, multiprotein machines that use energy derived from ATP hydrolysis to

1. INTRODUCTION

remodel chromatin. Remodeling activities include sliding of nucleosomes as well as incorporation and eviction of canonical histones and its variants. These activities result in nucleosome assembly and DNA accessibility and thus play important roles in transcriptional regulation, DNA replication, DNA damage repair, cell cycle progression and genomic stability.

The ATPase subunit of chromatin remodelers originates from the SNF2 family of DNA helicases which can be subdivided into four major subfamilies: SWI/SNF, ISWI, INO80 and CHD [59]. Due to importance for this thesis, the following section will solely focus on the CHD-containing Nucleosome Remodeling and Deacetylase (NuRD) complex that was first identified in 1998 [60-63]. NuRD is highly conserved among metazoans and uniquely combines chromatin remodeling and histone deacetylase enzymatic activity [64, 65]. The chromatin remodeling subcomplex comprises the chromodomain-helicase-DNA-binding protein (CHD3/4, also known as Mi-2 α/β), methyl-CpG-binding domain proteins (MBD2/3) and GATA-binding protein 2A/B (GATA2A/GATA2B, also known as p66 α/β). The histone deacetylase subcomplex contains class I histone deacetylase proteins HDAC1 or HDAC2, the retinoblastoma-binding proteins and histone chaperones RBBP4 and 7 (also known as RbAp46 and RbAp48) and the metastasis tumor antigen family of proteins, MTA1/2/3. The subunit composition of the complex varies, thus NuRD comes in different flavors contributing to the diverse functional consequences. The complex fulfills multifaceted biological roles, ranging from gene transcription, DNA damage repair, maintenance of genome stability to chromatin assembly and is crucial for embryogenesis and embryonic stem cell differentiation [66, 67]. Genome-wide mapping of binding features of NuRD components in different cell types displayed occupancy of active enhancers and promoters (see 1.6 for characterization) [68-71]. Originally identified and characterized as a transcriptional corepressor complex, presently there is growing evidence that NuRD is likewise associated with transcriptional activation and is particularly responsible for maintaining an equilibrium between the two [58, 59, 67, 72, 73].

1.4 Core Histone Variants

The incorporation of core histone variants is an important means to influence nucleosome structure, stability and DNA accessibility. Compared to their canonical counterparts, histone variants differ to varying degrees in their primary sequences and are usually expressed from either single-copy or two genes, which may contain introns giving rise to distinct splice isoforms [74, 75]. In contrast to canonical histones, where the encoding mRNAs are devoid of polyA tails and feature a stem loop structure to meet the cells' demand, the mRNA of histone variants is polyadenylated [74]. While canonical histones are synthesized during replication only, most histone variants are expressed throughout the cell cycle and thus are deposited into chromatin via replication-independent

1. INTRODUCTION

pathways [76]. In this way, histone variants can fulfil specific functions without spatial or temporal constraints. Histone variants and canonical histones are usually exchanged by specialized histone chaperones. So far, no variants have been described for histone H4 in higher eukaryotes [77]. In the following, predominately human histone variants and their functions will be described (**Figure 1.2**).

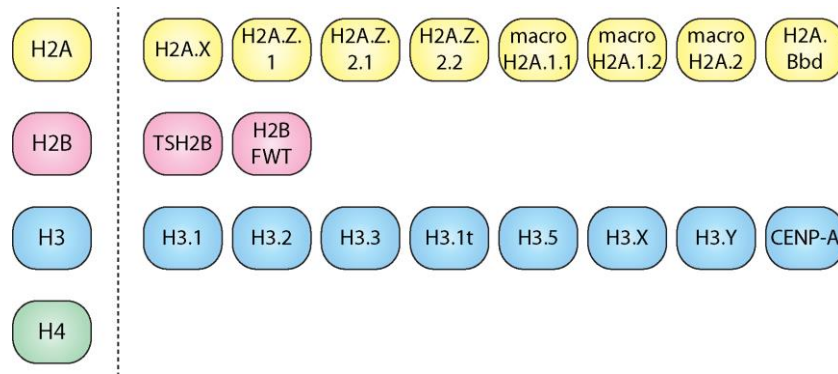


Figure 1.2: Schematic overview of human core histone variants. Variants of the histone H2A (yellow), H2B (red) and H3 (blue) family of the human core histones are depicted. To date, no histone H4 (green) variant has been described in humans.

Histone H3 family

The histone H3 family comprises two canonical histones H3.1 and H3.2, and the variants H3.3, H3.1t, H3.5, H3.X, H3.Y and CENP-A. Interestingly, H3.3 only differs from canonical H3.1 and H3.2 in five or four amino acids, respectively, attributing to H3.3 dissimilar function. H3.3 is not only found at gene bodies and regulatory regions, thereby being associated with transcriptional activity, but also with heterochromatic sites such as pericentromeres, transposons and telomeres and is incorporated by either HIRA or DAXX chaperone complexes [6, 78]. Primate-specific H3 variant H3.Y, possibly also H3.X, is found at actively transcribed genomic regions and is expressed in different brain regions and cancer tissues [79]. H3.1t and H3.5 are testis-specific H3 variants and their function is largely elusive [80, 81]. Histone H3-like centromeric protein A (CENP-A) distinctly localizes at the centromere and ensures proper centromere establishment and function by being involved in kinetochore assembly and chromosome segregation [82].

Histone H2B family

The histone H2B variant family to date comprises only three members. Human H2B variants TSH2B and H2BFWT are testis- and/or oocyte-specific and differ only slightly in their amino acid sequence from canonical H2B. Hence, TSH2B-containing and H2B-containing nucleosomes are highly similar in

1. INTRODUCTION

structure [83]. During spermatogenesis, TSH2B mediates the exchange of histones with protamines [84]. Moreover, expression of TSH2B in oocytes regulates reprogramming and enhances the generation of induced pluripotent stem cells [85]. H2BFWT's function is largely elusive although it has been proposed to associate with telomeres [86].

Histone H2A family

For the histone H2A family, the highest number of variants exists with four different classes - H2A.B, H2A.X, macroH2A and H2A.Z - and will be further discussed with a special focus on H2A.Z in the next section.

Human H2A variant H2A.B (also known as H2A.Bbd, Barr body-deficient) is exclusively expressed in brain and testes [87]. H2A.B shares only 50% sequence identity with H2A and is devoid of an acidic patch region thereby leading to a less stable nucleosome [88, 89]. Moreover, H2A.B is enriched over the gene body, correlating with active gene expression, and further localizes at the TSS where it mediates gene activation during spermatogenesis [90].

Generally known as guardian of the genome, histone variant H2A.X participates in DNA damage signaling pathways. In response to DNA double strand breaks, H2AX is phosphorylated on its Ser139 residue, termed γ H2A.X, thereby initiating a repair cascade [91, 92]. Moreover, H2A.X also accomplishes functions aside from DNA damage such as chromosome inactivation in germ and somatic cells, mitosis, stem cell development and aging and is found at promoters of active genes [93, 94].

Uniquely, histone variant macroH2A contains a large C-terminal globular domain that connects to the histone fold region through a flexible linker region. The histone fold domain shares 60% sequence identity with canonical H2A and the addition of the non-histone macrodomain gives rise to a large protein, three times the size of H2A [95]. In vertebrates, macroH2A exists in three isoforms: the alternative splice isoforms macroH2A.1.1 and macroH2A.1.2 as well as macroH2A.2. Generally, macroH2A is associated with transcriptional repression and localizes on the female inactive X-chromosome [96-99]. Moreover, macroH2A impairs recruitment of the chromatin remodeling complexes SWI/SNF and ACF [97, 100]. Interestingly, macroH2A localizes at developmental genes influencing differentiation and vertebrate development [96, 101].

1. INTRODUCTION

1.5 Histone Variant H2A.Z

Structural aspects of H2A.Z

Among eukaryotes, H2A.Z is highly evolutionary conserved and shares only 60 % sequence identity with canonical histone H2A. They differ in the L1 domain which mediates the interaction between the two H2A-H2B dimers, in the C-terminal docking domain, that mediates the interaction with the H3-H4-tetramer as well as in an extended acidic patch in H2A.Z that slightly alters the nucleosome structure and chromatin folding and promotes a higher affinity to the H4 tail [102]. Nevertheless, the crystal structure of an H2A.Z-containing nucleosome is overall highly similar to that containing the canonical counterpart [103]. While the H2A.Z-H2B dimer seems to be less stable than the H2A-H2B dimer, H2A.Z has also been reported to increase nucleosome stability [104-107]. Other studies report that H2A.Z is less tightly associated with chromatin and hence generates a more mobile nucleosome than canonical H2A [108, 109]. To date, it is widely accepted that H2A.Z may stabilize nucleosomes *in vitro* and functions as a destabilizer *in vivo* [110, 111]. The existence of homo- or heterotypic H2A.Z nucleosomes has been subject to much debate. Due to the steric properties of the L1 regions of H2A and H2A.Z it seemed reasonable that a coexistence may be ruled out although heterotypic H2A-H2A.Z nucleosomes have been reported [103, 112-114].

In humans, H2A.Z exists in three isoforms, encoded by the non-allelic genes *H2AFZ* and *H2AFV* for H2A.Z.1 and H2A.Z.2, respectively. They differ in only 3 amino acids on protein level arguing towards a separate evolution [115-117]. Alternative splicing of the H2A.Z.2 primary RNA (encoded by *H2AFV*) gives rise to an additional isoform H2A.Z.2.2, which only occurs in primates and leads to a drastic destabilization of the nucleosome [118]. Crystal structures of H2A.Z.1- or H2A.Z.2-containing nucleosomes revealed structural differences of the L1 loop regions of both isoforms despite their identical amino acid sequence [119]. Recently, using a label-free quantitative mass spectrometry approach, it was shown that the isoform specific interactomes are highly similar [120, 121]. However, due to the lack of an isoform specific antibody, most studies do not address whether the isoforms have independent functions.

Deposition and eviction of H2A.Z

In yeast, H2A-H2B dimers are substituted with H2A.Z-H2B by the histone chaperones Chz1, Nap1 and FACT [122, 123]. In human cells, H2A.Z is incorporated into chromatin independently of replication by YL1 and is removed by acidic leucine-rich nuclear phosphoprotein 32 family member E (ANP32E) and [124-127]. While YL1 is part of both ATP-dependent chromatin remodeler complexes SWI2–SNF2-related CBP activator protein (SRCAP) and p400-Tip60, ANP32E seems to be only present in p400-Tip60 [128-130]. Like ANP32E, YL1 specifically binds H2A.Z's extended acidic patch and,

1. INTRODUCTION

additionally, to H2A.Z's DNA-binding groove [124]. Another key interactor of H2A.Z essential for its deposition is GAS41, a component of both H2A.Z deposition complexes SRCAP and p400-Tip60, as its depletion leads to a dramatic reduction in H2A.Z occupancy [131].

Versatile functions of H2A.Z

Comprehensively, H2A.Z is involved in a vast number of DNA related processes (Figure 1.6 B). In metazoans, H2A.Z is essential while in yeast, H2A.Z is required for chromosome stability and normal growth [132, 133]. In *Drosophila melanogaster*, H2A.V, a combined homolog of the histone variants H2A.Z and H2A.X, contains residues in the α C helix within the highly conserved extended acidic patch that are required for viability [134, 135]. H2A.Z is expressed throughout frog development and RNAi-mediated loss of H2A.Z in *Xenopus laevis* impairs cell movement leading to defective gastrulation and defects in mesodermal and neuronal crest development [136, 137]. In mice, knockout of H2A.Z.1 results in embryonic lethality as H2A.Z.2 is unable to compensate for the loss of H2A.Z.1 function [138]. Similarly, in rat neurons, knockdown of either variant leads to deregulation of nonoverlapping gene cohorts, underlining H2A.Z.1's and H2A.Z.2's nonredundant functions [139]. In chicken cells, depletion of either H2A.Z paralogue leads to distinct abnormalities in cell growth and gene expression [117, 140]. Furthermore, an inducible knockout of H2A.Z in chicken cells results in a mitotic progression defect [141].

Generally, H2A.Z is an important regulator of transcriptional initiation and active gene expression. Consistently, H2A.Z is found at promoter regions (Figure 1.6 A) [142-147]. In line with this, H2A.Z resides at DNase hypersensitive sites marking open and accessible chromatin regions [145, 146]. During transcription initiation, H2A.Z is exchanged to recruit and modulate RNAPII kinetics at the TSS as well as gene bodies thereby reducing the nucleosome barrier for RNAPII [126, 143, 148]. Due to its predominant association with active transcription, H2A.Z is anticorrelated with DNA methylation at TSS and gene bodies [149, 150]. A recent study corroborates the theory of placeholder nucleosomes where H2A.Z is present in a nucleosome that changes its histone and/or its histone modification code pattern when transcriptional onset is desired during development [151]. H2A.Z is found together with the active chromatin mark H3K4me3 in the same nucleosome [152, 153]. In detail, H2A.Z is well-positioned at the -1 and the +1 nucleosome flanking nucleosome free region at the TSS of actively transcribed genes [154]. Generally, -1 H2A.Z-containing nucleosomes are associated with gene activity [154]. Several studies suggest that the presence of H2A.Z at the +1 nucleosome may function as a barrier for RNA polymerase II [126, 148, 155]. Besides localizing to actively transcribed promoters, H2A.Z also resides at regulatory regions such as enhancers where it is predominately found together with the histone variant H3.3 (Figure 1.6 A) [110, 144, 145, 156].

1. INTRODUCTION

H2A.Z is crucial for estrogen receptor enhancer activity by recruiting RNAPII and promoting the transcription of enhancer RNAs [157]. The level of H2A.Z at enhancers positively correlates with the H3K27ac level [144].

Although predominately described as a variant accompanied with a positive role in transcription and open chromatin conformation, H2A.Z also exhibits contrasting functions with being involved in transcriptional repression [158, 159]. H2A.Z contributes to the formation of pericentric and centromeric heterochromatin and co-occupies H3K9me3-enriched and / or CENP-A-bound regions [102, 143, 160-162]. Moreover, H2A.Z can mimic H3K9me3 via H2A.Z's acidic patch to enhance HP1 α binding which is mediated [102, 163]. H2A.Z represses transcription of p21 and Δ Np63 α target genes and is positioned at genes that are silenced in mitosis [130, 164, 165].

H2A.Z has been reported to be especially important in ESCs as it facilitates access to active and repressive complexes and transcription factors in ESCs and during differentiation [144, 166, 167]. Furthermore, it promotes maintenance of pluripotency and self-renewal in ESCs [144, 166, 168]. By recruiting pioneer transcription factor Foxa2 (Forkhead box protein A2), H2A.Z facilitates nucleosome depletion at TSS during differentiation [169]. The enrichment of H2A.Z at PRC2 target genes underlines the variants importance in the regulation lineage commitment [166, 167]. Together with H3.3, H2A.Z coordinately finetunes the enzymatic activity of PRC2 and H2A.Z localizes at H3K27me3-enriched genome-wide sites [170]. Moreover, H2A.Z activates differentiation-associated genes and regulates epithelial-mesenchymal transition by either activating or repressing epithelial or mesenchymal gene expression, respectively [171, 172].

Recent studies emphasize H2A.Z's role regarding neuronal aspects. Upon learning, H2A.Z is exchanged and is involved in fear conditioning and suppresses memory formation and retention by modulating gene expression [173]. Furthermore, H2A.Z is evicted from genes that are actively transcribed upon learning and accumulates in the mouse hippocampus during aging [174]. When the H2A.Z genes were knocked out in adult mice during brain development, deletion of H2A.Z causes impaired neuronal progenitor cell (NPC) differentiation, as well as behavioral abnormalities, such as reduced exploratory behavior and depression [175]. The occurrence of dendritic malformations upon H2A.Z depletion underlines the importance of H2A.Z during neuronal development as dysfunctions lead to neurodevelopmental disorders. In line, SNPs in the *H2AFZ* gene correlate with the occurrence of schizophrenia, substantiating H2A.Z.1 as a potential marker of predisposition [176].

Notably, H2A.Z is essential for mitosis. In mitotic chromatin, H2A.Z localizes at the centromere, indicating a role in centromere formation or a contribution in centromere–kinetochore attachments [161, 177]. Strikingly, depletion of H2A.Z in mammalian cells results in chromosome segregation defects with lagging chromosomes and issues in chromosome cohesion ultimately leading to

1. INTRODUCTION

genome instability [178]. Consistent with this observation is the mitosis progression phenotype observed in chicken cells upon H2A.Z knockout [141].

Furthermore, H2A.Z is involved in the early stages of the DNA damage response. H2A.Z is rapidly deposited into sites of DNA damage to enable DNA repair by lessening chromatin compaction [179-181]. Exchange of H2A.Z at sites of DNA damage is only transient and shortly after DNA damage; ANP32E removes H2A.Z from DNA lesions to facilitate end resection [126, 127, 180]. Moreover, also INO80, which replaces H2A.Z-H2B dimers with H2A-H2B in yeast, can similarly evict H2A.Z from damaged chromatin promoting homologous recombination [179, 182, 183].

In various cancer types H2A.Z is overexpressed or dysregulated. Both H2A.Z isoforms are overexpressed in melanoma and are linked with poor prognosis in disease progression [120]. Knockdown of H2A.Z.2, but not H2A.Z.1 decreases global acetylation levels on H3 and H4 in melanoma cells and restrains the recruitment of BRD2 and E2F1 to its target genes [120]. Moreover, H2A.Z is involved in hepatocellular carcinoma, breast cancer, bladder cancer and prostate cancer [153, 184-186].

PTMs of H2A.Z

Adding another layer to the complex and versatile functions of H2A.Z, its tails are subjected to posttranslational modifications (Figure 1.6 C). While lysine residues on N-terminal H2A.Z tails can either be acetylated (K4, K7, K11; H2A.Zac) or methylated (K4, K7; H2A.Zme), C-terminal lysines are prone to ubiquitination (K120, K121, K125; H2A.Zub) as well as methylation (K101) [187, 188]. H2A.Zub is enriched at facultative heterochromatin and is associated with a repressive chromatin state [152]. E3 ligase RING1B of the PRC1 sets the ubiquitination mark on H2A.Z, which can be removed by Ubiquitin Specific Peptidase 10 (USP10) to activate transcription [152, 189]. Monomethylation of K4 and K7 is mediated by SET domain containing 6 (SETD6) and is important for maintaining self-renewal of mESCs [190]. Furthermore, dimethylation of H2A.Z.1K101 by histone methyl-transferase SMYD3 prevents eviction of H2A.Z by ANP32E [191]. Recently, SUMOylation of H2A.Z.2 was described to be involved in the DNA-damage mediated exchange of H2A.Z but without identifying the SUMOylation target amino acid [192]. Acetylation of the N-terminal tails of H2A.Z on residues K4, K7 and/or K11 variations of singly- di and tri-acetylated forms exist [115, 193]. While H2A.Z is acetylated by Tip60 in yeast and drosophila, a recent study proposes that this is also true in mammalian cells [194-196]. Recently, the bromodomain of Bromodomain PHD Finger Transcription Factor (BPTF), which has previously only been described as a H4K16ac reader, was shown to also recognize diacetylated H2A.Z [197]. Acetylated H2A.Z is generally correlated with an open chromatin conformation by destabilizing the nucleosome while non-acetylated H2A.Z associates more tightly

1. INTRODUCTION

to DNA [104, 193, 198]. H2A.Zac is predominantly found at the TSS of actively transcribed genes and correlates with the level of gene expression [144, 156, 173, 199-201]. Moreover, H2A.Zac also localizes to enhancers and intergenic regions [200, 201]. In mESCs, acetylated H2A.Z is found at promoters of bivalent regions enriched in both H3K4me3 and H3K27me3 to facilitate cellular differentiation [156]. These bivalent sites may further comprise H2A.Zub marks [156]. The acetylation of H2A.Z plays an important role during differentiation and developmental processes as it is crucial for MyoD-activated myoblast differentiation and supports expression of Notch target genes [196, 202]. Moreover, H2A.Zac promotes oncogene activation in cancer and is associated with poor prognosis [200].

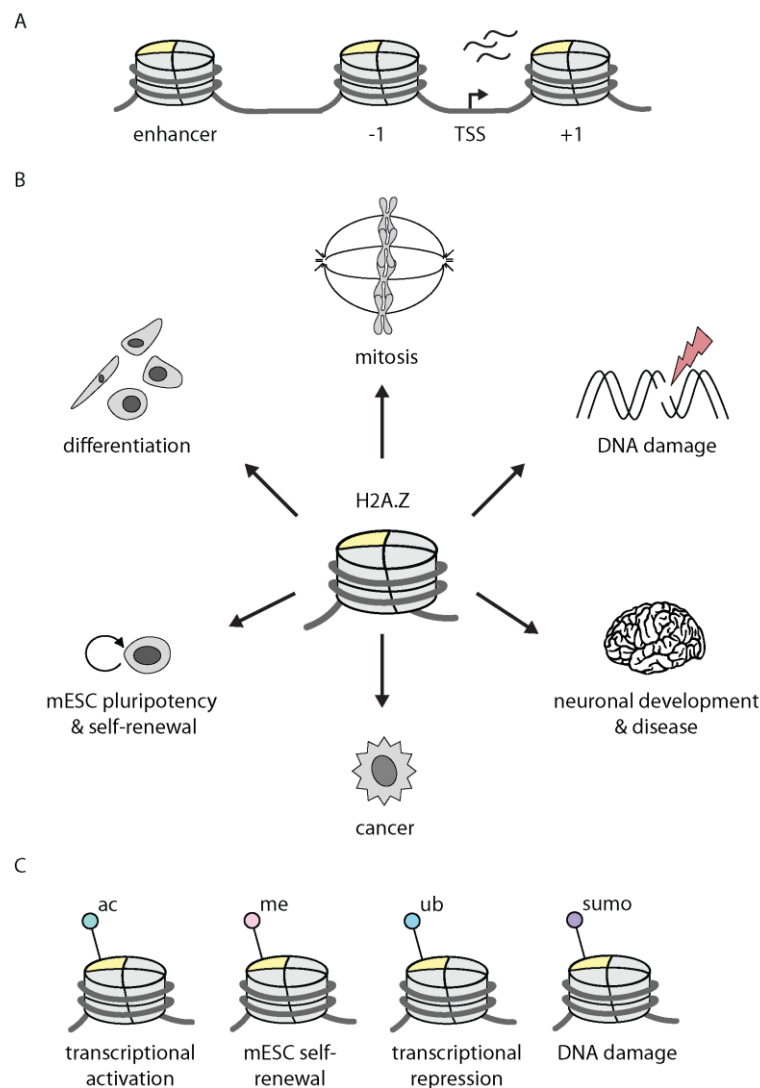


Figure 1.3: Summary of H2A.Z's main genome-wide localization, functions and PTMs. **A.** Genome-wide H2A.Z localizes at active regulatory regions such as enhancers and promoters of actively transcribed genes. **B.** H2A.Z is involved in manifold chromatin-related processes including DNA damage response, neuronal development and disease, cancer, mESC pluripotency and self-renewal, differentiation and mitosis. **C.** H2A.Z can be post-translationally modified contributing to H2A.Z's versatile functions.

1. INTRODUCTION

1.6 Functional genomic elements

Gene expression is regulated by dynamic changes in the structure and composition of chromatin, leading e.g. to the enhanced accessibility of the DNA allowing in turn binding of transcription factors (TFs). Accordingly, genome-wide data from ChIP-seq of histone modifications and variants and RNA-seq as well as DNA accessibility and TF binding profiles enabled the categorization of the genome into functional regulatory elements containing specific chromatin features. Genomic regulatory elements that are involved in the spatio-temporal regulation of gene expression as well as genomic organization are promoters, enhancers and insulators [203]. The promoter localizes around the TSS and is crucial for gene transcription by RNAPII. Specific DNA sequences within the promoter are referred to as core promoter motifs, of which the best known is the TATA box, and that among others interact with RNAPII as well as transcription factor II D (TFIID). Additionally, transcription is regulated spatio-temporally by distal non-coding *cis*-regulatory modules called enhancers. Enhancers are typically placed 3' or 5' relative to the promoter or within introns of the transcribed target gene irrelevant of the orientation or distance of the latter. A widely accepted model of enhancer function implies that enhancers, and transcription factors that bound to enhancers, are brought into contact with promoters via DNA looping in order to promote RNAPII performance mediated by the mediator core initiation complex [204]. More than 400.000 putative enhancers are predicted to allocate about 10% of the genome of human cells [205]. With an estimated number of 25.000 genes, it is still under debate how to specify which gene is regulated by which enhancer. Moreover, enhancer elements may be transcribed into RNA (eRNA), which are bidirectional and non-polyadenylated RNAs that are likewise involved in regulating enhancer activity and gene expression [206]. Complicating enhancer function even further, they can be found in an active, poised or silenced state. While promoters function as transcriptional on/off-switch, enhancers modulate the level of transcription by strengthening or dimming transcriptional activity. In addition to promoters and enhancers, insulators are long range *cis*-regulatory boundary elements that are involved in the regulation of chromatin architecture/conformation by promoting DNA looping and consequently aiding to cohere chromatin regions into domains [207]. Insulator function in mammals is primarily executed by CCCTC-binding factor (CTCF), which cooperates with cohesin to block gene transcription by preventing promoter-enhancer interaction [208].

Due to the importance for this thesis, in the following mainly chromatin features corresponding to active chromatin states will be explicated. In addition to signature histone modifications and histone variants, accessibility of chromatin and DNase sensitivity are summarized in the following (Figure 1.4).

1. INTRODUCTION

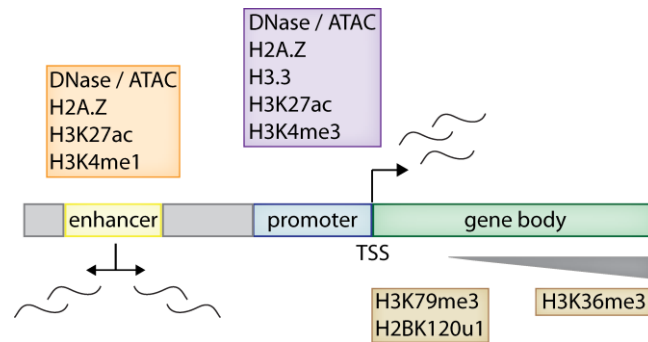


Figure 1.4: Combinatorics of the most common active genomic features. The genome can be segmented according to chromatin features, marking functional regulatory elements. Among others, enhancers are predominantly classified by a high DNA accessibility and enrichment in H2A.Z, H3K27ac and H3K4me1. Likewise, promoters show a high DNA accessibility as well as H2A.Z enrichment, but also high levels of H3.3 and H3K4me3. While enhancers are transcribed to eRNAs mostly in a bidirectional manner, within promoters, genes are transcribed from the TSS. Typically, gene bodies exhibit H3K79me3, H2BK120ub1 and H3K36me3 marks. Shown are only chromatin features related to gene activity.

Since enhancers and promoters exhibit an open chromatin conformation, both feature a high DNA accessibility as determined by DNase digest and Assay for Transposase-Accessible Chromatin using sequencing (ATAC) followed by high-throughput sequencing (DNase-seq or ATAC-seq). Consistently, nucleosomes containing histone variants H2A.Z and H3.3 localize not only at the nucleosome depleted promoter region at the TSS of actively transcribed genes but also at active and poised enhancers [144-146, 156, 166]. In general, enhancers are marked by mono- or dimethylated H3K4 while promoters feature di- or trimethylated H3K4 [209]. In combination with H3K27ac, those marks are considered to be chromatin signatures of an active state [210]. Active enhancers are also enriched in H3K56ac and H4K16ac [51, 211]. Additionally, enhancers are occupied by coactivator complexes p300 and CREB-binding protein (CBP) or H2A.Zac [144, 156, 157, 200, 209, 212, 213]. Further, TET proteins localize at enhancer regions that are hence enriched in 5hmC [214, 215]. Moreover, some enhancers are found in a poised state, in which both activating, such as H2A.Z or H3K4me1/2, as well as repressing marks, such as H3K9me3 and H3K27me3, are present at the same locus [144, 209, 216]. At promoter regions, H3K4me3 localizes at so called CpG islands and the level of H3K4me3 occupancy correlates with gene activity [146, 217]. Furthermore, promoters of active genes are enriched in acetylated H3 and H4 [218, 219]. Likewise, actively transcribed gene bodies feature high levels of H3ac and H4ac but also H3K79me3 and H2BK120u1 [220-223]. Importantly, H3K36me3 classifies gene body regions and increases in enrichment toward the 3'-end of actively transcribed genes [44, 224]. Repressive chromatin states are usually marked by low DNA accessibility and high levels of 5mC and H2AK119u1, H3K9me3 and H3K27me3 at promoters [225].

1. INTRODUCTION

Accordingly, enhancers and promoters serve as platforms for TFs and chromatin modifying proteins such as reader proteins and remodeling complexes that are tethered to these specific chromatin features thereby contributing to the complexity of spatio-temporal chromatin.

1.7 PWWP2A

H2A.Z localizes at regulatory genomic regions (see 1.6) and is crucial for various biological processes (see 1.5). How H2A.Z functions is largely unknown. Possibly, different proteins or protein complexes are recruited to and recognize H2A.Z within its specific chromatin environment and aid H2A.Z in fulfilling its functions. To identify specific interactors of H2A.Z-containing nucleosomes, our group previously solved the H2A.Z interactome via label-free quantitative mass-spectrometry [120, 121]. Among several other proteins that bound strongly to both H2A.Z.1 and H2A.Z.2 was PWWP2A, a protein that had already been detected in an earlier, non-quantitative H2A.Z-screen, but was not further characterized [226]. Owing to its eponymous PWWP domain, PWWP2A is part of the PWWP domain containing protein group, which was first found in Wolf-Hirschhorn syndrome candidate 1 (WHSC1) [227]. PWWP2A is a multidomain protein of 755 amino acids that contains two proline-rich regions (P1, P2), an intrinsically disordered internal stretch (I), which does not exhibit any similarity to domains present in other proteins, a serine rich region (S) and a PWWP domain (Figure 1.5).

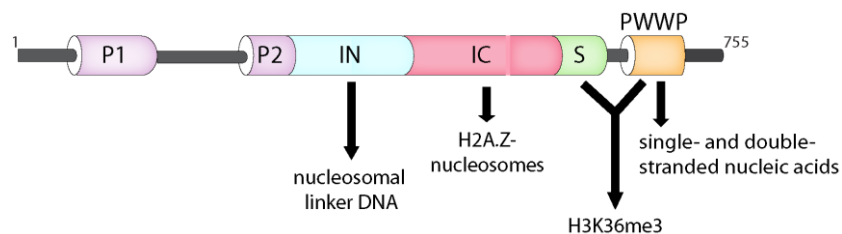


Figure 1.5: Domain structure and *in vitro* binding features of the human PWWP2A protein. PWWP2A consists of two proline-rich stretches in the N-terminal part (P1, P2; purple), a N-terminal (IN; light blue) and a C-terminal internal region (IC; red), a serine-rich stretch (S; green) and a PWWP domain (orange). PWWP2A binds to chromatin in a multivalent manner *in vitro*: The N-terminal part of I (IN) binds nucleosomes via nucleosomal linker DNA, the C-terminal part of I (IC) binds H2A.Z-containing nucleosomes, the serine rich stretch (S) in combination with the PWWP domain binds H3K36me3-containing nucleosomes and the PWWP domain alone binds single- and double-stranded nucleic acids.

In vitro experiments demonstrated that the internal region divides its labor and can thus be further subdivided into a nucleosomal linker DNA-binding N-terminal internal region and a C-terminal internal region which specifically interacts with H2A.Z-containing nucleosomes [121, 228]. PWWP domains of other proteins have been reported to bind to H3K36me3 via an aromatic cage as well as

1. INTRODUCTION

DNA with low affinity [229-231]. Likewise, regarding PWWP2A, the S together with the PWWP domain mediate binding to H3K36me₃-containing nucleosomes and the PWWP domain alone interacts weakly with single- as well as double stranded nucleic acids *in vitro* [228]. Fluorescence Recovery After Photobleaching (FRAP) experiments in HeLa Kyoto (HK) cells verified that PWWP2A uses at least three different regions - the IN, IC and PWWP region - to exert its strong chromatin binding ability. On a genome-wide basis, PWWP2A resides at the -1 and +1 nucleosome surrounding the TSS of highly transcribed genes (Figure 1.6) [121].

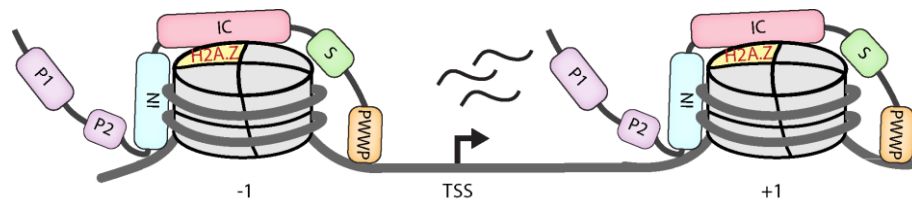


Figure 1.6: Schematic outline of PWWP2A nucleosome binding at the TSS of active genes. PWWP2A binds to chromatin in a multivalent manner: The N-terminal part of I (IN) binds nucleosomes, the C-terminal part of I (IC) binds H2A.Z and the PWWP domain binds naked DNA. Genome-wide, PWWP2A and H2A.Z co-occupy the -1 and the +1 nucleosome at the TSS of highly transcribed genes.

Depletion of PWWP2A in HK cells results in the deregulation of gene expression and a defect in cell cycle progression [121], both of which are further explored in this thesis. In *Xenopus laevis* and *tropicalis*, morpholino-mediated knockdown of PWWP2A leads to severe cranio-facial defects assumedly due to deficient neural crest cell differentiation and migration [121].

1.8 Objective

PWWP2A was previously characterized as a multivalent chromatin binding protein featuring strong interaction with H2A.Z-containing nucleosomes. Further, it was shown that loss of PWWP2A in human HeLa cells impairs gene expression programs and cell cycle progression. In this thesis, I set out to gain deeper insights into the mechanism(s) by which PWWP2A influences mitosis and transcriptional regulation. To investigate how PWWP2A might affect mitosis progression, I performed live cell imaging as well as immunofluorescence staining of fixed cells and metaphase spreads upon PWWP2A knockdown. Potential candidates deregulated upon PWWP2A depletion and implicated in cell cycle-related processes were validated via RT-qPCR and immunoblotting. As PWWP2A is a strong interactor of H2A.Z, I determined the effect of PWWP2A depletion on H2A.Z's chromatin association and occupancy using FRAP and nChIP, respectively. Further, to obtain first clues on the mechanism by which PWWP2A influences gene regulation, PWWP2A's interacting

1. INTRODUCTION

proteins were identified. Interesting binding candidates were further characterized and assessed on their effect on histone deacetylation and transcriptional output after PWWP2A depletion.

2. MATERIAL AND METHODS

2.1. Material

2.1.1 Technical devices

Description	Supplier
2100 Bioanalyzer	Agilent
CASY Cell Counter	Innovatis
Centrifuges	Beckmann Coulter Optima Max-XP Eppendorf 5424R Heraeus Biofuge pico Roth Rotilabo-mini-centrifuge Thermo Shandon Cytospin 4 Thermo Scientific Multifuge X3R
Developer machine	AGFA Curix
Freezer (-20°C)	Beko, Liebherr
Freezer (-80°C)	Thermo Scientific
Fridge	Liebherr
Gel documentation system	BioRad ChemiDoc
H ₂ O purification system	Millipore
Hood	Binder
Incubator 37°C tissue culture	New Brunswick
LightCycler 480 II	Roche
Mass spectrometer	Thermo Scientific Easy-nLC 1000 or 1200
Mastercycler nexus GX2	Eppendorf
Microscopes	Leica SP5 confocal scanning Leica SP5 II confocal scanning Leica SP8X WLL confocal scanning PerkinElmer UltraVIEW VoX spinning disc
pH meter	inoLab
Pipetboy	Neolab
Pipettes	Gilson
Power supply unit	BioRad
Protein gel chamber	Serva BlueVertical PRiME
Qubit fluorometer	Invitrogen
Rotating wheel	Neolab
Scales	Sartorius
Shaker	Roth
Spectrophotometer	Peqlab Nanodrop ND1000
Thermomixer	Eppendorf 5436 Thermomixer C
Trans Blot SD semi-dry transfer cell	BioRad
Vortex mixerGenie2	Bachofer

2. MATERIAL AND METHODS

2.1.2 Consumables

Description	Supplier
1.5 ml low binding tubes (DNA and protein)	Sarstedt
1.5 ml and 2 ml reaction tubes	Greiner, Sarstedt
15 ml and 50 ml tubes	Sarstedt
μ-slide 8-well glass bottom dishes	Ibidi
Cell culture plates	Sarstedt
Coplin jar	Sigma
Coverslips	Hecht-Assistant
Cryovials	Roth
Filter paper Whatman	Whatman
Filter tips	Biozym, Gilson
Glassware	Schott
LightCycler R 480 multiwell plate 384, white	Sarstedt
LightCycler R 480 Sealing foil	Sarstedt
MaXtract High Density Column	Qiagen
Microscope slides SuperFrost	Roth
Multiply μStripPro with 8 x 0.2 ml tubes	Sarstedt
Pipette tips	Biozym, Greiner, Sarstedt
Protein gels precast	Serva
Protran nitrocellulose transfer membrane	Whatman
Qubit assay tubes	Invitrogen
X-ray films	Fujifilm

2.1.3 Chemicals

Description	Supplier
Acetic acid	Sigma
Acetone	Sigma
Acetone nitrile	Sigma
AMPure XP beads	Beckman Coulter
BSA 98%	Sigma
Colcemid	Sigma
Complete Protease Inhibitor (PI) Cocktails Tablets	Roche
DAPI	Invitrogen
Developer	AGFA
Digitonin	Promega
DMEM	Sigma
DMSO	Sigma
DNA oligonucleotides	Eurofins MWG
DTT	Roth
Dynabeads	M-280 sheep anti-rabbit, life technologies Protein G, life technologies

2. MATERIAL AND METHODS

ECL Western Blotting detection reagents	Amersham
EDTA	Sigma
EGTA	Sigma
Ethanol, absolute	Roth
FCS dialyzed	Sigma
Fixer	AGFA
Formic acid	Sigma
G418-sulfate	Sigma
GFP-Trap®_M (magnetic)	Chromotek
Glycerol	VWR
Glycogen	Roche
HEPES	Serva
KCl	VWR
Methanol	Sigma
MgCl ₂	VWR
NaCl	VWR
Na-deoxycholate	Sigma
Nail polish	DM
NP-40	Sigma
Oligofectamine Transfection Reagent	Invitrogen
Opti-MEM Reduced-Serum Medium	Invitrogen
Penicillin / streptomycin (P/S)	Sigma
PMSF	Sigma
Polyethylenimine (PEI)	Polysciences
Proteinase K	Life technologies
RNase A	Life technologies
Roti-Phenol/Chloroform/Isoamylalcohol	Roth
SDS	Serva
siRNAs	Eurofins MWG
β-mercaptoethanol	Sigma
Sulfuric acid	Sigma
Trichloroacetic acid (TCA)	Sigma
Tris	Invitrogen
Triton X-100	Sigma
Trypsin/EDTA (cell culture)	Sigma
Tween20	Sigma
Urea	Sigma
VECTASHIELD® mounting medium	Vector Laboratories
X-treme Gene HP Transfection Reagent	Roche

2. MATERIAL AND METHODS

2.1.4 Kits, enzymes and markers

Description	Supplier
DNA 1000 or HS Kit	Agilent
Fast SYBR Green Master Mix	Applied Biosystems
Micrococcal nuclease	Sigma
MicroPlex Library Preparation Kit	Diagenode
MinElute PCR Purification Kit	Qiagen
NEBNext 2x PCR Master Mix	NEB
Nextera DNA Library Preparation Kit	Illumina
peqGOLD Protein Marker IV, V	Peqlab
Phalloidin Alexa 594-conjugated	Life technologies
ProtoScript First Strand cDNA Synthesis Kit	NEB
Qubit dsDNA HS Assay Kit	Invitrogen
RNase-Free DNase Set	Qiagen
RNeasy Mini Kit	Qiagen

2.1.5 Antibodies

2.1.5.1 Primary antibodies

Table 2.1: Primary antibodies used for Western Blot (WB), Immunofluorescence (IF), Chromatin immunoprecipitation (ChIP) or immunoprecipitation (IP)

Antibody (order number)	Host species	Application and dilution	Supplier
Aurora B (ab2254)	rabbit	1:400 for IF	Abcam
CAPZA1 (6606-1-Ig)	mouse	1:2.000 for WB	Proteintech
CENP-E (39620)	mouse	1:1.000 for IF	Active motif
F-actin (ABIN731498)	rabbit	1:1.000 for WB	Antibodies-online GmbH
FLAG M2 (F1804)	mouse	1:80.000 for WB 3 µg per IP	Sigma
GFP (ab290)	rabbit	15 µg for IP	Abcam
H2A.Z (ab4174)	rabbit	1:3.000 for WB	Abcam
H2A.Zac (C15410202)	rabbit	1:2.000 for WB 2 µg per ChIP	Diagenode
H2AT120ph (61196)	rabbit	1:400 for IF	Active motif
H3 (61475)	mouse	1:5.000 for WB	Active motif
H3 (ab1791)	rabbit	1:30.000 for WB	Abcam
H3K27ac (ab4729)	rabbit	2 µg per ChIP 1:2.500 for WB	Abcam
H3S10ph (39636)	mouse	1:1.000 for IF	Active motif
HA-HRP (2999S)	mouse	1:40.000 for WB	Cell Signaling Technology
HDAC1 (5356S)	mouse	1:20.000 for WB	Cell Signaling Technology
IgG (I8765)	mouse	3 µg per IP	Sigma
INCENP (39260)	mouse	1:1.000 for IF	Active motif

2. MATERIAL AND METHODS

MBD3 (ab157464)	rabbit	1:5.000 for WB	Abcam
MTA1 (ab50209)	rabbit	3 µg per IP	Abcam
MTA1 (ab71153)	rabbit	1:1.000 for WB	Abcam
PWWP2A (NBP2-13833)	rabbit	1:1.000 for WB 1:100 for IF	Novus
α-Tubulin (39527)	mouse	1:1.000 for IF	Active motif

2.1.5.2 Secondary antibodies

Table 2.2: Secondary antibodies used for Western Blot (WB) or Immunofluorescence (IF)

Antibody (order number)	Application and dilution	Supplier
α-mouse HRP (NA931)	1:10.000 for WB	VWR
α-rabbit HRP (NA934)	1:10.000 for WB	VWR
α-mouse IRDye 680RD (926-68070)	1:10.000 for WB	LICOR Biosciences
α-rabbit IRDye 800CW (926-32211)	1:10.000 for WB	LICOR Biosciences
α-mouse Alexa 488 (715-545-151)	1:400 for IF	Jackson Laboratories
α-rabbit Alexa 488 (711-545-152)	1:400 for IF	Dianova
α-rabbit Alexa 555 (A31572)	1:1.000 for IF	Thermo Fisher Scientific
α-mouse Alexa 594 (715-585-151)	1:400 for IF	Dianova
α-rabbit Alexa 594 (711-585-152)	1:400 for IF	Dianova

2.1.6 Cell lines

Name	Origin	Source/Supplier
HeLa Kyoto (HK)	Cervical cancer, human	Leonhardt laboratory, Biocenter LMU Munich
HK GFP #4	Cervical cancer, human	[118]
HK GFP-H2A #4	Cervical cancer, human	[118]
HK GFP-H2A.Z.1 #5	Cervical cancer, human	[118]
HK GFP-PWWP2A #5.2	Cervical cancer, human	[121]
EXPI293F™ (A14527)	293 embryonic kidney, human	Thermo Fisher Scientific, Mackay laboratory, University of Sydney
mESC Mbd3-Avi-3×FLAG	E13tg2a embryonic stem cells, mouse	[232], Hendrich laboratory, Wellcome Trust-MRC, Cambridge
mESC Mta1-Avi-3×FLAG	E13tg2a embryonic stem cells, mouse	[233], Hendrich laboratory, Wellcome Trust-MRC, Cambridge
mESC Mta2-GFP	E13tg2a embryonic stem cells, mouse	[233], Hendrich laboratory, Wellcome Trust-MRC, Cambridge
mESC Mta3-Avi-3×FLAG	E13tg2a embryonic stem cells, mouse	[233], Hendrich laboratory, C Wellcome Trust-MRC, Cambridge

2. MATERIAL AND METHODS

2.1.7 Oligonucleotides

Table 2.3: Oligonucleotides used for nChIP quantitative PCR in 5' to 3'

Name	Sequence F	Sequence R
B3GALNT2 remote	TGTCTCCCTGAAACTCATCTCT`	GCACTAATCCTGCCTTCCTG
CCDC71 TSS	GTGGTGCATTGACATCTGGG	CTGGGACTGAAGTGGGCATT
CCL5 remote	GGATCCCAAGAGAAGCCTGA	CAGGGGCAAAGAAGGAGAGA
CCL5 TSS	ATTTCTCTGCTGACATCCTTAGT	TCCTAACTGCCACTCCTTGT
FST close	TGCCATCCTTAGACCTCAGA	AGCACTGCCAGGACTACATT
NUF-	GCATCTAACAAAACCCGGCAC	GTCCGAGTTGAAGAGCAAAC
NUF+	CACTGTAGGTGAGCGCGAGA	CGCTGAGCACGACGAAAACA
PARS2-	AGACGCCTTTATTACAGTGCCC	TCTACGTGGTAGCAGCTCAAAA
PARS2+	GGGATGCAAGTGGGAAAAC	ATTGCGGTAGGTGAACGTG
RPL11	ACAGCTTTGGGTGATGCAGT	TTGTTGGACCAAAACACGGC
ZNF19 remote	CACACAAAACATTTCTCCATCAGG	AGGTTTTCTGCCTTGAACA

Table 2.4: Oligonucleotides used for quantitative PCR in 5' to 3'

Name	Sequence F	Sequence R
ANTXR1	CACTCCAGGTCAGCATGAAC	CCAGAACCACCAGAGGAGAG
B3GALNT2	TGGCTGCCATAGGACCTAA	TCCACAGTTCGTCAGTTCC
CAPZA1	AGTTCACCATCACACCACCT	CTTGGCAGTTTGGGCTTCAT
CCDC71	AAAGCTGCTGAAGTTCGGTG	TGGAGCCGTATTACAGGTGA
CCL5	CTCGCTGTCATCCTCATTGC	TACTCCTTGATGTGGGCACG
FST	TGCCTGCCACCTGAGAAAG	TCTCCCAACCTTGAAATCCCA
HPRT	AAGGGTGTTTATTCCTCATGGA	AATCCAGCAGGTCAGCAAAG
MTA1	GGCGGATGAACTGGATCGA	CAGCACGCTTGGTTTCCG
PREX1	CTGAGCGTGTCCTGGAG	GTCCTTGACTCGCAGGTTTT
TPGS2	GGTTCCTGGACAGAGCGTTA	GCAGGTTTGTGTTGTAGGTGA
VASP	AGTCGTCTTCTCGGTGACC	GAGAACCCCGTTCCTCAG
ZNF19	CCCAGCAGAGAGGACCAAAA	GCTGACCATGTGACATCATCC

2. MATERIAL AND METHODS

Table 2.5: siRNA oligonucleotides used for RNAi in 5' to 3'

Name	Sequence (sense)
ctrlii	UAAGGCUAUGAAGAGAUACTT
Luciferase	CUUACGCUGAGUACUUCGATT
MTA1#1	GGGAAAUAGAAGAGGAAUUTT
MTA1#2	GAAAU AUGGUGGCUUGAAATT
PW#1	GGACAGAAGUCAAGUGUGAUUTT
PW#2	GCUAUUAAACUACGACCCAUUTT

2.1.8 Plasmids

Plasmid	Description	Source	Resistance
Cherry-PWWP2A	pIRESneo-Cherry-PWWP2A; cloned via Gateway from pIRESneo-EGFP-PWWP2A plasmid	Andrea Schmid, BMC	Amp; Neo
FLAG-PWWP2A	pcDNA3.1 expression vector backbone	Mackay laboratory, University of Sydney	Amp; Neo
GFP-PWWP2A Δ IC	pIRESneo-eGFP-PWWP2A_ Δ IC; cloned via Gibson from pIRESneo-EGFP-PWWP2A plasmid	Ramona Spitzer and Martina Peritore, BMC	Amp; Neo
HA-MTA1	pcDNA3.1 expression vector backbone	Mackay laboratory, University of Sydney	Amp; Neo
HA-MTA2	pcDNA3.1 expression vector backbone	Mackay laboratory, University of Sydney	Amp; Neo
HA-RBBP7	pcDNA3.1 expression vector backbone	Mackay laboratory, University of Sydney	Amp; Neo

2.1.9 Buffers and solutions

Buffer	Components
Laemmli buffer (5x)	314 mM Tris 50% Glycerol (v/v) 5% SDS (v/v) 5% beta-Mercaptoethanol (v/v) 0.01% Bromphenol blue (w/v)
PBS (10x)	137 mM NaCl 2.7 mM KCl 10 mM Na ₂ HPO ₄ 2 mM KH ₂ PO ₄ adjust to pH 7.4 with HCl
TE	10 mM Tris

2. MATERIAL AND METHODS

	1 mM EDTA
Transfer buffer (Western Blot)	48 mM Tris-HCl 39 mM Glycine 0.0375% SDS (w/v) 20% Methanol (v/v)

2. MATERIAL AND METHODS

2.2 Cell biological methods

2.2.1 Cultivation and manipulation of mammalian cells

2.2.1.1 Cultivation, passaging, freezing and thawing of cells

HeLa Kyoto (HK) wild type cells were grown in Dulbecco's modified Eagle medium (DMEM) supplemented with 10% fetal calf serum (FCS) and 1% penicillin/streptomycin at 37°C and 5% CO₂ in a humidified incubator. In case of cultivating cell lines stably expressing GFP-tagged proteins, medium was additionally supplemented with 400 – 600 µg/ml G418-sulfate. When cells reached 80-90 % confluency, cells were usually passaged every second day in a 1:10 ratio into 10 cm dishes. After removal of old medium, cells were washed with 10 ml PBS and cells were dissociated by the addition of 1 ml trypsin/EDTA for 5 min at 37°C. 9 ml of fresh medium was added to stop the trypsin reaction, cells were resuspended and either partly discarded and replaced with fresh medium or seeded into new dishes. If cells were seeded into new dishes, the cell number was determined using the CASY cell counter. To store cells, trypsinized cells from a 10 cm dish were spun down for 5 min at 200 x g, resuspended in 1 ml normal medium + 10% DMSO, transferred into cryo vials and kept at -80°C or in liquid nitrogen for long term storage. To thaw cells, cryo vials were shortly incubated in a water bath (37°C), the cell suspension was resuspended in 9 ml medium and spun down for 5 min at 200 x g to remove DMSO and plated into a 10 cm dish.

EXPI293F™ suspension cells were cultured by our collaborators from the Mackay laboratory (University of Sydney) in Expi293™ Expression Medium.

Epitope tagged mouse embryonic stem cells (mESCs) were grown by our collaborator Dr. Thomas Burgold (Wellcome Trust-MRC, Cambridge) on 0.1% gelatin in 2i/LIF conditions.

2.2.1.2 Transfection of plasmid DNA

24h prior to transfection, 4×10^4 HK cells were seeded into in µ-slide 8-well glass bottom dishes containing 150 µl of medium when cells were used for Fluorescence Recovery After Photobleaching (FRAP) analyses while 2×10^7 HK cells were seeded into 150 cm plates when cells were subjected to Fluorescence-Activated Cell Sorting (FACS) experiments. For the transfection of cells growing in µ-slide 8-well glass bottom dishes, 100 ng of plasmid DNA was diluted in 10 µl of Opti-MEM and 0.3 µl X-tremeGENE transfection reagent was added and incubated for 15-30 min at room temperature (RT). For the transfection of cells growing in 150 cm plates, 20 µg of plasmid DNA was diluted in 1.5 ml of Opti-MEM and 60 µl of X-tremeGENE transfection reagent was added and likewise incubated.

2. MATERIAL AND METHODS

Afterwards, the transfection suspension was added dropwise onto the cells. After 48 h cells were subjected to FRAP or FACS.

Expi293F™ cells were transfected by our collaborators from the Mackay laboratory (University of Sydney) using polyethylenimine (PEI).

2.2.1.3 Transfection of small interfering RNAs (siRNAs)

One day prior to transfection 2×10^5 HK cells were seeded into a 6-well containing 2 ml of medium. 4 μ l Oligofectamine transfection reagent was added to 11 μ l Opti-MEM and incubated for 5 min at RT. 10 μ l of small interfering RNA (siRNA, for sequences see 2.1.7, table 2.5; 100 μ mol stock solution diluted 1:5 in sterile water) dilution was mixed with 175 μ l Opti-MEM. The oligofectamine mix was added to the siRNA mix and incubated for 20 min at RT. In the meantime, cells were washed twice with 2 ml of PBS, 800 μ l DMEM without FCS or antibiotics was added and the transfection mix was added drop wise. After incubating for 4 h at 37°C, 500 μ l DMEM containing 30% FCS was added. Usually, cells were harvested and processed 48 h after transfection. If cells were needed for immunofluorescence (IF), cells were transferred onto coverslips 24 h after transfection and fixed after 48 h. If cells were used for FRAP, one tenth of cells was transferred into μ -slide 8-well glass bottom dishes 24 h after transfection.

2.2.2 Immunofluorescence Microscopy

2.2.2.1 IF staining

48 h after transfection of siRNAs (see 2.2.1.3), coverslips with adherent HK cells were washed three times with 2 ml of PBS and cells were fixed for 10 min with 4% formaldehyde in PBS. The fixation solution was exchanged stepwise with PBST (PBS + 0.02% Tween 20). After this step, coverslips were stored at 4°C for several days or directly subjected to immunofluorescence staining. To permeabilize cells, coverslips were incubated for 15 min in 2 ml of PBS + 0.5% Triton X. After two washing steps with 2 ml of PBST, coverslips were incubated in blocking solution (2 % BSA in PBST) for 1 h. The coverslips were then incubated for 1 h with 50 μ l primary antibody solution (antibody diluted in blocking solution) on parafilm in a dark humidified chamber. Next, coverslips were washed four times with 2 ml of PBST and incubated for 45 min with 50 μ l secondary antibody solution on parafilm in a dark humidified chamber. Coverslips were washed two times with 2 ml of PBST and DNA was counterstained with 200 ng/ml DAPI in 2 ml of PBST for 6 min in the dark. Finally, coverslips were

2. MATERIAL AND METHODS

washed two times with 2 ml of PBS, briefly rinsed with ddH₂O, mounted on slide with a few drops of VECTASHIELD® and carefully sealed with nail polish.

2.2.2.2 Metaphase Spreads Preparation and Staining

Metaphase spreads were prepared as previously described [234] with a few adjustments. Usually, confluent cells growing in 6-well plates (approximately 8×10^6 cells) were used. To arrest cells in metaphase, cells were incubated with 0.1 µg/ml colcemid for 3 h prior to harvest. Cells were gently washed off with medium, collected in a 50 ml falcon, shortly spun down and placed on ice. 1 ml of ice-cold 75 mM KCl was added dropwise and mixed with the pellet. The suspension was incubated for 20 min at 37 °C and then directly put back on ice. 0.1 % Tween20 was added to the suspension and 400 µl of cell suspension were spread at 1600 rpm for 8 min at medium acceleration using a Shandon cytospin 4. Slides were transferred into a Coplin Jar filled with 35 ml of KCM and incubated for 20 min followed by blocking in 35 ml of blocking solution (KCM + 2% BSA) for 1 h. 50 µl of primary antibody solution (antibody diluted in blocking solution) was pipetted directly onto the slide, covered with a piece of parafilm and incubated in a dark humidified chamber for 1 h. Slides were washed three times in 35 ml of KCM and secondary antibody solution was likewise incubated. After washing three times in 35 ml of KCM, slides were fixed with 35 ml of 4% formaldehyde in KCM for 10 min. Slides were washed two times in 35 ml of KCM and DNA was counterstained with 500 ng/ml DAPI diluted in 35 ml KCM followed by one short washing with 35 ml of KCM. A coverslip was mounted onto the slide using a few drops of VECTASHIELD® and sealed with nail polish.

KCM: 120 mM KCl
20 mM NaCl
10 mM Tris pH 8.0
0.5 mM EDTA

2.2.3 Confocal Microscopy

Single optical sections or z-stacks of optical sections were collected using SP5, SP5 II or a SP8 (Leica) confocal microscopes equipped with Plan Apo 63x/1.4 NA oil or Plan Apo CS 63x/1.3 NA glycerol immersion objectives and lasers with excitation lines 405, 488, 543 and 594 nm. Laser intensities were adjusted using the acousto-optical tunable filters (AOTFs). Photomultiplier tubes (PMTs) were used in sequential mode and a smart gain of 600 – 800V. Images were processed using Fiji/ImageJ or Adobe Photoshop CS5.

2. MATERIAL AND METHODS

2.2.4 Fluorescence Recovery After Photobleaching (FRAP) and live cell imaging

After transfection and seeding of cells into μ -slide 8-well glass bottom dishes, live cell imaging and FRAP experiments were essentially performed as described before [235] using an UltraVIEW VoX spinning disc microscope with integrated FRAP PhotoKinesis accessory (PerkinElmer) assembled to an Axio Observer D1 inverted stand (Zeiss) and using a 63x or 100x/1.4 NA Plan-Apochromat oil immersion objective. The microscope was equipped with a heated environmental chamber set to 37°C and 5% CO₂. Fluorophores were excited with 488 nm solid-state diode laser line. Microscopy of living cells and image analysis were supervised by Dr. Yolanda Markaki (LMU Biocenter, Munich). FRAP analyses were performed by our collaborator Susanne Leidescher (LMU Biocenter, Munich). Confocal image series were typically recorded with 14-bit image depth, a frame size of 512 × 512 pixels, a pixel size of 68.5 nm and with time intervals of 154 ms. For photobleaching experiments, the bleach regions, typically with a length of 8–10 μ m, were chosen to cover the anterior half of the oval-shaped nucleus. Photobleaching was performed using two iterations with the acousto-optical tunable filter (AOTF) of the 488 nm laser line set to 100% transmission. Typically, 20 prebleach frames were recorded at maximum speed (197 ms). Postbleach frames were recorded as follows: 150 images at maximum speed and 180 images at a rate of 1 frame per second for each series. Data correction, normalization and quantitative evaluations were performed by automated processing with ImageJ using a set of self-developed macros followed by calculations in Excel. In long-term imaging experiments, a z-stack of 10.8–14.4 μ m with a step size of 1.2 μ m was recorded every 20 min for up to 24 h. To avoid photodamage of the cells, the AOTF of the laser was set to low transmission values of 6–10%. Image analysis was performed by automated processing with Fiji using a set of macros developed by Dr. Katrin Schneider (LMU Biocenter, Munich).

2.2.5 Fluorescence-Activated Cell Sorting (FACS)

Fluorescence-Activated Cell Sorting was carried out together with Dr. Martha Smets (LMU Biocenter, Munich). Two days after transfection of HK cells stably expressing GFP-H2A.Z.1 with Ch-PWWP2A, cells were sorted using a FACS Aria II according to their level of Ch-expression. Accordingly, 4×10^6 cells with low or high expression of Ch-PWWP2A were sorted in separate tubes and subsequently used for nChIP experiments (see 2.3.5).

2. MATERIAL AND METHODS

2.3 Biochemical methods

2.3.1 SDS polyacrylamide gel electrophoresis (SDS-PAGE)

Proteins were separated usually using precast 4-20% gradients gels from Serva via SDS-polyacrylamide gel electrophoresis (SDS-PAGE). To determine protein molecular weights, pEqGOLD protein marker IV and V were additionally loaded onto gels. Prior to loading, samples were boiled in Laemmli buffer. Gels were run at 150 – 180 V until the dye front had run out of the gel. Typically, gels were immediately used for immunoblotting.

2.3.2 Immunoblotting

Polyacrylamide gels were blotted onto a nitrocellulose membrane using a semidry blotting system. The polyacrylamide gel, a nitrocellulose membrane and four Whatman paper were shortly soaked in transfer buffer and assembled as a blotting sandwich with two Whatman paper, the membrane, the gel and Whatman paper. Proteins were transferred from the gel to the membrane for one hour at 250 mA or 300 mA in case more than one sandwich was blotted. The membrane was blocked for one hour in 10 ml of blocking buffer (5% milk powder PBST (PBS + 0.1% Tween20)) and subsequently incubated with the primary antibody diluted in blocking buffer ON at 4°C. The membrane was washed three times with 10 ml PBST and incubated with the secondary antibody diluted in blocking buffer for one hour at RT. After three washing steps with 10 ml of PBST, membranes were imaged and developed using the Chemidoc or X-ray films and a developing machine if HRP-conjugated secondary antibodies and ECL detection reagent were used or the LICOR system if fluorescent secondary antibodies were applied.

2.3.3 Preparation of cell lysates

To prepare whole cell lysates, 2×10^6 freshly harvested HK cells were resuspended in 200 μ l 5x Laemmli and boiled for 10 min at 95°C.

2.3.4 Preparation of mononucleosomes

The isolation of mononucleosomes was initially described by [236] and can be scaled down according to the cell number. Typically, 4×10^7 HK cells were harvested and washed once with PBS. Cells were resuspended and permeabilized with 5 ml PBS + 0.3% Triton X-100 + protease inhibitors (PI) for 10

2. MATERIAL AND METHODS

min at 4°C under rotation. Nuclei were pelleted for 5 min at 3.000 x g and washed once with 5 ml PBS + PI. Next, nuclei were resuspended in 500 µl EX100 buffer and transferred to a low-binding tube. CaCl₂ concentration was adjusted to 2 mM and 1.5 U micrococcal nuclease (MNase) was added and incubated for 20 min at 26°C. Samples were placed on ice and the addition of EGTA to a final concentration of 10 mM terminated the digestion. Subsequently, samples were centrifuged at 14.000 x g for 30 min at 4°C. The supernatant (S1) almost exclusively contains the mononucleosome fraction that was used for further experiments.

EX100: 10 mM HEPES pH 7.6

100 mM NaCl

1.5 mM MgCl₂

0.5 mM EGTA

10% Glycerol

10 mM β-Glycerol phosphate

add prior to use:

1 mM DTT

1x PI

2.3.5 Native chromatin immunoprecipitation (nChIP)

S1 mononucleosomes (see 2.3.4) isolated from 5 x 10⁶ HK cells or stably expressing GFP-tagged proteins and/or subjected to PWWP2A or control siRNAs were used per nChIP. After washing with PBS, cells were resuspended and permeabilized with 500 µl PBS + 0.3% Triton X-100 + PI for 10 min at 4°C under rotation. Nuclei were pelleted for 5 min at 3.000 x g and washed once with 500 µl PBS + PI. Next, nuclei were resuspended in 50 µl EX100 buffer and transferred to a low-binding tube. CaCl₂ concentration was adjusted to 2 mM and 1.5 U micrococcal MNase was added and incubated for 20 min at 26°C. Samples were placed on ice and the addition of EGTA to a final concentration of 10 mM terminated the digestion. Subsequently, samples were centrifuged at 14.000 x g for 30 min at 4°C and the supernatant was transferred to a fresh tube. The supernatant (S1) almost exclusively contains the mononucleosome fraction that was used for further experimental steps. 5 µl from the S1 suspension was kept as an input and 455 µl EX100 was added to the remaining 45 µl of S1. Depending on the nChIP, either 15 µl magnetic Dynabeads Protein G were precoupled for 2.5 h with 2 µg anti-H3K27ac or anti-H2A.Zac antibodies or, for GFP-tagged proteins, 15 µl GFP-Trap® beads were equilibrated and incubated with mononucleosomes ON at 4°C under rotation. Beads-only IP served as negative control. Beads were washed twice with 1 ml of WB1, twice with 1 ml of WB2, once with 1 ml of TE + 0.2% Triton-X and once with 1 ml of TE buffers. Beads were then incubated in 100 µl TE, 3 µl 10% SDS and 5 µl of 20 mg/ml proteinase K for 1 h at 65 °C. After magnetic separation,

2. MATERIAL AND METHODS

the supernatant was transferred to a fresh tube. Next, beads were resuspended in 100 μ l TE + 0.5 M NaCl, magnetically separated and the supernatant was added to the first supernatant. DNA was isolated using a standard Phenol/chlorophorm/isoamylalcohol extraction and ethanol precipitation protocol. Subsequently, the DNA pellet after IP and the input DNA pellet were resuspended in 12 μ l or in 32 μ l 10 mM Tris-HCl (pH 7.5), respectively. DNA was either used for nChIP-qPCR (see 2.4.5) or subjected to library preparation if nChIP-seq (see 2.4.4) was applied.

WB1: 10 mM Tris-HCl, pH 7.5
1 mM EDTA
0.1% SDS
0.1% sodiumdeoxycholate
1% TritonX-100

WB2: 10 mM Tris-HCl, pH 7.5
150 mM NaCl
1 mM EDTA
0.1% SDS
0.1% sodiumdeoxycholate
1% Triton X-100

2.3.6 Native chromatin immunoprecipitation followed by quantitative label-free mass spectrometry (nChIP-MS)

S1 mononucleosomes (see 2.3.4) isolated from 4×10^7 HK cells stably expressing GFP or GFP-PWWP2A were used for nChIP-MS. nChIP were essentially performed as described before [120] with a few adjustments. 40 μ l of GFP-Trap[®] beads were added to the pooled S1 mononucleosome fractions from 8×10^7 cells and incubated for 2.5 h at 4°C. IPs were carried out in triplicates and washed using the wash buffers WB1 and WB2 but without the addition of detergents. Samples were subsequently prepared for and analysed by label-free quantitative mass spectrometry by our collaborator Dr. Eva Keilhauer (MPI of Biochemistry, Martinsried) as described previously [120]. Briefly, samples were prepared for on-beads tryptic digestion by incubating the beads with buffer E1 (50 mM Tris pH 7.5, 2 M Urea, 1 mM EDTA) for 20 min at 25 °C. The supernatant was transferred to a fresh low-binding tube and beads were resuspended in buffer E2 (50 mM Tris pH 7.5, 2 M Urea, 5 mM CAA). Subsequently, trypsin was added to a final concentration of 5 μ g/ml and incubated for 1 h at 25°C while shaking at 500 rpm. The supernatants were pooled and incubated ON at RT. StageTips were loaded with tryptic peptides and subjected to LC-MS/MS analysis. Peptides were analyzed by reversed-phase liquid chromatography on an EASY-nLC 1000 or 1200 system coupled to a Q Exactive plus or HF mass spectrometer.

2. MATERIAL AND METHODS

2.3.7 Immunoprecipitation of MTA paralogues and MBD3 or recombinant PWWP2A

Nuclear extracts from mESCs followed by immunoprecipitation of MTA1 and MBD3 was performed by our collaborator Dr. Thomas Burgold (Wellcome Trust-MRC, Cambridge) according to a modified version of previously described procedures [232, 237].

Immunoprecipitation of recombinant FLAG-PWWP2A were performed by our collaborators from the Mackay laboratory (University of Sydney) using lysates from EXPI293F™ and standard FLAG affinity pull downs.

2.3.8 Acid extraction of histones

After harvest of $1 - 2 \times 10^6$ cells, cell pellets were washed with 1 ml PBS and resuspended in 1 ml ice-cold hypotonic lysis buffer. Subsequently, samples were incubated for 30 min under rotation at 4 °C to promote hypotonic swelling of cells and lysis by mechanical shearing. Intact nuclei were pelleted at 10.000 x g for 10 min at 4 °C, resuspended in 400 µl 0.4 N H₂SO₄ and incubated under rotation for at least 30 min at 4 °C. To remove nuclear debris, samples were spun down at 16.000 x g for 10 min at 4 °C and the supernatants were transferred into a fresh tube. To precipitate the histones, 132 µl 100% TCA was added dropwise, the tube was inverted several times and incubated on ice ON. Extracted histones were pelleted at 16.000 x g for 10 min at 4 °C, the supernatant was carefully removed, and the cloudy histone pellet was washed twice with 500 µl ice-cold acetone without disturbing the histone pellet. Then, the histone pellet was air-dried for 20 min at RT. The histone pellet, which appears as a smear-like pellet on the tube wall, was dissolved in 50 µl of sterile water and transferred into a fresh 1.5-ml tube. Histones were stored at -20 °C. To run on a SDS-PAGE gel, 2 µl of 5x Laemmli were added to 5 µl of extracted histones and boiled for 10 min at 95°C.

Hypotonic lysis buffer: 10 mM Tris pH 8.0
1 mM KCl
1.5 mM MgCl₂
add prior to use:
1 mM DTT
0.4 mM PMSF
1x PI

2. MATERIAL AND METHODS

2.4 Molecular biological methods

2.4.1 RNA extraction

Total RNA from 2×10^6 cells HK cells was isolated using the RNeasy Mini Kit according the manufacturer's instructions. The quality of the RNA was determined using a Nanodrop ND1000 spectrophotometer. RNA was stored at -80°C .

2.4.2 cDNA synthesis

1 μg of total RNA was reverse transcribed utilizing the NEB ProtoScript M-MuLV First Strand cDNA Synthesis Kit according the manufacturer's instructions. A sample without reverse transcriptase served as control. Typically, a GAPDH-specific PCR was run to verify faithful cDNA preparation.

2.4.3 Quantification of mRNA levels with quantitative PCR (qPCR)

To investigate changes in gene expression upon PWWP2A knockdown, qPCR was applied on cDNA. qPCR was performed on a LightCycler[®] 480 Instrument II using Fast SYBR Green Master Mix. Primers were designed using the Primer3 tool and were *BLASTed* to ensure specificity (see 2.1.7, table 2.4). PCR efficiency and primer pair specificity were examined using a standard curve of serially diluted cDNA and melting curve, respectively. Samples were analyzed in technical triplicates with a total reaction volume of 15 μl . 10 μl of a premix containing 1.5 μl of a forward and reverse primer mix (128 μl ddH₂O + 4 μl of each primer), 7.5 μl Fast SYBR Green Master Mix and 1 μl of ddH₂O were first added to a well of the 384-well plate. Then a premix of 0.2 μl cDNA plus 4.8 μl ddH₂O was added. After sealing with self-adhesive foil, the plate was shortly centrifuged, loaded into the LightCycler[®] and the following program was run:

Table 2.6: PCR program

step	temperature	duration	
preincubation	95°C	20 sec	
amplification	95°C	3 sec	} repeat 45 x
	60°C	20 sec	
melting curve	5°C/min		

Resulting CT (cycle threshold) values were normalized to the transcript level of HPRT1 (hypoxanthine phosphoribosyltransferase 1) and further analyzed based on the $2^{-\Delta\Delta\text{CT}}$ method. To incorporate the

2. MATERIAL AND METHODS

standard error of the mean (SEM) of the $\Delta\Delta\text{CT}$ values into the fold-difference, the range of the error bars were calculated as $2^{-\Delta\Delta\text{CT}+\text{SEM}}$ and $2^{-\Delta\Delta\text{CT}-\text{SEM}}$.

2.4.4 Preparation of libraries for nChIP-seq

Prior to nChIP-seq library preparation, quality of nChIP samples was assured. Therefore, DNA concentrations were determined using the Qubit dsDNA HS Kit and DNA size was monitored using the Bioanalyzer and a DNA 1000 Kit. Illumina Sequencing libraries were established with the MicroPlex Library Preparation Kit following the manufacturer's instructions. The number of amplification cycles was scaled according to the amount of input material and amplification was validated by determination of DNA concentrations using the Qubit dsDNA HS Kit. Quality of purified libraries was assessed using the Bioanalyzer and a DNA 1000 Kit. Sequencing was performed on the Illumina 1500 platform using the TruSeq Rapid SR Cluster Kit-HS (Illumina) and single read 50 nucleotide sequencing on a HiSeq Rapid SR Flow Cell (Illumina) by Dr. Stefan Krebs (Laboratory of Functional Genome Analysis, LAFUGA, Munich) or Dr. Andrea Nist (Genomics Core Facility, Philipps-University Marburg). Bioinformatic data analyses were performed by our collaborators Dr. Tobias Straub (Bioinformatics Core Unit, BMC, Munich) and Dr. Marek Bartkuhn (Institute for Genetics, JLU, Giessen).

2.4.5 Validation of nChIP-sequencing results with quantitative PCR (nChIP-qPCR)

To investigate GFP-H2A.Z.1 occupancy after PWWP2A depletion or overexpression as well as to validate H3K27ac and H2A.Zac nChIP-seq results, nChIP-qPCR was conducted. qPCR was performed as described in 2.4.3. with the following exceptions. Primer pairs were described and established before [121] or designed using the Integrated Genome Browser software (BioViz) and Primer3 tool and were *BLASTed* to ensure specificity (see 2.1.7, table 2.3). Instead of 0.2 μl cDNA, 0.15 μl DNA was used. Data were analyzed according to the percent input method.

2.4.6 Assay for Transposase Accessible Chromatin with high-throughput sequencing (ATAC-seq)

ATAC-seq was performed using 50.000 HK cells subjected to PWWP2A or control siRNAs as described before [238]. In brief, cells were harvested and washed once with 50 μl PBS + PI. Centrifugation steps were carried out at 500 x g for 5 min at 4°C. Cell pellets were resuspended in 50 μl transposase mixture of the Nextera DNA Library Preparation Kit and incubated at 37°C for 30 min under agitation.

2. MATERIAL AND METHODS

Transposed DNA was purified using a MinElute PCR Purification Kit and eluted in 10 µl elution buffer (10 mM Tris-HCl, pH 8). Transposed DNA fragments were amplified according to the following conditions:

Table 2.7: Pipetting scheme

component	µl for one reaction
Transposed DNA	10 µl
forward primer [25 µM]	2.5 µl
reverse primer [25 µM]	2.5 µl
NEBNext 2 x PCR Master Mix	10 µl
Nuclease-free H ₂ O	10 µl

Table 2.8: PCR program

temperature	duration	
72°C	5 min	
98°C	30 sec	} repeat 4 x
98°C	10 sec	
63°C	30 sec	
72°C	1 min	
4°C	-	

After 4 cycles of PCR amplification, a qPCR side reaction was set up to monitor the PCR amplification prior to saturation via the LightCycler®:

Table 2.9: Pipetting scheme

component	µl for one reaction
PCR-amplified DNA	5 µl
forward primer [25 µM]	0.25 µl
reverse primer [25 µM]	0.25 µl
SensiMix SYBR 2x PCR Master Mix	7.5 µl
Nuclease-free H ₂ O	2 µl

Table 2.10: PCR program

temperature	duration	
95°C	10 min	
98°C	10 sec	} repeat 19 x
63°C	30 sec	
72°C	1 min	
4°C	-	

The additional number of cycles needed for the remaining 45 µl PCR reaction was determined by calculating the number of cycles that corresponds to ¼ of the maximal reached fluorescence. The

2. MATERIAL AND METHODS

amplified library was size-selected to enrich for fragments < 600 bp and purified using AMPure XP beads. Quality of libraries were assessed using the Bioanalyzer and a DNA HS Kit. ATAC libraries were sequenced using the Illumina Hiseq 1500 platform.

Transposase mixture: 25 µl 2x TD buffer
2.5 µl TDE1
0.25 µl 2% digitonin
22.25 µl nuclease-free water

2.5 Bioinformatics

2.5.1 nChIP-seq analysis

2.5.1.1 nChIP-seq analysis of GFP-H2A.Z.1

Analysis of nChIP-seq data concerning GFP-H2A.Z was carried out by our collaborator Dr. Tobias Straub (Bioinformatics Core Unit, BMC, Munich) [121].

Raw sequencing reads were mapped to the human genome (hg19) using bowtie (version 0.12.9) omitting reads with more than one match. Coverage vectors were created after read extension to 150 bp corresponding to the expected fragment size after MNase digestion. Peak calling was performed on the pooled replicates of each target against the pooled input chromatin libraries using Homer (v4.7) applying parameters `-style histone`, `-fragLength 150` and `-inputFragLength 150`. Cumulative plots were obtained by averaging the signals across all genes.

2.5.1.2 nChIP-seq analysis of H3K27ac and H2A.Zac

Analysis of nChIP-seq data concerning H3K27ac and H2A.Zac was executed by our collaborator Dr. Marek Bartkuhn (Institute for Genetics, JLU, Giessen) [228].

Image analysis and base calling were performed using the Illumina pipeline v 1.8 (Illumina Inc.). Public ChIP-seq data from additional histone modifications (H3K4me1, H3K4me3, H3K27ac, H3K27me3 and H3K36me3) was downloaded from ENCODE. Raw sequencing reads were mapped to the human genome (hg19) using bowtie (1.1.2) with parameters `-k` and `-m` set as 153. PCR duplicates were removed with samtools rmdup function. Coverage vectors were generated after read extension to 150 bp corresponding to the expected fragment size after MNase digestion using Deeptools bamCoverage function normalizing to 1x sequencing depth (`--normalizeTo1x` option) [239]. Peak calling was done using MACS2 version 2.1.155. with default settings. Cumulative coverage plots and heatmaps were generated with deeptools computeMatrix and plotHeatmap functions. The Venn

2. MATERIAL AND METHODS

diagram (Figure 3.14) was generated as described in [240]. As gene models, UCSC hg19 gene models were downloaded from Illumina's iGenome repository. For collection of binding data around meta-genes, 6 kb up- and downstream regions were collected as 50-bp bins and gene bodies were represented by 120 bins of variable size. Differential binding analysis was done using csaw57 and validated by a custom analysis pipeline. For csaw we binned the human genome into 100 bp bins with a step size of 300 bp. Normalization was performed by extraction of scaling factors based on 10 kb bins basically normalizing for total read count. Differentially regulated bins were selected as those bins with a p-value < 0.001. For representation of significantly changed regions in heatmaps we merged neighboring significantly changed bins by a sliding window approach (width: 2 kb). In an alternative approach, we calculated the peaks overlapping between control treatments as well as those overlapping between RNAi treatments. Peaks were combined and overlapping peaks were merged into single features spanning the original features' intervals. Read counts overlapping these intervals were determined for the 4 experimental conditions (untreated, Luci siRNA, PWWP2A siRNA 1 and 2) and DESeq2 was used for normalization as well as for the identification of differentially bound peak intervals [241]. In order to assign chromatin states, publicly available H3K4me1/3, H3K27ac, H3K27me3 and H3K36me3 data from HeLa cells generated by the ENCODE consortium were used [205]. The human genome was discretized into 1 kb bins and trained a 10-state HMM using the ChromHMM application using default parameters [19]. All downstream analysis was done in R/BioConductor [242]. Genome browser snap shots were generated using the Gviz package [243]. Manipulation of sequencing reads was done using Rsamtools and genomic intervals were represented as GenomicRanges objects [244]. The analysis of the association between peak intervals and known genomic annotation feature were done using the CHIPseeker package [245] with default setting using the UCSC hg19 gene definitions. As statistical tests, Wilcoxon rank sum tests were performed.

2.5.2 nChIP-MS analysis

nChIP-MS data were analyzed by our collaborator Dr. Eva Keilhauer (MPI of Biochemistry, Martinsried). MS raw data were processed using the MaxQuant software version 1.4.3.13 [246]. Fragmentation spectra were searched against a human sequence database obtained from Uniprot in May 2013 and a file containing frequently observed contaminants such as human keratins. Cysteine carbamidomethylation was set as a fixed modification; N-terminal acetylation and methionine oxidation were set as variable modifications. Trypsin was chosen as specific enzyme, with 2 maximum missed cleavages allowed. Peptide and protein identifications were filtered at a 1% FDR.

2. MATERIAL AND METHODS

Label-free quantification was performed using the MaxLFQ algorithm [247] integrated into MaxQuant. The match between runs option was enabled with a matching time window of 0.5 min and an alignment time window of 20 min. All other parameters were left at standard settings. MaxQuant output tables were analyzed in Perseus [248] version 1.5.8.6 as follows: After deleting proteins only identified with modified peptides, hits to the reverse database, contaminants and proteins with one or less razor and unique peptides, label-free intensities were log₂ transformed. Next, proteins were required to have 3 valid values in at least one triplicate, then remaining missing values in the data matrix were imputed with values representing a normal distribution around the detection limit of the mass spectrometer. Now a two-sample t-test was performed to identify proteins enriched in the PWWP2A pull-downs compared input control. Only those proteins were kept for further analysis. Significant outliers were determined using a permutation-based FDR. The S0 and FDR parameters were set to 0.5 and 0.05, respectively.

2.5.3 ATAC-seq analysis

Analysis of ATAC-seq data was performed by our collaborator Dr. Marek Bartkuhn (Institute for Genetics, JLU, Giessen). ATAC-seq reads were quality controlled with fastqc (<https://www.bioinformatics.babraham.ac.uk/projects/fastqc/>). Trimming of low quality reads and adaptor removal was done using Trim Galore! (https://www.bioinformatics.babraham.ac.uk/projects/trim_galore/) with default settings. Reads were aligned against the UCSC version of the human genome (hg19) downloaded from Illumina's iGenome repository (http://emea.support.illumina.com/sequencing/sequencing_software/igenome.html?langsel=/de/#) using Bowtie2 [249]. Samtools were used for filtering and conversion to BAM format (-uq 10 -F 4) [250]. Subsequently, Picard tools *SortSam* and *MarkDuplicates* were used for sorting of BAM files and removal of duplicated reads.

Downstream processing was done in R (<https://www.r-project.org>) using BioConductor [242] packages and custom R code. For differential ATAC-seq analysis we used the *csaw* package [251]. For this, the genome was binned into 100 bp bins with a 300 bp spacing between bins. Reads were extended to 200 bp. Bins were filtered for abundance, such that we expected a 4-fold difference as compared to global background for a bin to be considered as containing an ATAC-seq signal. For each bin, we calculated the log₂-transformed fold change when comparing specific siRNA and control treatment. In order to study the relationship between chromatin availability as measured by ATAC-seq and H3K27ac changes occurring after knock-down of PWWP2A, we selected bins significantly changed for H3K27ac and extracted the corresponding log₂-fold changes observed in the same

2. MATERIAL AND METHODS

contrast for the ATAC-seq signals. Differences between background bins and bins associated with significant H3K27ac changes (p-value < 0.01) were tested using Wilcoxon rank sum test using R's *wilcox.test* function (with option *alternative* set as "greater").

3. RESULTS

Parts of this section of the Ph.D. thesis are published in the following manuscripts:

Pünzeler, S., **Link, S.**, Wagner, G., Keilhauer, E.C., Kronbeck, N., Spitzer, R.M., Leidescher, S., Markaki, Y., Mentele, E., Regnard, C., *et al.* (2017). Multivalent binding of PWWP2A to H2A.Z regulates mitosis and neural crest differentiation. *The EMBO journal*, 36(15), 2263–2279.

Link, S., Spitzer, R.M., Sana, M., Torrado, M., Völker-Albert, M., Keilhauer, E.C., Burgold, T., Pünzeler, S., Low, J., *et al.* (2018). PWWP2A binds distinct chromatin moieties and interacts with an MTA1-specific core NuRD complex. *Nature Communications*, 9, 4300.

3.1 PWWP2A mediates mitosis progression

The RNAi-mediated knockdown of PWWP2A not only leads to the deregulation of ~ 600 genes, but also to decelerated cell proliferation and enlarged nuclei in HK cells in comparison to control cells as determined by Dr. Sebastian Pünzeler, a previous member from the Hake group. Using FACS analysis as well as H3S10ph immunofluorescence staining, he could further show that the depletion of PWWP2A resulted in an accumulation of cells in mitotic prometaphase [121].

To gain deeper insights into the cellular processes upon PWWP2A depletion, I employed live-cell imaging under the supervision of Dr. Yolanda Markaki (LMU Biocenter, Munich). Therefore, HK cells stably expressing GFP-H2A [118] were transfected with Luciferase-specific (Luci, control) or PWWP2A-specific (PW#1, PW#2) siRNAs. Two days after knockdown of PWWP2A, stacks of cells were acquired every 20 minutes for up to 24 hours. While control cells (wt, Luci) traversed through mitosis within less than two hours, cells treated with PWWP2A-specific siRNAs needed up to 20 hours to successfully complete mitosis (Figure 3.1 A). Strikingly, depletion of PWWP2A caused cells to repeatedly shuffle back and forth between prometaphase and metaphase. Cells were unable to properly align all chromosomes at the equatorial plate during metaphase and chromatin generally appeared more condensed indicated by brighter GFP-H2A signal upon PWWP2A depletion. Of note is that while some cells were able to escape mitotic arrest and proceed to anaphase to complete mitosis, some cells accomplished cytokinesis without previous sister chromatid segregation but formed micronuclei and some cells underwent apoptosis (Figure 3.1 B).

3. RESULTS

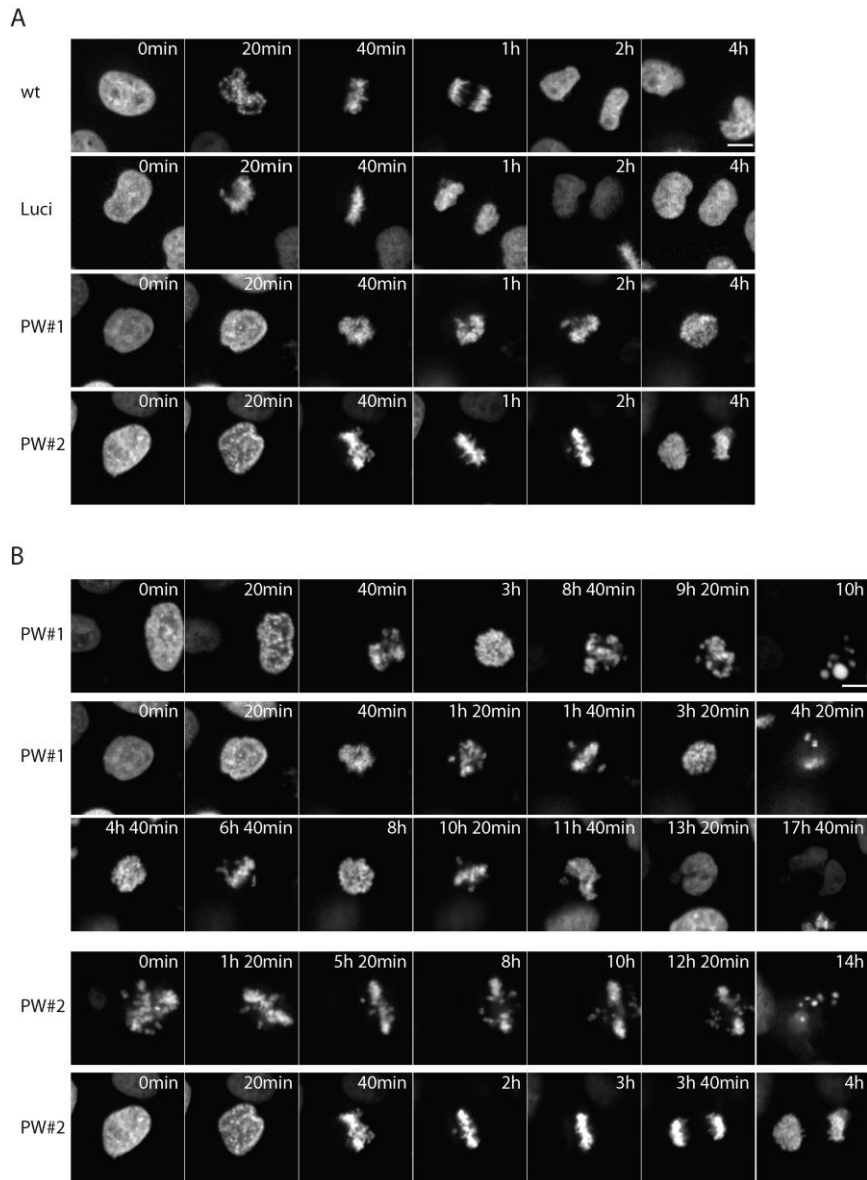


Figure 3.1 PWWP2A is crucial for proper mitosis progression. Selected frames from live cell imaging series showing from HK cells stably expressing GFP-H2A for visualization of chromatin. Two days after control (wt, Luci) and PWWP2A (PW#1, PW#2) siRNA-mediated knockdown, cells were imaged for (A) four hours or (B) indicated duration exemplifying occurring phenotypes starting from nuclear breakdown at prophase. Scale bar = 10 μ m.

As it seemed as if chromosomes were either not aligning properly at equatorial plate and/or sister chromatids were futilely pulled away from the equatorial plate, I next investigated whether tubulin fibers were successfully formed and attached to the centromeres. After PWWP2A depletion, cells were fixed, stained with an α -tubulin-specific antibody and confocal stack images were obtained. Notably, tubulin fibres were formed but showed slightly abnormal morphology and appeared less directed in comparison to control stainings (Figure 3.2).

3. RESULTS

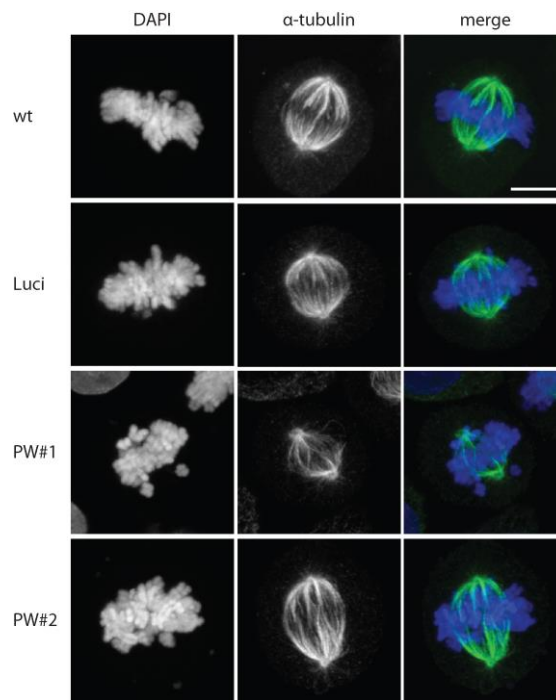


Figure 3.2 HK cells form morphologically slightly abnormal tubulin fibres upon PWWP2A knockdown. Representative z-projections of confocal images of mitotic metaphases from HK cells. Two days after control (wt, Luci) and PWWP2A (PW#1, PW#2) siRNA-mediated knockdowns, HK cells were fixed and stained with an α -tubulin-specific (green) antibody. DNA was counterstained with DAPI (blue). Scale bar = 10 μ m.

Interestingly, the observed mitotic phenotype strongly copies the previously described mitotic defects in chicken cells upon H2A.Z knockout that is mechanistically not understood [141]. Mitosis is a tightly regulated process mediated by sophisticated complexes such as chromosomal passenger complex (CPC), mitotic checkpoint complex (MCC), spindle assembly checkpoint (SAC) and anaphase-promoting complex (APC) with many factors involved [252-254]. Analysis of some of the factors involved in mitotic regulation by the CPC and SAC, such as the kinase Aurora B that phosphorylates H3S10 or the inner centromere protein (INCENP), did not show an altered distribution (Figure 3.3 A). Members of the SAC and MCC, such as mitotic arrest deficient 2 (MAD2) and budding uninhibited by benzimidazole-related 1 (BUBR1), and members of the APC, were likewise tested in immunofluorescence staining, but could not be corroborated due to antibody specificity limitations and reproducibility issues (data not shown). Moreover, also staining of posttranslational histone marks featuring a specific localization pattern during mitosis such as H3S10ph enrichment at chromosome ends and H2AT120ph at centromeres did not exhibit a difference in localization after PWWP2A depletion (Figure 3.3 B).

3. RESULTS

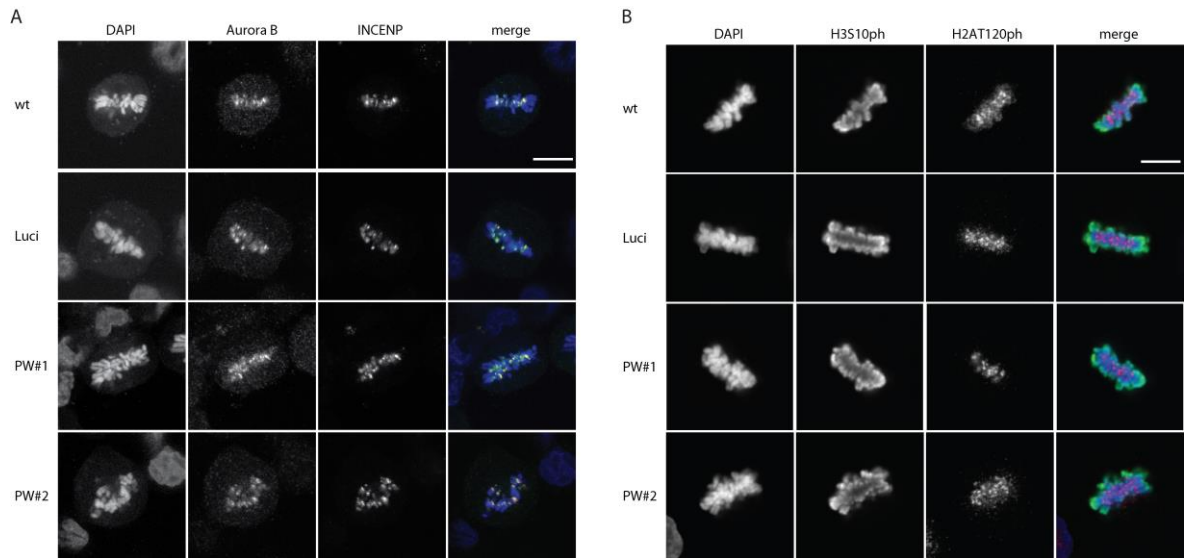


Figure 3.3 Localization of mitotic markers remain unchanged in HK cells after depletion of PWWP2A. Representative confocal images of mitotic HK cells. Two days after control (wt, Luci) and PWWP2A (PW#1, PW#2) depletion, HK cells were fixed and co-stained with (A) Aurora B (green) and INCENP (red) or (B) H3S10ph (green) and H2AT120ph (red) antibodies. DNA was counterstained with DAPI (blue). Scale bar = 10 μm .

3.2 PWWP2A indirectly influences mitosis

These results raised the question of how PWWP2A can influence mitosis. At least two different scenarios can be envisioned. First, PWWP2A fulfils a structural role in mitosis, implying that by localizing close to a structural component of a chromosome such as the kinetochore, PWWP2A could directly interfere with e.g. proper spindle attachment and PWWP2A's loss might impair the latter. Secondly, PWWP2A indirectly influences mitosis by regulating the expression of genes that are important for proper mitotic progression. To investigate whether PWWP2A has a structural role in mitosis, I specified PWWP2A's localization on chromosomes and performed metaphase spreads. Cells were transfected with siRNAs two days prior to harvest and arrested in metaphase using colcemid to enrich for the mitotic cell population. Extracted metaphase spreads were stained with anti-PWWP2A and anti-CENP-E, a microtubule binding kinetochore-associated protein [255], antibodies and DNA was counterstained with DAPI. Subsequently, confocal stack images were obtained. On metaphase chromosomes, PWWP2A localizes at distinct regions on both sister chromatids but does not co-localize with CENP-E nor localizes at the centromeric region in general (Figure 3.4). Interestingly, a loss of chromosome cohesion and/or a loss or sliding of CENP-E was observed for some of the chromosomes but only when treated with PW#1 siRNA. Hence, PWWP2A does not seem to be structurally involved in mitosis and it is thus unlikely that it directly regulates mitosis.

3. RESULTS

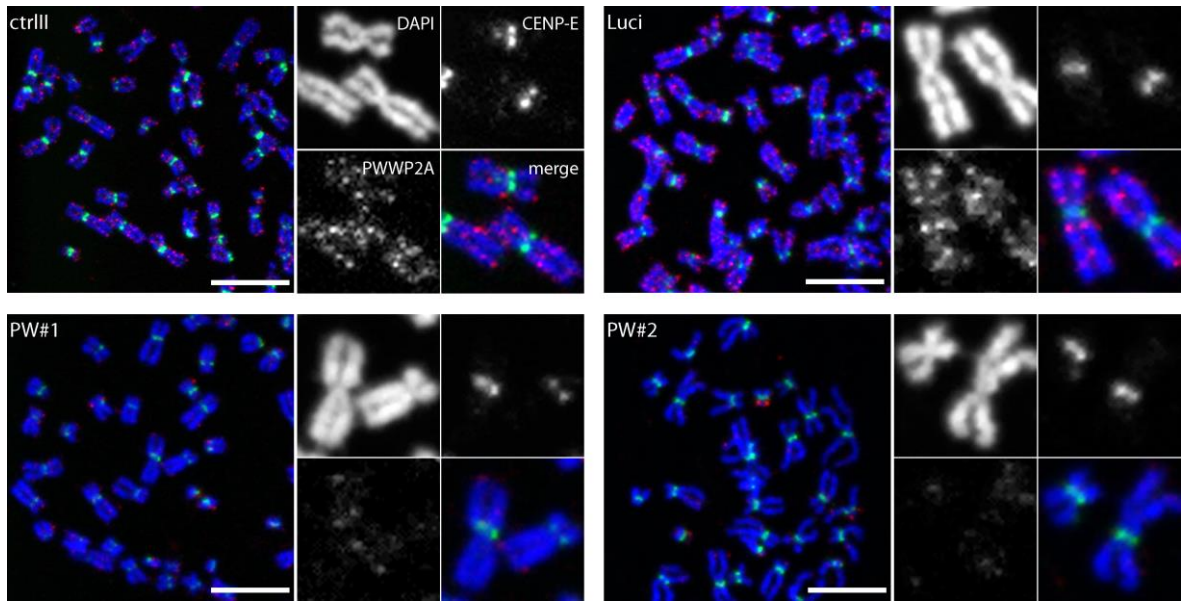


Figure 3.4 PWWP2A localizes at distinct regions on mitotic chromosomes. Representative z-projections of confocal images of chromosomes from HK cells. Two days after control (wt, Luci) and PWWP2A (PW#1, PW#2) depletion, chromosomes were co-stained with CENP-E- (green) and PWWP2A-specific (red) antibodies, fixed and DNA was counterstained with DAPI (blue). Scale bar = 10 μ m.

Subsequently, I set out to decipher whether PWWP2A influences mitosis indirectly. RNA-seq after knockdown of PWWP2A, previously carried out by Dr. Sebastian Pünzeler and Dr. Tobias Straub (Bioinformatics Core Unit, BMC, Munich), showed that \sim 600 genes were deregulated with many involved in the regulation of developmental processes, metabolism and cell morphogenesis according to gene ontology analysis [121]. Some of the most deregulated genes are involved in actin and tubulin regulation including F-actin-capping subunit alpha-1 protein (CAPZA1), tubulin polyglutamylase complex subunit 2 (TPGS2), phosphatidylinositol 3,4,5-trisphosphate-dependent Rac exchanger 1 (PREX1), vasodilator-stimulated phosphoprotein (VASP) and ANTXR Cell Adhesion Molecule 1 (ANTXR1). There is emerging evidence that actin not only plays a role in cell mobility and cytokinesis, but also during mitosis by spanning to the spindle poles and being involved in controlling spindle length and shape [256-258]. CAPZA1 regulates actin filament growth by capping the filaments' fast growing plus end [259]. As part of a large protein complex that adds polyglutamate chains to tubulin, TPGS2 promotes centrosome stability [260, 261]. PREX1 is involved in actin dynamics thereby influencing neuronal cell migration and elongation [262, 263]. VASP is part of the Ena-VASP protein family whose members are known to bind both globular (G) and filamentous (F) actin [264, 265]. There, VASP fulfils an anti-capping activity by promoting elongation of actin filaments [266]. ANTXR1 interacts with the actin cytoskeleton and mediates cell migration [267, 268]. Indeed, a downregulation of CAPZA1, TPGS2 and PREX1 as well as a slight upregulation of VASP and

3. RESULTS

ANTXR1 could be verified by RT-qPCR in three independent replicates (Figure 3.5 A). Furthermore, loss of PWWP2A also led to a decrease in CAPZA1 protein levels detected via immunoblotting but did not impair global F-actin protein levels (Figure 3.5 B).

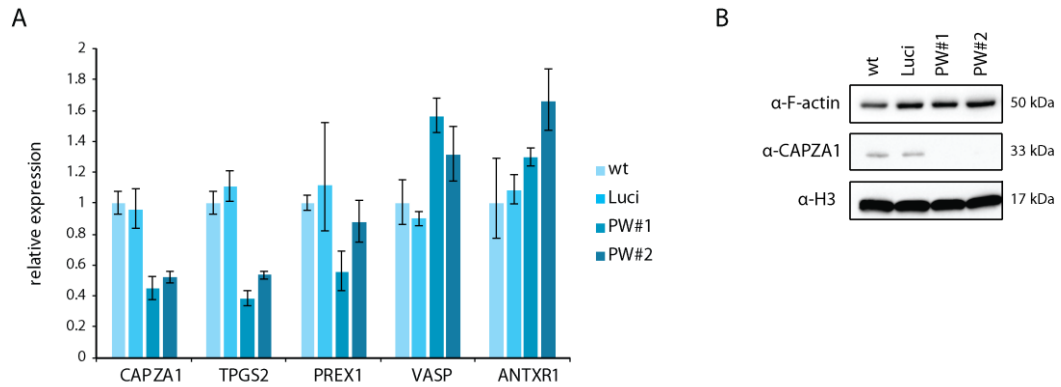


Figure 3.5 Knockdown of PWWP2A in HK cells leads to the deregulation of genes involved in tubulin- and actin-related processes. **A.** Relative expression levels of selected genes implicated in tubulin and actin regulation two days after control (wt, Luci) or PWWP2A (PW#1, PW#2) siRNA-mediated knockdown. Shown is the fold-change of three replicates compared to wt and normalized to HPRT expression. Error bars depict SEM (n=3). **B.** Representative immunoblot of F-actin and CAPZA1 after control (wt, Luci) or PWWP2A (PW#1, PW#2) siRNA-mediated knockdown. H3 served as loading control.

As genes involved in actin and tubulin regulation were deregulated and tubulin fibers exhibited altered morphology, I speculated whether actin filament morphology was also compromised by PWWP2A depletion although global F-actin levels remained unaffected. To this end, fixed HK cells were stained with a Phalloidin-conjugate, a reagent specifically binding F-actin, and overview confocal stack images were taken. Interestingly, knockdown of PWWP2A resulted in an altered appearance of actin filaments with thicker filaments and more stress fibers occurring (Figure 3.6). With both proteins influencing the capping activity at actin filaments, the downregulation of CAPZA1 as well as the upregulation of VASP upon PWWP2A loss thus may provide an explanation for the altered morphology of actin fibers.

3. RESULTS

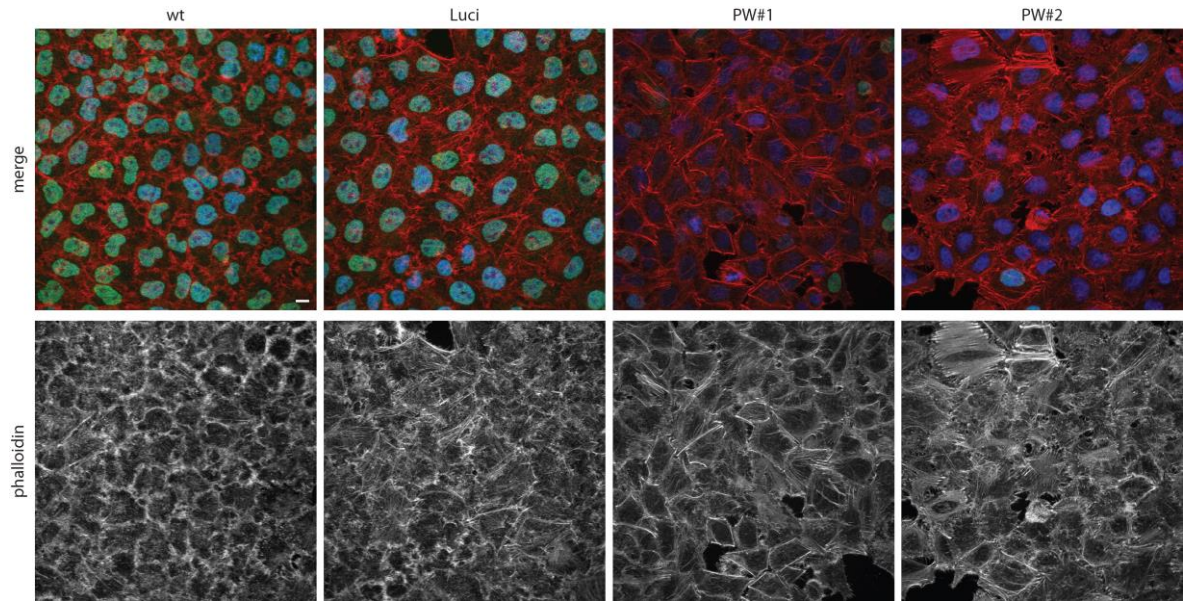


Figure 3.6 HK cells form morphologically altered actin filaments upon PWWP2A knockdown. Representative z-projections of confocal images of HK cells. Two days after control (wt, Luci) and PWWP2A (PW#1, PW#2) depletion, HK cells were fixed and co-stained with PWWP2A (green) and phalloidin (F-actin, red) and DNA was counterstained with DAPI (blue) (merge images, upper panel). Lower panel: Phalloidin staining from upper panel in grayscale. Scale bar = 10 μ m.

In summary, PWWP2A is involved in the regulation of mitotic progression. While it is unlikely that PWWP2A plays a direct role in mitosis it is probable that PWWP2A indirectly affects mitosis by regulating the expression of genes involved in processes that regulate proper distribution and function of actin and tubulin.

3.3 H2A.Z's chromatin association is unimpeded by PWWP2A

As the mitosis phenotype caused by loss of PWWP2A is similar to the phenotype observed after H2A.Z knockout in chicken cells [141], it was next investigated whether the phenotype upon PWWP2A depletion could be the result of changes in H2A.Z occupancy due to either defects in its chromatin binding ability or its deposition. First, to investigate whether PWWP2A influences H2A.Z's chromatin association, FRAP experiments in collaboration with Susanne Leidescher (LMU Biocenter, Munich) were performed. HK cells stably expressing GFP-H2A or GFP-H2A.Z.1 [118] were transfected with control (Luci) or PWWP2A specific siRNAs and subjected to FRAP. Interestingly, PWWP2A depletion did not alter the mobility of GFP-H2A nor of GFP-H2A.Z.1 and thus did not affect their chromatin binding ability (Figure 3.7).

3. RESULTS

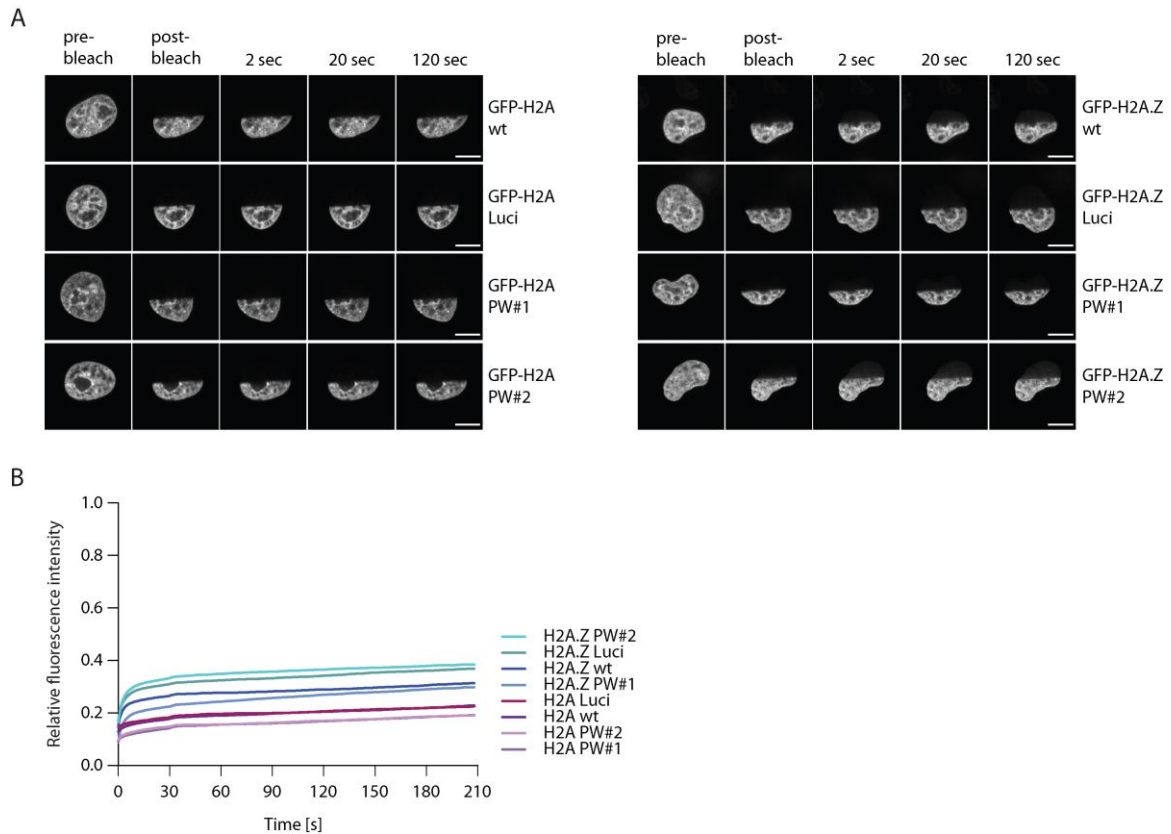


Figure 3.7 PWWP2A depletion does not influence H2A.Z's chromatin binding ability. (A) Representative confocal images before and after half-nucleus photobleaching of HK cells stably expressing GFP-H2A (H2A, left) or GFP-H2A.Z.1 (H2A.Z, right) two days after control (wt, Luci) or PWWP2A (PW#1, PW#2) knockdown. (B) FRAP quantification curves from (A) (n=9-19). Scale bar = 5 μ m.

Next, to assess whether PWWP2A is involved in the regulation of H2A.Z occupancy, GFP-H2A.Z.1 nChIP-seq upon PWWP2A knockdown, sequenced by Dr. Stefan Krebs (LAFUGA, Munich) and analyzed by Dr. Tobias Straub (Bioinformatics Core Unit, BMC, Munich), was carried out. Mononucleosomes isolated from HK cells stably expressing GFP-H2A.Z.1 and treated with control (wt, Luci) or PWWP2A-specific siRNAs (PW#1, PW#2) were precipitated using GFP-Trap® beads. Bound DNA was isolated, libraries prepared and subjected to sequencing. nChIP-seq analysis revealed only subtle, non-significant changes in H2A.Z peak heights and no effect on global H2A.Z occupancy (Figure 3.8 A-C). Notably, the observed reduction in peak heights was apparent on sites bound by PWWP2A as well as PWWP2A-unbound sites, arguing for a PWWP2A-unspecific effect (Figure 3.8 A+B). qPCR analyses of selected sites verified the nChIP-seq results (Figure 3.8 C). Accordingly, as determined by immunoblot, expression levels of endogenous H2A.Z remained unaffected by the loss of PWWP2A (Figure 3.8 D).

3. RESULTS

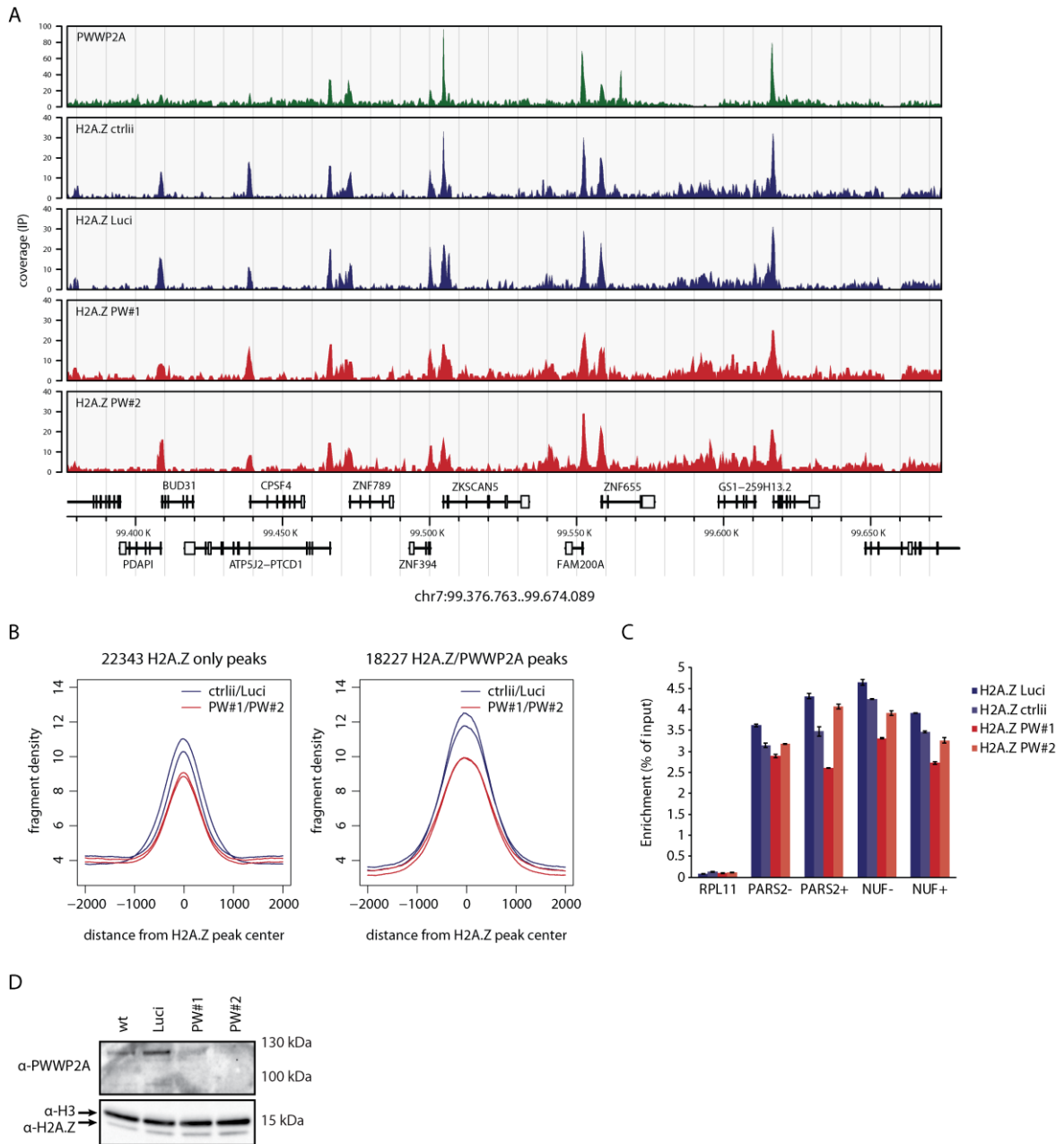


Figure 3.8 PWWP2A depletion does not influence H2A.Z occupancy or global H2A.Z levels. **A.** Snapshot from genome browser of a representative region in human chromosome 7 with gene structure annotations displayed below. Depicted are nChIP-seq signals of GFP-PWWP2A (green) and GFP-H2A.Z two days after control (ctrlII, Luci; blue) or PWWP2A (PW#1, PW#2; red) knockdown. **B.** Density plot displaying GFP-H2A.Z only (left, 22.343 peaks) or GFP-H2A.Z overlapping with GFP-PWWP2A (right, 18.227 peaks) nChIP-seq peaks upon control (ctrlII, Luci; dark blue) or PWWP2A (PW#1, PW#2; red) depletion. **C.** Verification of nChIP-seq results of GFP-H2A.Z from (B) by nChIP-qPCR. RPL11 is a gene body site devoid of H2A.Z-containing nucleosomes and serves as negative control. PARS and NUF represent H2A.Z-containing promoter sites (- = -1 nucleosome relative to the TSS, + = +1 nucleosome relative to the TSS). Shown is percent input of two replicates of GFP-H2A.Z nChIPs two days after control (wt, Luci) or PWWP2A (PW: PW#1, PW#2) siRNA-mediated knockdown. Error bars indicate SEM of two to three technical replicates. **D.** Representative immunoblot of cell extracts from HK cells two days after control (wt, Luci) or PWWP2A (PW#1, PW#2) knockdown with anti-PWWP2A, -H3 and -H2A.Z antibodies. H3 served as loading control.

3. RESULTS

As the depletion of PWWP2A did not influence H2A.Z's occupancy, I next investigated whether overexpression of PWWP2A affects H2A.Z levels. To this end HK cells stably expressing GFP-H2A.Z.1 were transiently transfected with Cherry-tagged PWWP2A (Ch-PWWP2A) and FACS sorted with the help of Dr. Martha Smets (LMU Biocenter, Munich) according to the Ch-expression level (Figure 3.9 A). Cells stably expressing GFP-H2A.Z wt, lowly expressing Ch-PWWP2A and highly expressing Ch-PWWP2A as well as GFP, as a control, were subjected to nChIP followed by qPCR of specific loci. Similar to the results obtained with PWWP2A depletion, also the overexpression of Ch-PWWP2A did not affect H2A.Z's occupancy at selected sites (Figure 3.9 B).

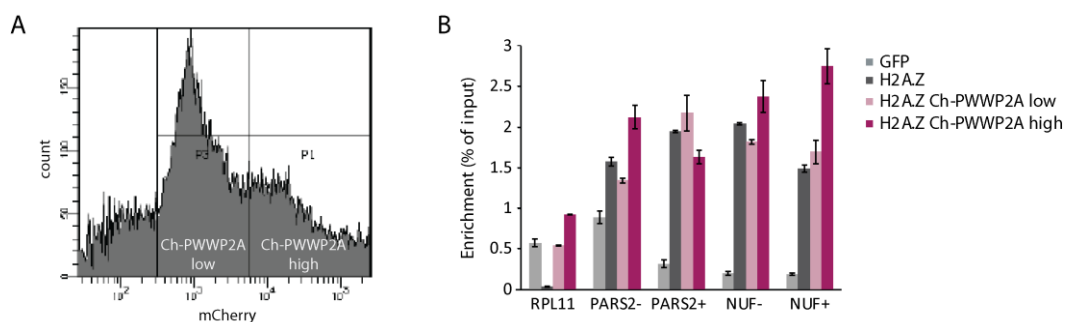


Figure 3.9 Overexpression of PWWP2A does not affect H2A.Z occupancy. **A.** FACS-based sorting of lowly (left) or highly (right) transiently expressed Ch-PWWP2A in HK cells stably expressing GFP-H2A.Z. **B.** nChIP-qPCR of selected loci using the same primer pairs as shown in 3.8 C. RPL11 is a gene body site devoid of H2A.Z-containing nucleosomes and serves as negative control. PARS and NUF represent H2A.Z-containing promoter sites (- = -1 nucleosome relative to the TSS, + = +1 nucleosome relative to the TSS). Shown is percent input of GFP (negative control, light gray), GFP-H2A.Z (H2A.Z, dark gray) or GFP-H2A.Z transiently expressing low (light red) or high (dark red) levels of Ch-PWWP2A. Error bars indicate SEM of two to three technical replicates.

To vice versa determine whether PWWP2A's chromatin association is dependent on H2A.Z-binding, I performed FRAP in collaboration with Susanne Leidescher (LMU Biocenter, Munich). Therefore, I transiently transfected HK cells with a GFP-PWWP2A construct lacking the IC region (Δ IC) that mediates H2A.Z-specificity (Figure 3.10 A). Indeed, depletion of the H2A.Z interaction domain within PWWP2A resulted in increased but not full mobility in comparison to full length PWWP2A (Figure 3.10 B+C). This result indicates that H2A.Z is one important but not the sole mediator of PWWP2A chromatin association and is in line with our previous finding that PWWP2A binds chromatin in a multivalent manner.

3. RESULTS

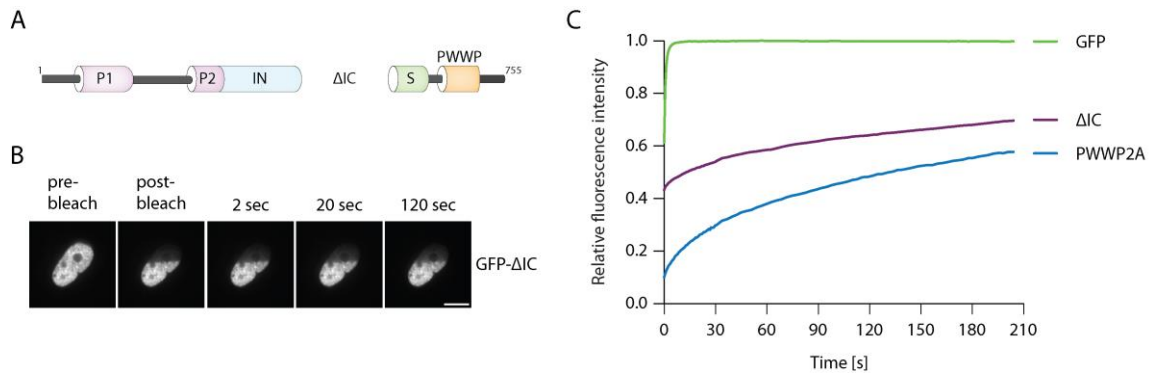


Figure 3.10 Depletion of the H2A.Z-interacting domain within PWWP2A influences PWWP2A's chromatin binding ability. **A.** Schematic depiction of PWWP2A's domain structure lacking the IC region. **B.** Representative confocal images before and after photobleaching of half-nucleus of HK cells transiently expressing GFP-ΔIC. **C** FRAP quantification curves from HK cells transiently expressing GFP, GFP- or GFP-PWWP2A (n=9-19). Scale bar = 5 μm.

In conclusion, H2A.Z's occupancy remains unaffected by the depletion of PWWP2A while the deletion of the H2A.Z-interacting internal region within PWWP2A decreases PWWP2A's chromatin binding ability.

3.4 PWWP2A binds weakly to H3K36me3-containing gene bodies and associates with regulatory regions

To determine whether the multivalent chromatin binder PWWP2A is also enriched at other chromatin features besides H2A.Z, Dr. Marek Bartkuhn (Institute for Genetics, JLU, Giessen) reanalyzed the earlier generated GFP-PWWP2A nChIP-seq data [121]. Notably, it was previously found that PWWP2A is also able to recognize H3K36me3, a chromatin mark typically associated with gene bodies, via its PWWP domain *in vitro* ([224], data from Ramona Spitzer, [228]). To assess whether these observations are also supported *in vivo*, first gene body regions with high H3K36me3 levels (data from ENCODE) were identified by cluster analysis, defining cluster 2 as prototypic for H3K36me3-enriched gene body peaks (Figure 3.11 A). Both PWWP2A as well as H2A.Z were strongly enriched at the promoters of cluster 2 genes (Figure 3.11 B). Further, the PWWP2A signal was slightly increased at H3K36me3-positive gene bodies of cluster 2 genes, while both H2A.Z isoforms were depleted in the gene body regions (Figure 3.11 B). By comparing signals of H2A.Z, PWWP2A and H3K36me3 in 3'-gene body ends with the corresponding non-transcribed downstream regions, a small but significant enrichment of PWWP2A across H3K36me3-high gene bodies was revealed (Figure 3.11 C). Vice versa, H2A.Z.1 and H2A.Z.2 were absent at these sites (Figure 3.11 C). This

3. RESULTS

indicates that PWWP2A is recruited to H3K36me₃-enriched sites independently of H2A.Z and might only occur in a transient manner.

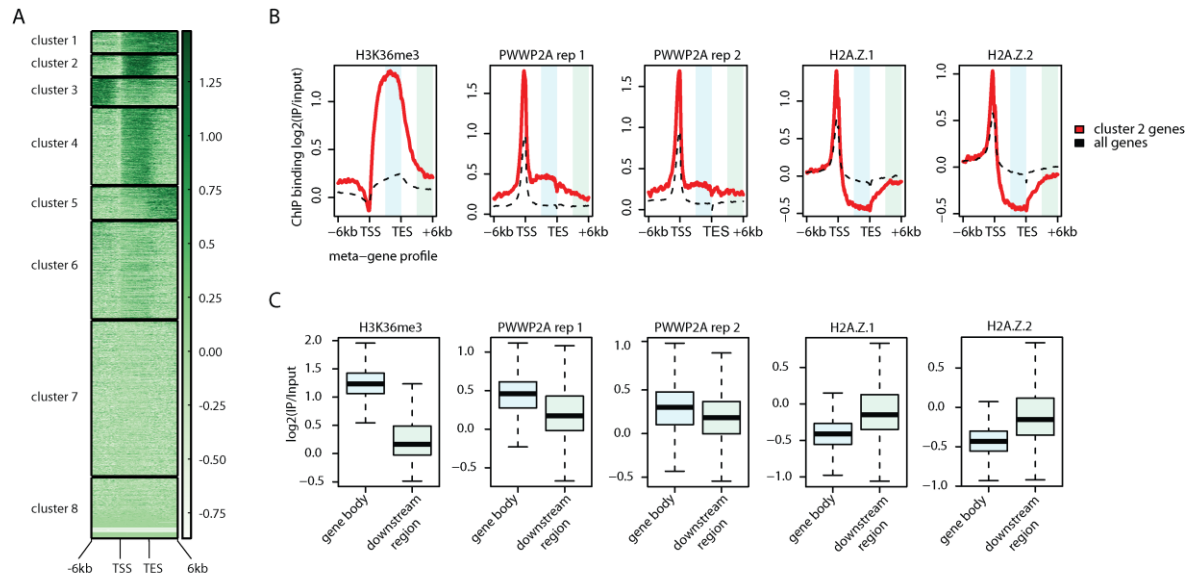


Figure 3.11 PWWP2A associates weakly with H3K36me₃-containing but H2A.Z-depleted gene body regions. A. Density heatmap of H3K36me₃ (ENCODE) ChIP-seq clustering analysis of meta-gene binding profiles encompassing gene bodies and 6 kb upstream and downstream regions of transcriptional start sites (TSS) and transcriptional end sites (TES). Color intensity represents normalized and scaled tag counts. Cluster 2, which represents H3K36me₃-enriched genes, was used for further analysis. **B.** Meta-gene profile correlations of ChIP-seq data for H3K36me₃, two GFP-PWWP2A replicates (rep), GFP-H2A.Z.1, and GFP-H2A.Z.2 mean coverage signals of cluster 2 genes (red line) and all genes (black dotted line) encompassing gene bodies and 6 kb upstream and downstream regions of TSS and TES. Regions highlighted in light blue (gene body) and light green (downstream region) were further analyzed in (C). **C.** Boxplots of H3K36me₃, two independent GFP-PWWP2A, GFP-H2A.Z.1, and GFP-H2A.Z.2 signal intensities comparing gene body with non-coding regions of same size within cluster 2.

To identify further binding modes of PWWP2A, the previously generated GFP-PWWP2A nChIP data was compared to chromatin states defined by training a 10-state model on ENCODE data for H3K4me₁, H3K4me₃, H3K27ac, H3K27me₃, and H3K36me₃ and using ChromHMM [18]. Interestingly, PWWP2A was anticorrelated with the heterochromatin mark H3K27me₃ (state 9) as well as H3K36me₃ (state 7), while a slight correlation of PWWP2A with H3K36me₃ was found, when sites were co-occupied with H3K4me₁ and/or H3K4me₃ and H3K27ac (states 2 and 6) (Figure 3.12 A+B). Notably, PWWP2A binding was strongly enriched at active promoters, which are marked by low levels of H3K4me, high levels of H3K4me₃ and H3K27ac (state 3). Moreover, enrichment of PWWP2A was observed at active as well as inactive or poised enhancers, which are characterized by low levels of H3K4me₃, high levels of H3K4me₁ and high or low H3K27ac, respectively (states 4 and

3. RESULTS

5) (Figure 3.12 A-C). Intriguingly, enrichment patterns of H2A.Z and PWWP2A not only at promoters but also at enhancers were highly identical, indicating a common role for both factors at respective chromatin regions and suggesting a mechanism by which PWWP2A is recruited to regulatory regions (Figure 3.12 C).

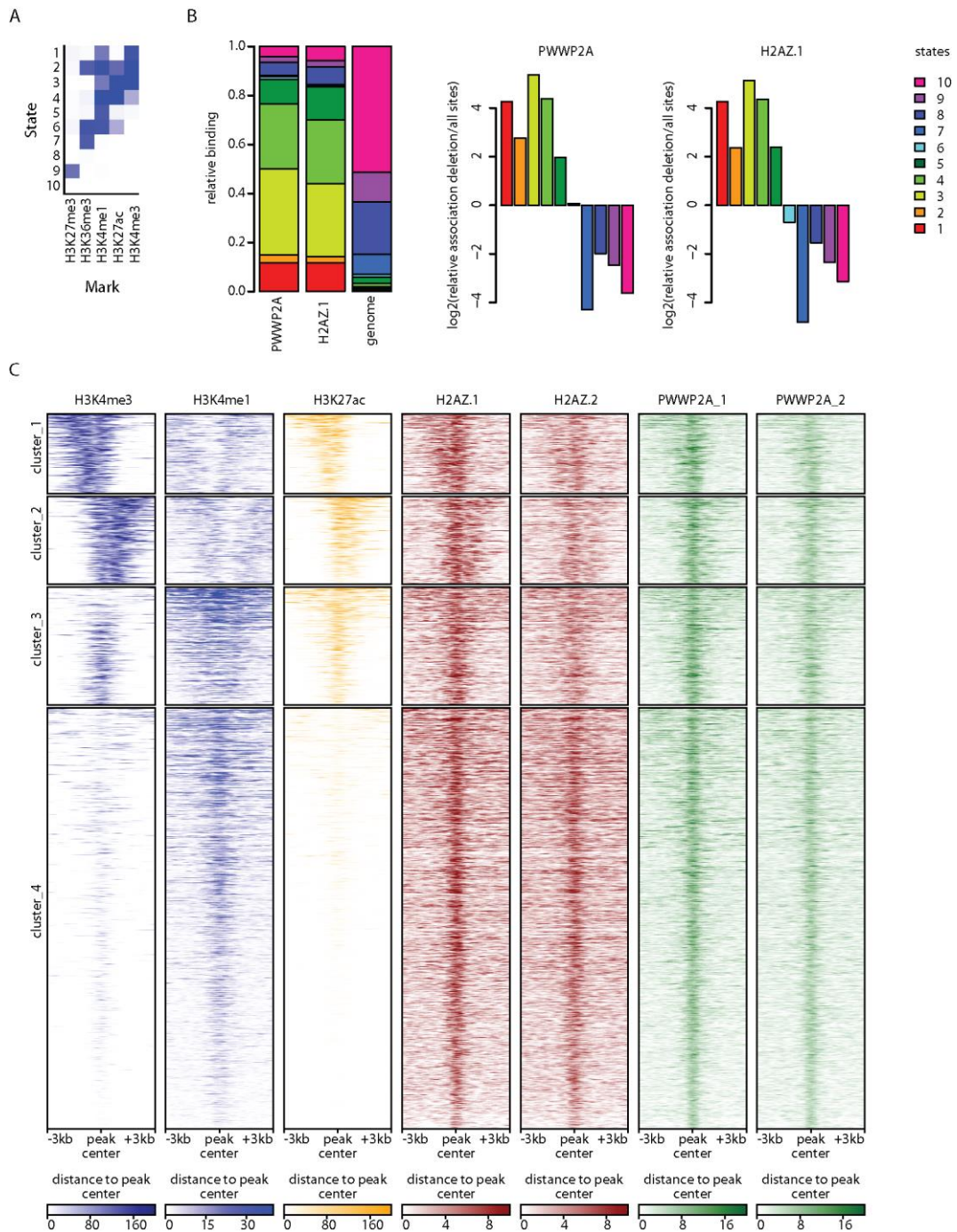


Figure 3.12 PWWP2A associates with regulatory regions genome-wide. A. Heatmap displaying the characterization of chromatin states of PWWP2A-containing genomic regions according to ChromHMM [19]. **B.** Comparison of enrichments of chromatin states of PWWP2A- or H2A.Z-containing sites to the human

3. RESULTS

genome (left). Fold enrichment or decrease of PWWP2A- or H2A.Z-containing sites in specific states calculated to frequency in complete genome (right). **C.** Density heat map of nChIP-seq signals of PWWP2A-enriched sites (two replicates, green) and intensities of H3K4me3 (dark blue, ENCODE), H3K4me1 (light blue, ENCODE), H3K27ac (yellow, ENCODE) and GFP-H2A.Z1 and -H2A.Z.2 variants (red) at these regions. Color intensity represents normalized and globally scaled tag counts. Bioinformatic analyses were performed by Dr. Marek Bartkuhn (Institute for Genetics, JLU, Giessen).

3.5 PWWP2A interacts with a MTA1-specific NuRD subcomplex

Our lab has previously found that PWWP2A interacts with a range of chromatin moieties via its distinct domains and affects transcription by a yet unknown mechanism [121]. As PWWP2A does not seem to contain any domains with known enzymatic activity, it is likely that PWWP2A mediates recruitment of chromatin modifiers to H2A.Z-containing nucleosomes that in turn affect chromatin structure and function. To identify interaction partners of PWWP2A, label-free quantitative MS was applied. Therefore, chromatin from HK cells stably expressing GFP or GFP-PWWP2A was MNase-digested and mononucleosomes were immunoprecipitated using GFP-Trap® in technical triplicates. In collaboration with Dr. Eva Keilhauer from the Matthias Mann group (MPI of Biochemistry, Martinsried) GFP- or GFP-PWWP2A bound nucleosomal proteins were subjected to on-bead tryptic digestion and then quantitated by label-free MS/MS. Dr. Sebastian Pünzeler had already determined PWWP2A-specific binding partners in one replicate which I aimed to confirm in a second replicate. Overall, results of the first replicate were largely verified with PWWP2A representing the strongest outlier and H2A.Z as one of PWWP2A's targets (Figure 3.13 A). While some of the interactors were previously identified to also bind H2A.Z (e.g. HMG20A, PHF14, PHF20L1, RAI1, ZNF512B) [120, 121] other proteins specifically interacted with PWWP2A only (e.g. ATRX, DAXX, MDC1, PWWP2B). Interestingly, comparison of the two replicates revealed a strong reproducible interaction with proteins previously shown to also bind H2A.Z-containing nucleosomes: MTA1, HDAC2, RBBP4 and RBBP7. These proteins are core components of the Nucleosome Remodeling and Deacetylase (NuRD) complex that is, among other functions, involved in gene regulation [64] (Figure 3.13 B). In line with our finding, PWWP2A binding to HDAC1/2 and MTA1 has been previously reported in different MS-based screens [269, 270]. Usually, NuRD also contains MBD2/3, GATAD2A/B and the ATP-dependent remodeling enzymes CHD3/4/5 [271]. Surprisingly, none of these subunits were isolated in my or Dr. Sebastian Pünzeler's previous PWWP2A or H2A.Z pulldowns, and also confirmed by immunoblots (data not shown, [228]). The MTA, HDAC and RBBP subunits seem to independently constitute a stable subcomplex that we termed MHR accordingly. In *Drosophila*, a corresponding PMR complex containing the three homologous proteins (p55, MTA-like, Rpd3) has been identified [272]. PWWP2A exhibited binding to all three MTA paralogues although the strongest interaction was observed with

3. RESULTS

MTA1. Thus, it was next tested whether PWWP2A is able to interact with all MTA isoforms equally well. Our collaborator Dr. Thomas Burgold from Dr. Brian Hendrich's group (Wellcome Trust-MRC, Cambridge) performed MTA isoform-specific IPs from mESC lysates followed by immunoblotting for PWWP2A and, as positive control, MBD3. Indeed, PWWP2A displayed strongest interaction with MTA1 over MTA2 or MTA3 (Figure 3.13 C). Reciprocally, only MTA1 but not MBD3 was able to bind PWWP2A (Figure 3.13 D). To determine which subunit(s) of the MHR complex is responsible for mediating the interaction with PWWP2A, members of the group of Prof. Joel Mackay (University of Sydney) carried out further experiments. They co-expressed FLAG-PWWP2A, HDAC1 (untagged), HA-RBBP4 and either HA-MTA1 or HA-MTA2 in HEK293 cells and performed FLAG-PWWP2A IPs from respective cell lysates (Figure 3.13 E). Remarkably, only when MTA1, but not MTA2, was present PWWP2A precipitated the other components of the MHR complex. This indicates, that MTA1 directly binds to PWWP2A and mediates the recruitment of HDAC and RBBP proteins to form an MTA1-specific M1HR module.

3. RESULTS

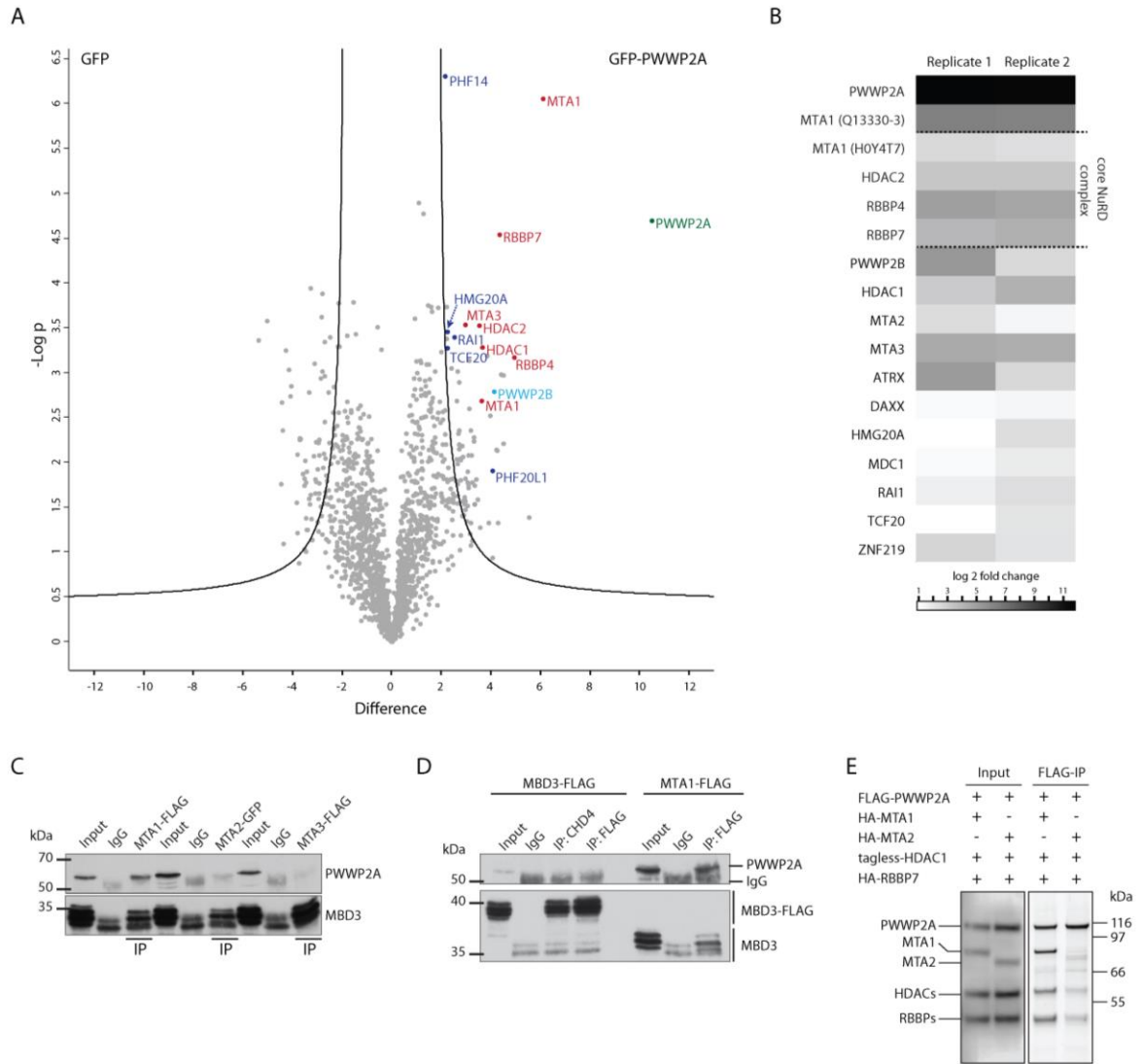


Figure 3.13 PWWP2A interacts with a MTA1-specific core NuRD complex. **A.** Volcano plot visualizing significantly enriched proteins after GFP-PWWP2A pulldowns from mononucleosomes (right) over GFP-enriched proteins (left). t-test differences were obtained by two-sample t-test. PWWP2A is highlighted in green, members of the MTA1-specific core NuRD (M1HR) complex as well as other proteins that have previously been identified to bind H2A.Z as well in dark blue and PWWP2B, as a specific-PWWP2A-binder in light blue. **B.** Heatmap depicting GFP-PWWP2A interacting proteins from two replicates (n=2). Shown are log₂ LFI intensities (fold-change for GFP-PWWP2A vs. GFP pulldowns) for the strongest binders of GFP-PWWP2A. **C.** Immunoblots of IPs from endogenously tagged MTA1-FLAG, MTA2-GFP or MTA3-FLAG from mouse embryonic stem cell (mESC) nuclear extracts using PWWP2A- or MBD3-specific antibodies. **D.** Immunoblot of endogenously tagged MBD3-FLAG or MTA1-FLAG, CHD4 or control (IgG) IPs from mESC nuclear extracts using PWWP2A- or MBD3-specific antibodies. **E.** Immunoblot of FLAG-PWWP2A IPs with cell lysates from HEK293 cells co-transfected with combinations of plasmids encoding for FLAG-PWWP2A, HDAC1 (tagless), HA-RBBP4, and either HA-MTA1 or HA-MTA2 (left). Precipitated proteins were detected via Sypro-staining (right). Experiments for figures (C) – (E) were carried out by our collaborators as indicated in the text.

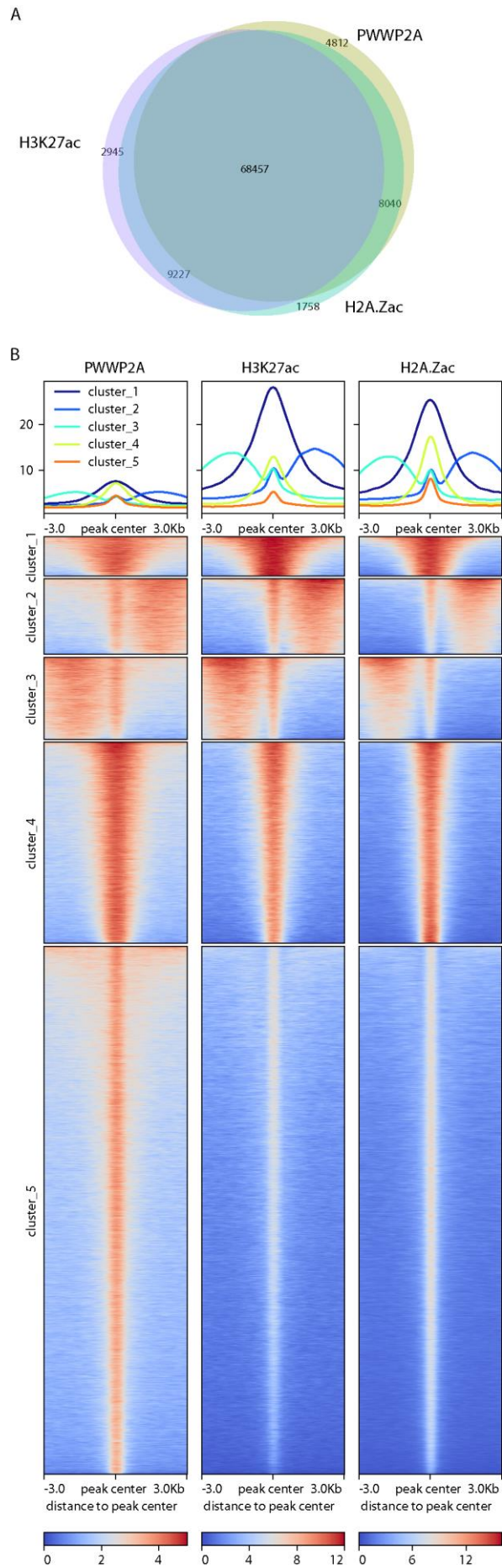
3. RESULTS

The interactome of PWWP2A revealed that PWWP2A binds to a range of chromatin modifying proteins and complexes, many of which have been previously identified in H2A.Z pulldowns. Notably, PWWP2A interacts with an MTA1-specific core NuRD complex (M1HR), presumably recruiting it to H2A.Z-containing nucleosomes.

3.6 PWWP2A mediates changes in histone acetylation levels

Previously, it was shown that H3K27ac levels correlate with the activity of the NuRD complex [273, 274]. The PWWP2A-associated M1HR complex contains the enzymatically active histone deacetylases HDAC1 and HDAC2, with the latter also being found to bind to H2A.Z-containing nucleosomes [121]. In general, HDACs were referred to as transcriptional co-repressors that remove histone acetylation marks thereby repressing transcription [275, 276]. However, recent studies indicate that HDACs may also be associated with active genes, in particular at gene promoters and enhancers [277, 278]. These data sets correlate with the observation that HDAC2 and HDAC1 are bound to H2A.Z and PWWP2A, which both localize to the -1 and +1 nucleosomes at the TSS of actively transcribed genes [121] and also occupy regulatory regions (Figure 3.12 C). Hence, I next set out to investigate whether the H2A.Z-PWWP2A-M1HR connection influences histone acetylation levels. To this end, I performed nChIPs of H3K27ac as well as H2A.Zac (which can be acetylated at lysines 4, 7 and 11) after PWWP2A knockdown that were sequenced by Dr. Andrea Nist (Genomics Core Facility, Marburg) and bioinformatically analyzed by Dr. Marek Bartkuhn (Institute for Genetics, JLU, Giessen). Intriguingly, H3K27ac shares a substantial number of binding peaks across the genome with acetylated H2A.Z especially at distal intergenic regions but also at promoters (Figure 3.12, Figure 3.14). Focusing on genome-wide distribution patterns of the H3K27ac (85.023 peaks) or H2A.Zac (87.482 peaks) nChIP-seq data indicated that the vast majority of sites (68.457 peaks; 72.171 peaks shared by H3K27ac and PWWP2A) were co-occupied by PWWP2A (84.343 peaks) (Figure 3.14), indicating that all three feature a highly similar genome-wide binding patterns.

3. RESULTS



3. RESULTS

Figure 3.14 Correlation between PWWP2A-enriched sites and H3K27ac as well as H2A.Zac regions. **A.** Venn diagram showing the overlap GFP-PWWP2A, H3K27ac and H2A.Zac sites on a genome-wide scale. The overlap was calculated according to [240]. **B.** Heatmap of PWWP2A, H3K27ac and H2A.Zac. Peak sets were combined into a unified set and binding data were collected in 6 k- spanning windows around the peak centres. In total, 98.953 peaks were analyzed. Data was portioned into 5 clusters by k-means clustering. Bioinformatic analyses were performed by Dr. Marek Bartkuhn (Institute for Genetics, JLU, Giessen).

Strikingly, depletion of PWWP2A strongly increased H3K27ac and H2A.Zac levels at 566 distinct regions (Figure 3.15 A). Moreover, differential acetylation of H3K27ac was simultaneously induced at the majority of H2A.Zac sites. (Figure 3.15 B). Vice versa, for H2A.Zac 423 differentially acetylated sites were identified, which likewise, although not as pronounced, exhibit an induction of acetylation of H3K27ac (Figure 3.15 B). Of note is that the differentially acetylated sites are typically occupied by PWWP2A and H2A.Z.

3. RESULTS

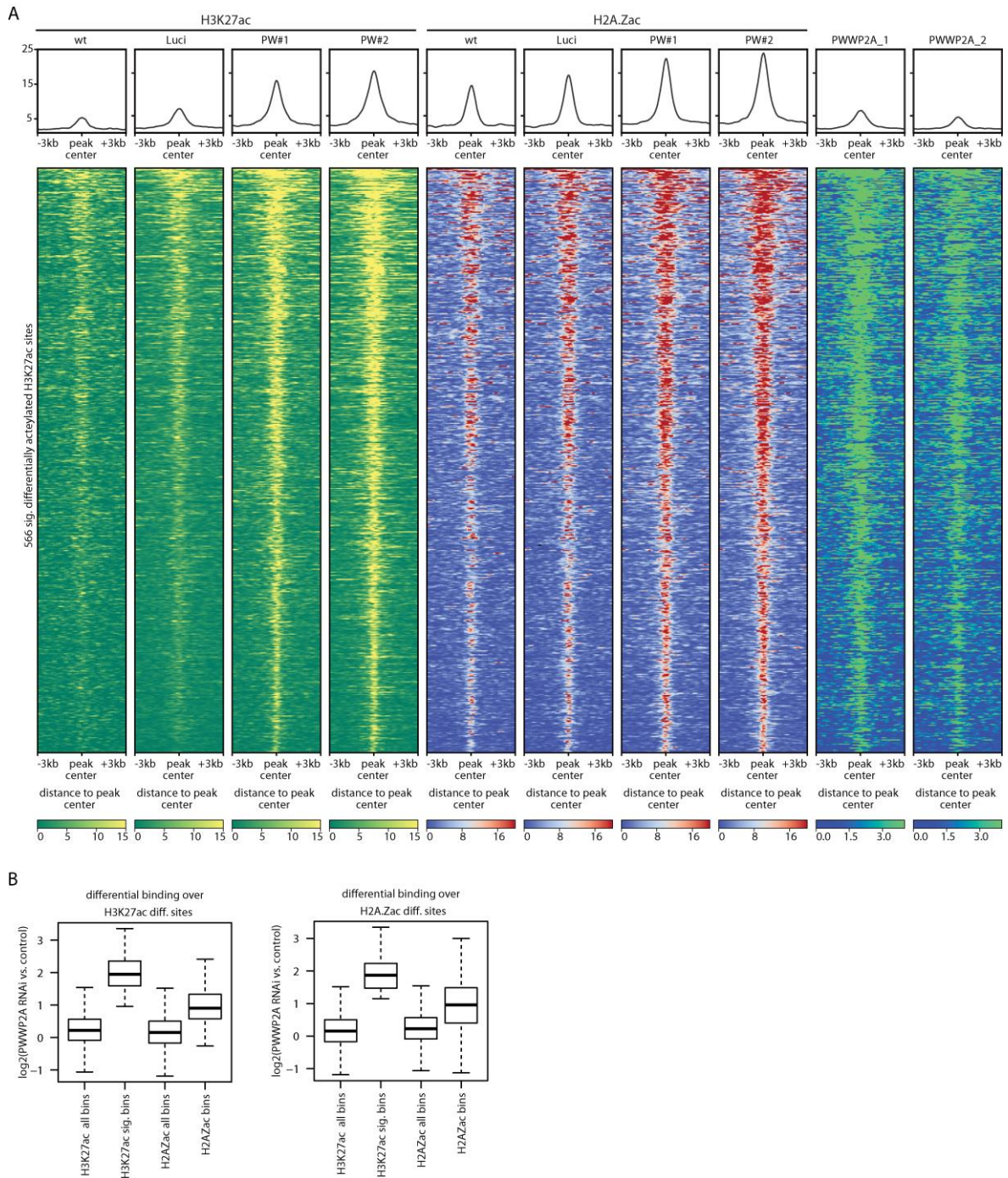


Figure 3.15 Depletion of PWWP2A leads to an increase of H3K27 and H2A.Z acetylation levels in a subset of genomic regions. A. Density heat map of nChIP-seq of 566 induced H3K27ac sites upon PWWP2A depletion. Shown are H3K27ac (yellow) and H2A.Zac (red) intensities upon control (wt, Luci) or PWWP2A (PW#1, PW#2) depletion. **B.** Boxplots quantifying binding events at 566 sites differentially acetylated at H3K27 ($p < 0.001$) after depletion of PWWP2A (left). Differentially regulated H2A.Zac (423 sites, right) are prevalently induced ($p < 2.2 \times 10^{-16}$). At these sites, H3K27ac is simultaneously induced, although not as strongly pronounced as for H2A.Zac (p value $< 2.2 \times 10^{-16}$). Bioinformatic analyses were performed by Dr. Marek Bartkuhn (Institute for Genetics, JLU, Giessen).

3. RESULTS

Interestingly, the increase in histone acetylation was predominantly apparent at distal intergenic regions (Figure 3.16). Typically, H3K27ac, H2A.Zac and PWWP2A binding sites are mainly found at promoter regions, yet differentially acetylated regions are found at distal intergenic regions (~50%) and to a much lesser extend at promoters (~10%). This suggests that the acetylation changes do not occur randomly but are happening at defined regions.

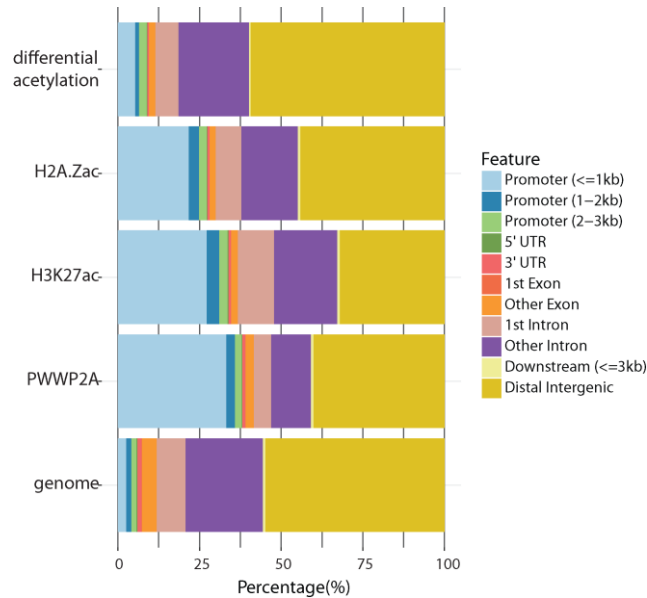


Figure 3.16 Genomic features of differentially acetylated sites. Feature distribution proportioning the human genome according to the indicated functional annotations based on UCSC hg19 gene annotations and in comparison to the genomic background. Bioinformatic analyses were performed by Dr. Marek Bartkuhn (Institute for Genetics, JLU, Giessen).

In line with the finding that acetylation levels are only increased at a subset of H3K27ac and H2A.Zac sites, global acetylation levels of H3K27 and H2A.Z remained unaffected by the depletion of PWWP2A as determined by immunoblotting from extracted histones (Figure 3.17).

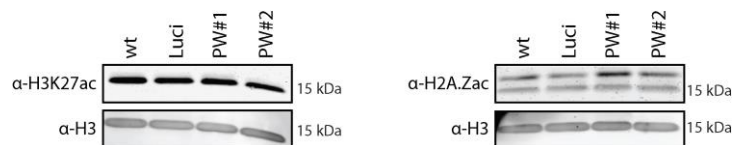


Figure 3.17 Depletion of PWWP2A does not influence global H3K27ac or H2A.Zac levels. Representative immunoblot of extracted histones from HK cells two days after control (wt, Luci) or PWWP2A (PW#1, PW#2) knockdown with antibodies against H3K27ac (left) or H2A.Zac (right), and H3 respectively. H3 served as loading control.

3. RESULTS

Furthermore, to examine whether the increase in histone acetylation is accompanied by an opening in chromatin conformation and hence an increase in the accessibility of chromatin, I made use of ATAC-seq. Therefore, I prepared transposed DNA samples and libraries for ATAC-seq from HK cells after PWWP2A depletion, which were sequenced by Dr. Andrea Nist (Genomics Core Facility, Marburg) and analyzed by Dr. Marek Bartkuhn (Institute for Genetics, JLU, Giessen). Interestingly, ATAC-seq displayed only a subtle increase in chromatin accessibility at differentially acetylated H3K27 loci (Figure 3.18).

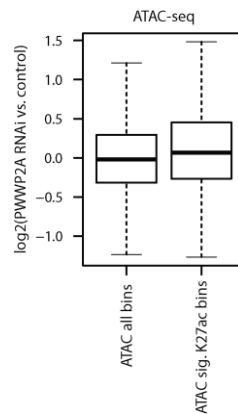


Figure 3.18 Depletion of PWWP2A slightly affects chromatin accessibility at differentially H3K27 acetylated regions. Boxplots showing quantification of accessible chromatin sites at sites differentially acetylated at H3K27 two days after siRNA-mediated knockdown of control (wt, Luci) or PWWP2A (PW#1, PW#2) in HK cells. Genomic regions with increased H3K27ac signals after PWWP2A knockdown that also had enriched number of ATAC-seq read counts (in total 433 genomic bins) were identified. Compared to all genomic bins (110.476 bins; left), differentially acetylated H3K27 loci (right) were marked by a slight increase in ATAC-seq read counts (median log₂FoldChange: 0.06 vs -0.02; Wilcoxon rank sum test p-value = 0.0003539).

Assumedly, regulatory regions such as enhancers are localized close to and influence the expression of nearby genes [279]. To test whether the increase in acetylation on H3K27ac and H2A.Zac upon PWWP2A depletion is robust and indeed affects the expression of nearby genes, I performed nChIP-qPCR to validate nChIP-seq results from corresponding regulatory regions and analyzed expression levels via RT-qPCR. To verify the increase in acetylation levels at defined loci, first loci for possibly affected regulatory regions were selected (Figure 3.19 A) and accordingly, nChIP-qPCR primers for chosen loci were established. Next, H3K27ac and H2A.Zac nChIPs after PWWP2A knockdown were repeated twice and enrichment of these histone PTMs at specific differentially acetylated loci as well as control loci was investigated by nChIP-qPCR. Consistently, differential acetylation of H3K27 as well as H2A.Z was highly reproducible at selected sites (Figure 3.19 B).

3. RESULTS

Subsequently, in order to assess whether the increase in acetylation on H3K27ac and H2A.Zac affects the expression of corresponding nearby genes, I analyzed expression levels via RT-qPCR. For this purpose, I established qPCR primers for selected genes from previously generated RNA-seq data [121]. RNA from three independent knockdown experiments was isolated, reverse transcribed to cDNA and analyzed via qPCR. Interestingly, the differential acetylation on H3K27ac and H2A.Zac led to the upregulation of expression of some genes (e.g. CCL5, FST), while the expression levels of other genes remained unchanged (e.g. ZNF19, B3GALNT2) (Figure 3.19 C).

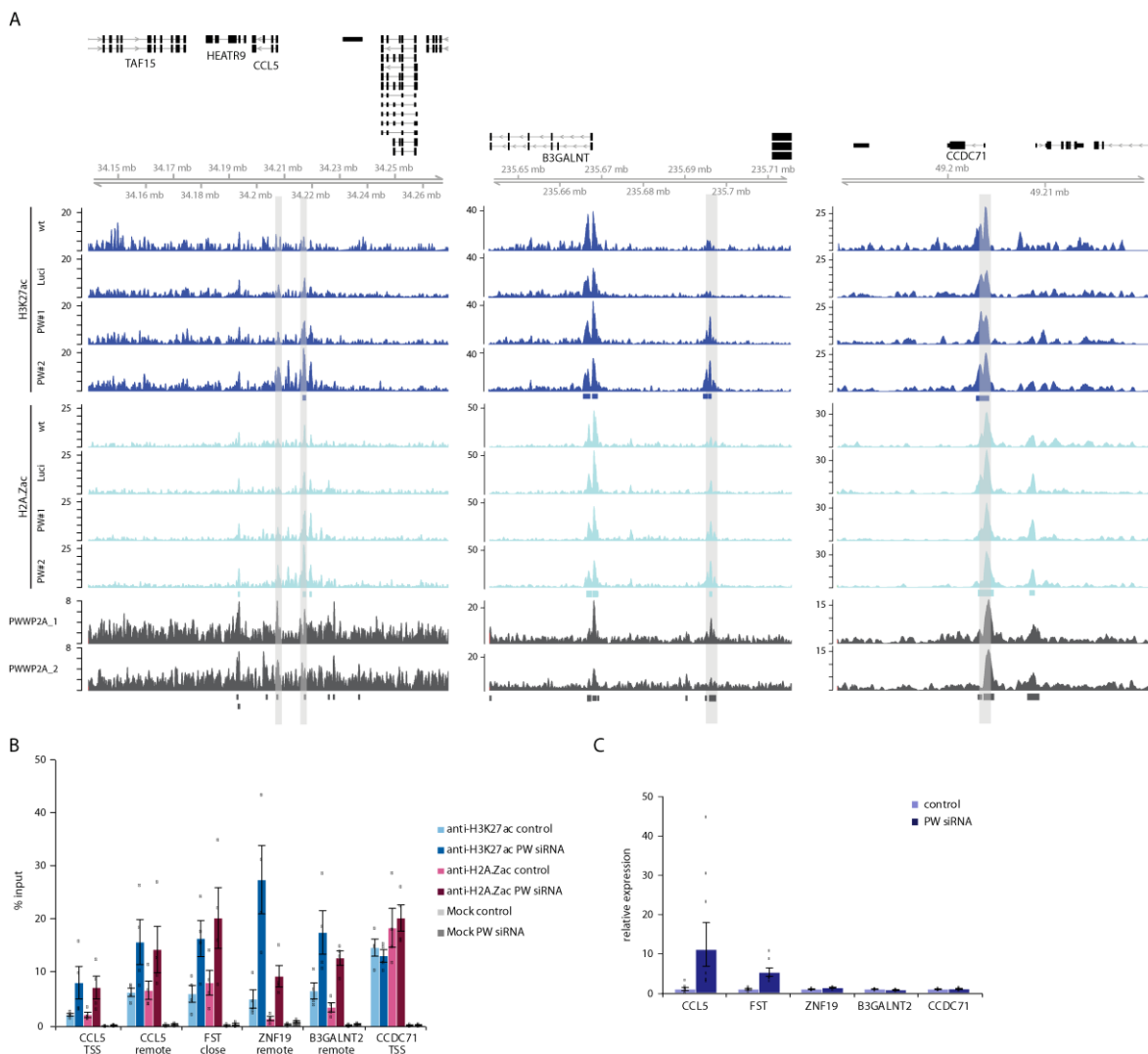


Figure 3.19 Depletion of PWWP2A leads to a site-specific increase of H3K27 and H2A.Z acetylation levels and a gene-specific induction of expression. **A**. Genome browser snap shots of three representative regions in the human genome displaying H3K27ac (from top to bottom: wt, Luci, PW#1, PW#2) (blue), H2A.Zac (wt, Luci, PW#1, PW#2) (light blue) and two GFP-PWWP2A replicates (dark gray) nChIP-seq signals. Differentially acetylated sites are highlighted in gray. **B**. Verification of nChIP-seq data (see Figure 3.15) by nChIP-qPCR at selected loci. As indicated CCL5, FST, ZNF19 and B3GALNT2 represent TSS (transcriptional start site) regions or remote (regulatory region close to a gene) regions at which acetylation levels of H3K27ac and H2A.Zac are

3. RESULTS

induced upon depletion of PWWP2A. Acetylation levels at CCDC71 TSS remain unaffected and serves as control. Shown is percent input of two replicates of H3K27ac or H2A.Zac nChIPs two days after control (wt, Luci) or PWWP2A (PW: PW#1, PW#2) depletion. Error bars depict SEM (n=4). **C.** Relative expression of selected genes corresponding to differentially acetylated sites (B) after control (wt, Luci) or PWWP2A (PW: PW#1, PW#2) siRNA-mediated knockdown. Shown is the fold-change of three replicates normalized to HPRT expression. Error bars depict SEM (n=6). Increase of H3K27 and H2A.Z acetylation levels can result in (i) upregulation of expression of a nearby gene (CCL5, FST) or (ii) no change in expression of a nearby gene (ZNF19, B3GALTN2).

Overall, PWWP2A not only binds to TSSs but also to regulatory regions and its depletion increases acetylation levels of H3K27ac and H2A.Zac at a subset of its binding sites.

4. DISCUSSION AND FUTURE PERSEPCTIVES

4.1 Towards understanding the role of PWWP2A in mitosis and *Xenopus* cranio-facial development

Depletion of PWWP2A in HK cells via RNAi resulted in severe consequences in mitotic progression (Figure 3.1, 4.1). Intriguingly, cells repeatedly shuffled back and forth between prometaphase and metaphase with some chromosomes failing to properly align on the equatorial plate with single chromosomes seemingly being pulled from the metaphase plate into the direction of the opposite mitotic spindle apparatus. Nonetheless, chromosomes realigned to the equatorial plate, thereby impeding successful progression to anaphase. Eventually, some cells were able to escape the seemingly endless loop of prometaphase-metaphase-shuffling and proceeded to anaphase to complete mitosis, fulfilling cytokinesis with some cells forming micronuclei due to chromosomes that were not properly segregated. Overall, when PWWP2A was depleted, cells needed up to 20 hours to complete mitosis. In some cases, cytokinesis was executed albeit sister chromatids had not been previously separated. Yet, a high number of cells formed micronuclei over cytokinesis or cytokinesis failed and cells went into apoptosis.

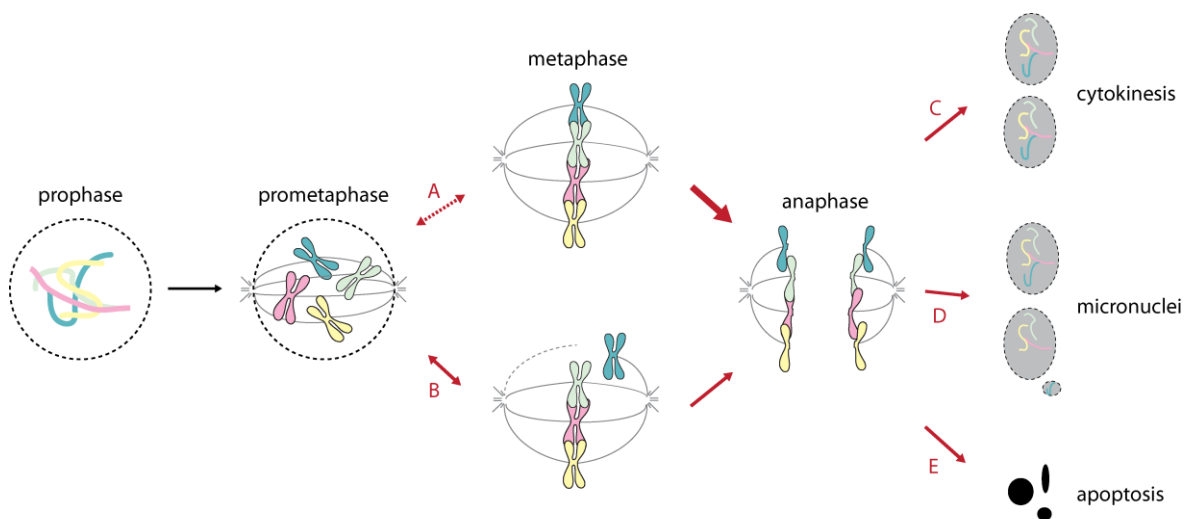


Figure 4.1 Consequences of PWWP2A depletion on mitosis. Mitosis consists of a series of phases starting from prophase, prometaphase, metaphase, anaphase, telophase (not shown) and cytokinesis. Depletion of PWWP2A causes **A**, a back-and-forth shuffling between prometaphase and metaphase, **B**, loop of improper pulling of chromosomes towards the spindle poles during metaphase and realignment of chromosomes at the equatorial plate, **C**, proper cytokinesis, **D**, formation of micronuclei during cytokinesis or **E**, apoptosis. Extended and modified from [280].

4. DISCUSSION AND FUTURE PERSPECTIVES

These observations strongly indicate that PWWP2A depletion causes a defect in chromosome congression very early in the series of mitosis stages. Within prometaphase, chromosomes position relative to the spindle poles and microtubules attach to the chromosomes' kinetochores and sister chromatid chromosomes align at the equatorial plate and bi-orientate, a process termed chromosome congression [281]. Together with motor protein dynein, CENP-E mediates the transport of chromosomes along microtubules, first in direction of the spindle poles and subsequently towards the equator. In mitotic metaphase, sister chromatids are pulled to the spindle which are then oppositely segregated towards the centrosomes in anaphase. The segregation of sister chromatids is executed by microtubulin fibers which attach to the kinetochore of chromosomes centromere as well as the centrosome and draw the chromatids to the latter. Cyclin-dependent protein kinases (CDKs) play an important role in the regulation of cell cycle processes and most notably in chromosome segregation [282]. By ensuring that chromosomes have properly attached to mitotic spindles, the SAC can delay chromosome segregation. In case kinetochores are not attached to mitotic spindles, the MCC is formed to delay chromosome segregation and thereby inhibits the APC. To hinder mitotic progression, SAC proteins bind to cell-division cycle protein 20 (Cdc20) and enclose it into a complex that interacts with the APC. The SAC is inactivated when chromosomes have bioriented and subsequently the APC is activated and initiates segregation of sister chromatids in anaphase. Active APC acts as an E3 ubiquitin ligase and induces the proteasomal degradation of securin and cyclins which is required for mitotic exit and allows separase-mediated cleavage of cohesin [254]. Only then, cells can proceed to telophase in which the nuclear envelope is rebuilt followed by cytokinesis and reformation into an interphase nucleus. IF stainings of Aurora B or INCENP, members of the CPC and SAC, did not exhibit differences in localization upon PWWP2A depletion (Figure 3.3), indicating that these checkpoints remain unaffected by the loss of PWWP2A. Maiato et al. summarized a long list of proteins that have been associated with chromosome congression defects, highlighting the fact that a plethora of proteins is involved in mitosis [281]. Kinetochore associated protein CENP-E was one of them. Loss of CENP-E has been shown to cause misalignment of chromosomes at the metaphase plate and an increase in lagging chromosomes [283, 284]. On some metaphase chromosomes, a loss or sliding of signal of CENP-E was apparent although only when PW#1 siRNA was used for PWWP2A depletion (Figure 3.4). Likewise, also some chromosomes were not properly connected at the centromere anymore when treated with PW#1 siRNA, indicating a loss of chromosome cohesion. After DNA replication the multi-protein complex cohesin mediates cohesion of sister chromatids until onset of anaphase. Making use of an inducible PWWP2A knockout cell line may contribute to understand whether this is due to an off-target effect of the siRNA. Defects in chromosome congression are often linked to aneuploidy, accompanied by

4. DISCUSSION AND FUTURE PERSPECTIVES

chromosome missegregation. Moreover, some other proteins mentioned to be involved in chromosome congression, such as Aurora B and Bub1, were tested in IF, but did not display any obvious impairment or led to inconclusive results.

On mitotic chromosomes, PWWP2A binds to distinct regions on the chromosome arms. Interestingly, localization of PWWP2A is absent at the centromeric region (**Figure 3.4**). The absence of PWWP2A at centromeres is in agreement with the heterochromatin composition of these regions marked by satellite repeat DNA to which PWWP2A generally does not locate according to ChIP-seq [121, 285]. Hence, PWWP2A seems not to interfere with the kinetochore and is likely not involved in the stability of the chromosome.

One other possibility by which PWWP2A mediates mitosis progression involves the regulation of genes that jointly ensure the formation of necessary cellular conditions for chromosome segregation. Indeed, PWWP2A depletion leads to the deregulation of around 600 genes, many being involved in metabolism or in actin- and tubulin-related processes [121]. Intriguingly, tubulin as well as actin are both involved in mitosis [256-258]. Proposedly, actin filaments are crucial for cleavage furrow formation and cytokinesis and loss of actin prevents centrosome separation thereby leading to a chromosome segregation delay [257, 286]. Interestingly, although microtubules were formed, they exhibited a slightly abnormal morphology with tubulin fibres appearing less directed when PWWP2A was depleted (Figure 3.2). This is in line with the observation, that chromosomes are indeed pulled towards the spindle poles. Likewise, actin fibres were perturbed in morphology as indicated by thicker actin filaments and the emergence of stress-like fibres (Figure 3.6). Among the genes that were deregulated upon PWWP2A and involved in actin and tubulin regulation were CAPZA1, TPGS2, PREX1, VASP and ANTXR1 (Figure 3.5, [121]). Analysis of H3K27ac and H2A.Zac levels of sites in close proximity to these genes remained largely unaffected by PWWP2A depletion, indicating that there is no link between the mitosis phenotype and the site-specific increase in acetylation. Interestingly, CAPZA1 and VASP perform antagonistic counteracting activities and balance actin filament growth [287]. While CAPZA1, characterized as the cap of growing actin filaments, was downregulated, VASP, which promotes actin filament elongation, was upregulated upon PWWP2A depletion, indicating a possible cause for the perturbed actin filament morphology [288]. Moreover, CAPZA1 is linked to tubulin stability, as siRNA-mediated knockdown of CAPZA1 led to a reduction in stable microtubuli and is thus needed for microtubule stability [289]. As CAPZA1 seems to be a fundamental target of PWWP2A, it is of interest to examine if depletion of CAPZA1 leads to a PWWP2A-resembling phenotype. Knockdowns using siRNAs specific for CAPZA1 should be applied and live-cell imaging and immunofluorescence approaches performed. This may validate if

4. DISCUSSION AND FUTURE PERSPECTIVES

the mitotic phenotype is correlated with a PWWP2A-CAPZA1 interconnection. Since actin is required for cell migration, deregulation of its polymerization upon PWWP2A depletion can also provide an explanation for the neural crest stem cell migration defects during *Xenopus* development. To identify a potential aberration in cell migration, a scratch assay after PWWP2A and CAPZA1 knockdown should be performed. With the help of a scratch assay, one can determine the rate of gap closure after the removal of a physical barrier using live cell microscopy [290]. In a previous study migration rate was increased upon CAPZA1 depletion in gastric cancer cells while overexpression of CAPZA1 had the opposite effect [291]. The regulation of gene expression might contribute to the phenotypes but may not be its only determinants.

There is a plethora of proteins involved in the regulation of mitosis and the list of associated proteins is far from exhausted. Of note is that also the *Xenopus* phenotype upon PWWP2A is not understood either and one should focus on proteins that participate in mitosis as well as cell migration and/or differentiation [121]. Strikingly, most phenotypes caused by H2A.Z depletion in different models exhibit similarities to the mitotic defects observed when PWWP2A is deleted in HK cells but also to the *Xenopus* phenotype, proposing that PWWP2A might serve as mediator in H2A.Z-dependent processes in a yet mechanistically unknown manner. In yeast, lack of H2A.Z leads to a defect in chromosome stability and segregation [132, 292, 293]. Likewise in human cells, knockdown of H2A.Z leads to a chromosome segregation defect [178]. In DT40 chicken cells, an inducible double knockout of both H2A.Z isoforms resulted in a chromosome segregation and progression defect with aberrant tubulin fiber and mitotic spindle formation and an increase in micronuclei formation as well as in the apoptotic cell population [141]. RNAi-mediated loss of H2A.Z in *Xenopus laevis* impaired cell movement leading to mesodermal and neuronal crest development issues [136, 137], a phenotype featuring parallels to the phenotype in *Xenopus* upon PWWP2A depletion. The frog phenotype is dependent on binding of PWWP2A to H2A.Z as a construct lacking the IC domain, which is the H2A.Z binding domain within PWWP2A, could not rescue the head malformation phenotype in *Xenopus* [121]. Moreover, upon H2A.Z depletion during mouse neuronal development some of the most downregulated genes were the ones involved in microtubule cytoskeleton organization [175]. The occurrence of mitotic defects upon H2A.Z loss among different species, hints towards a rather evolutionary conserved mechanism by which H2A.Z influences mitosis. Histone variant H2A.Z is implicated in the regulation of genome stability providing a possible mechanistic explanation for the phenotypes occurring when H2A.Z is depleted. The amount of H2A.Z dramatically increases at the centromere but also at subtelomeric regions when cells enter mitosis [177]. Further, H2A.Z contributes to a specialized 3D structure of the centromere and adjacent pericentromeric regions, which is essential in anaphase for faithful chromosome segregation [161, 178]. With PWWP2A and

4. DISCUSSION AND FUTURE PERSPECTIVES

H2A.Z both being involved in mitosis regulation, and PWWP2A serving as a recruiter for certain proteins or protein complexes, it is tempting to speculate that loss of PWWP2A or H2A.Z leads to a loss of recruitment of chromatin binders to specific chromatin sites. The latter are then unable to fulfil their function and e.g. cellular processes cannot be activated anymore. Particular focus of future experiments needs thus to be placed on whether phenotypes are truly conferred through the interplay of PWWP2A and H2A.Z. FRAP experiments indicated, that the deletion of the H2A.Z-interacting domain within PWWP2A indeed impairs PWWP2A's chromatin binding ability (Figure 3.10). Hence, the effect of H2A.Z depletion on PWWP2A needs to be assessed. Technically it is extremely challenging to obtain cells in which both H2A.Z alleles (*H2AFZ* and *H2AFV*) are depleted. Thus, many studies focus on only one of the H2A.Z isoforms. As H2A.Z is essential in higher eukaryotes and others had failed to generate H2A.Z ko mESCs before [170], best an inducible double knockout of H2A.Z should be generated. Our collaborators from Masahiko Harata's group (Tohoku University, Japan) developed a tetracycline-inducible H2A.Z double knockout system in DT40 chicken cells [141], which may aid to shed light on PWWP2A's dependence on H2A.Z. Although PWWP2A seems to be highly dependent on H2A.Z, PWWP2A does not affect H2A.Z's chromatin association and genome-wide occupancy as assessed by FRAP and ChIP-seq, respectively (Figure 3.7, 3.8, 3.9).

Hints from the PWWP2A interactome

Furthermore, also interactors of PWWP2A may provide missing explanations for the observed phenotypes upon PWWP2A knockdown. Notably, some proteins, such as RAI1, HMG20A, TCF20, PHF14, PHF20L1, ZNF512B and M1HR members, were previously also identified to bind H2A.Z, while other proteins are PWWP2A-specific interactors: PWWP2B, ATRX, DAXX, MDC1 ([121], Figure 3.13). Interestingly, phenotypes upon depletion of some of the above mentioned PWWP2A interactors bear similarities to the PWWP2A-associated phenotypes. With PWWP2A hypothetically serving as a platform for proteins or protein complexes to H2A.Z, loss of PWWP2A will likely impair recruitment of the latter.

PWWP2A specifically interacts with members of a RAI1 complex, containing RAI1, TCF20 (also known as SBPB), PHF14 and HMG20A (also known as iBRAF) proteins (Figure 3.13), and that was first identified as a H3K4me-repelling complex by the Mann laboratory [294, 295]. Interestingly, each member of the RAI1 complex not only has been found to interact with PWWP2A as well as H2A.Z but also has implications in neuronal development, providing a possible explanation for the observed defect in neural crest development. As depletion of PWWP2A in *Xenopus* results in defects during neuronal crest development and perturb cerebellar development, a possible interplay between

4. DISCUSSION AND FUTURE PERSPECTIVES

PWWP2A and RAI1 complex could provide explanations for the neuronal phenotype observed in *Xenopus* upon PWWP2A knockdown. RAI1 is highly conserved among vertebrates and its deletion or mutation in humans is linked to the neuronal developmental disorders Smith–Magenis syndrome as well as Potocki–Lupski syndrome [296]. Both syndromes are characterized by neurodevelopmental and behavioral symptoms. A study in *Xenopus* indicates that loss of RAI1 principally affects neural crest development and proper cartilage formation and features aberrant neural crest migration [297]. Like PWWP2A, RAI1 is thus implicated in craniofacial and neural development. As RAI1 expression during development is induced by retinoic acid [297], using an inducible PWWP2A mESC system and neuronal differentiation techniques utilizing retinoic acid may shed light on PWWP2A's function. RAI1 and TCF20 feature a high sequence similarity and are structural paralogues [298]. TCF20 functions as transcriptional coactivator and is associated with craniofacial development and mental diseases such as autism and schizophrenia [299-301]. PHF14 is linked to Dandy-Walker syndrome, a disease of the central nervous system [302]. Moreover, knockdown of PHF14 led to a prolonged mitosis with misaligned chromosomes, incomplete separation of chromatids in anaphase and defects in spindle organization [303].

Another possible candidate, involved in mitosis regulation and interacting with both PWWP2A and H2A.Z, represents MTA1 (see also 4.2), member of the M1HR NuRD complex. Overexpression of MTA1 in MCF7 and HC11 cancer lines leads to an abnormal spindle formation with an increased number of cells exhibiting more than three centrosomes [304]. The occurrence of more than two spindle poles was also observed for HK cells upon PWWP2A depletion but was not further statistically evaluated. Further, it was shown via IF, that cytoplasmic MTA1 localizes to microtubules [305]. As assessed by a wound healing assay, also referred to as scratch assay, loss of MTA1 in human and cancer cells resulted in a significantly lower ability to migrate [306, 307]. Given the observed defect in neural crest cell migration and differentiation in *Xenopus* upon PWWP2A depletion [121], a scratch assay experiment should be employed in HK cells upon PWWP2A as well as MTA1 knockdown. Moreover, F-actin staining using phalloidin showed altered actin fiber morphology in human cancer cell lines treated with MTA1 shRNA [307]. This finding is similar to the changed actin fiber morphology upon PWWP2A knockdown (Figure 3.6), although the phenotypes are not identical. Generally, a possible correlation between PWWP2A and MTA1 phenotypes upon respective knockdowns needs to be determined (see also 4.2). One other possibility is that indeed gene expression changes contribute to the observed phenotypes upon PWWP2A depletion and that these transcriptional alterations are, at least in part, due to M1HR (HDAC) influenced changes in histone acetylation. But, one must keep in mind that our MS/MS analyses revealed several other PWWP2A interacting proteins, of which many are also found in H2A.Z pulldowns, while some others seem to

4. DISCUSSION AND FUTURE PERSPECTIVES

be PWWP2A-specific. As most of the other binding factors are also able to influence or act on chromatin structure, and some have been shown to influence normal brain development [294], it is likely that they all may contribute, to a different extent, to mitotic progression and cranial-facial development.

Besides interactors of H2A.Z and PWWP2A, also PWWP2A-specific binders may provide explanations for loss of PWWP2A-mediated phenotypes. Mediator of DNA-damage checkpoint protein 1 (MDC1) interacts with the APC and knockdown of MDC1 resulted in a metaphase arrest due to impaired ubiquitin ligase activity of the APC towards cyclin A and B1 [308, 309]. Despite similarities between the phenotypes upon MDC1 or PWWP2A knockdown with cells being unable to proceed to anaphase the mitosis phenotype, in terms of PWWP2A this is more likely due to a defect in chromosome congression. Moreover, PWWP2A-interactor ATRX is important for mitosis. ATRX forms a complex with DAXX that serves as a histone chaperone depositing H3.3 at heterochromatic regions. Cells exhibit a defect in chromosome congression with misaligned chromosomes at metaphase and defective sister chromatid cohesion when ATRX is depleted [310].

Future studies regarding changes in gene expression in *Xenopus* development upon PWWP2A depletion will assess whether the observed mitotic defect in HK cells and the defect in cranio-facial development in *Xenopus* are interconnected or are based on different molecular pathways. Continuative experiments such as RNA-seq during *Xenopus* development need to be employed to gain further knowledge regarding this phenotype. Likewise, putting loss-of-PWWP2A-studies into other systems, like mESCs, in which additionally differentiation into different lineages can be traced, will contribute to a clearer understanding of the individual phenotypes. The faithful differentiation into the three germ layers should be validated by using lineage markers. Here, a special focus on differentiation into ectoderm and subsequent neuronal lineages may aid to understand the cell differentiation in *Xenopus*.

4.2 Probable functions of PWWP2A in NuRD recruitment and histone deacetylation

PWWP2A – a repellent of NuRD remodeling activities?

PWWP2A is a multivalent chromatin binder that is involved in cell cycle progression and transcriptional regulation [121]. Based on homology searches, it is highly unlikely that PWWP2A has any enzymatic activity by means of any of its domains, raising the question of how PWWP2A is able to affect gene expression. Hypothetically, PWWP2A may act as a recruiter, mediating the binding of other chromatin modifying proteins or complexes to H2A.Z-containing nucleosomes. PWWP2A-

4. DISCUSSION AND FUTURE PERSEPECTIVES

specific interactors were determined via nChIP-MS and among the potential candidates were MTA1, HDAC2, RBBP4 and RBBP7, members of the NuRD complex (Figure 3.13). Typically, NuRD combines both chromatin remodeling and histone deacetylase activities [271]. The canonical NuRD complex is composed of a chromatin remodeling subcomplex, containing CHD3/4, MBD2/MBD3 and GATA2A/GATA2B and a histone deacetylase subcomplex, comprising HDAC1/2, MTA1–MTA3 and RBBP4/RBBP7 [67]. Strikingly, PWWP2A only interacted with members of the histone deacetylase subcomplex but not with chromatin remodeling subcomplex members. For the mammalian system, PWWP2A seems to be the first protein found to be associated solely with the deacetylase subcomplex. Recently, drosophila p55 (RBBP4/7 in mammals), MTA1 and Rbd3 (HDAC2 in mammals) were described to be part of also called “PMR”-NuRD subcomplex, a preinitiation complex containing proteins that first associate when the NuRD complex assembles [272]. According to structural studies, mammalian NuRD consists of two HDAC1s and four RBBP4/7s that bind a dimer of MTA1, implying a MTA, HDAC and RBBP ratio of 2:2:4, and form a core NuRD whereby MTA proteins serve as scaffold around which the other subunits assemble [311-314] (Figure 4.2). As determined by electron microscopy, MTA1 dimerizes with HDAC1 and recruits RBBP4 which forms a lobe-like structure around the dimer thereby interacting with both MTA1 as well as HDAC1 [313-315]. In line with the assumption that MTA proteins represent the scaffold around which the NuRD assembles, depletion of all three MTA paralogues constitutes a complete NuRD null [233, 272]. One copy of CHD3/4, MBD2/3 and one or two GATAD2A/B in varied compositions mount around this core NuRD and MBD2/3 bridges the core NuRD with the chromatin remodeling subcomplex and is essential for a stable complex formation. In contrast, Smits et al. suggested a stoichiometry of three MTA1/2/3, one HDAC1/2, six RBBP4/7, one CHD3/4, one MBD3 and two GATAD2A/B using a mass spectrometry-based approach [316].

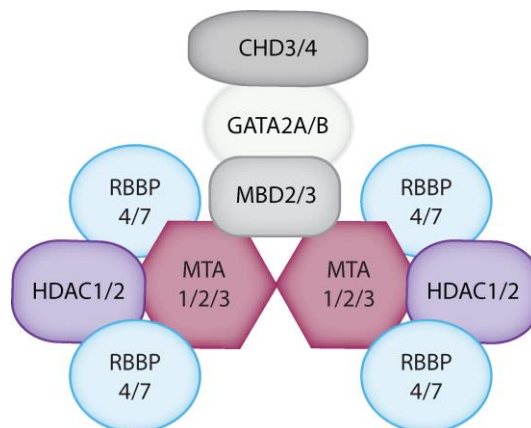


Figure 4.2: NuRD complex architecture. The NuRD complex contains a histone deacetylase and an ATPase subcomplex. Around a dimer of MTA proteins (red), four RBBP (blue) and two HDACs proteins (purple)

4. DISCUSSION AND FUTURE PERSPECTIVES

assemble and form a core MHR NuRD complex. The ATPase subcomplex (gray) consists of MBD2/3, GATA2A/B and CHD3/4, where MBD2/3 interaction with MTA1/2/3 bridging the two subcomplexes.

In line with the finding that a stable core NuRD complex exists, components like CHD3/4 as well as MBD2/3 are only found transiently associated with or devoid of NuRD [311, 313]. Further, MBD3 directly interacts with an MTA subunit, indicating that MBD3 may function as a bridge between M1HR and the CHD-containing remodeling subcomplex [317]. It is tempting to speculate that PWWP2A competes with the MBD proteins for binding to the M1HR module, explaining why MBD, GATA and CHD proteins are not enriched in PWWP2A purifications. While MTA proteins are exclusively found in NuRD complex, HDAC and RBBP proteins are not restricted to NuRD but are also part of other complexes. While HDAC1 and 2 are also present in corepressor for repressor element 1-silencing transcription factor (CoREST) complexes, RBBPs are moreover associated with ATP-dependent nucleosome-remodeling factor (NURF) and polycomb repressive complex 2 (PRC2) and both protein groups are found in the Swi-independent (SIN3) co-repressor complex. HDAC1 and HDAC2 are largely identical in sequence and are able to form homo- as well as heterodimers, which are crucial for proper deacetylase function [318].

Drosophila "PMR" subcomplex exerts catalytic activity *in vitro* [272], thus it seems likely, that human M1HR fulfils deacetylase function *in vivo*. Traditionally, HDACs have been described as important transcriptional repressors but conversely they also prime genes for successive transcriptional rounds, are involved in gene activation and fine-tune transcriptional output [277, 319]. Concordantly, the current view of HATs and HDACs implies that they are involved in balancing acetylation states and promoting a dynamic acetylation turnover rather than setting static acetylation states [277, 320]. HDAC 1 and 2 both localize at promoters of active genes, which correlates with PWWP2A's as well as H2A.Z's genome-wide occupancy [277]. PWWP2A and H2A.Z are enriched at H3K4me3/H3K27ac-positive active promoters as well as H3K4me1/H3K27ac-positive active enhancers (Figure 3.12), both of which are characteristic NuRD-enriched regions [69, 274]. We speculate that PWWP2A recruits HDACs in the context of M1HR complex, to transcriptionally active or bivalent H2A.Z-containing regions in order to balance transcriptional output at these sites. Interestingly, it was recently shown that also MTA proteins are found at these sites, although sites where only MTA1 (and the core deacetylase NuRD) was found and not CHD4 where mostly inactive enhancers, not enriched in H3K27ac or H3K4me3 but in H3K4me1 [233]. Purified RBBP4 and RBBP4-MTA1 complex exhibited enhanced affinity for H3K27me3 and H3K27ac peptides indicating that, additionally to recruitment by PWWP2A, NuRD can also be tethered by RBBP4 to chromatin [313]. Moreover, it was previously that shown H3K27ac levels correlate with the activity of the NuRD complex [273, 274]. In mESCs,

4. DISCUSSION AND FUTURE PERSPECTIVES

NuRD is thought to deacetylate H3K27ac to allow subsequent methylation of H3K27me3 by PRC2 [72, 273, 321]. Typically, also H2A.Z occupies H3K27ac-enriched sites and H2A.Zac is found at these sites as well [156, 199, 200]. Of note is the finding that PWWP2A co-occupies H3K27ac as well as H2A.Zac regions (Figure 3.12, 3.14). Concordantly, H3K27ac and H2A.Zac constitute valid targets for NuRD/M1HR-mediated histone deacetylation. Strikingly, loss of PWWP2A led to a site-specific increase in acetylation on H3K27 and H2A.Z levels at 566 sites that are usually likewise occupied by PWWP2A and H2A.Z (Figure 3.15). The changes in acetylation levels occurred at defined regions, primarily at distal intergenic regions such as enhancers (Figure 3.16). Enhancers are thought to modulate the expression of nearby genes, nonetheless, the exact gene targets of enhancers are difficult to determine [279]. To assess whether the changes in acetylation at promoters and enhancers are likewise reflected by changes in gene expression, expression levels of selected genes near differentially acetylated sites were examined. Notably, two different classes of genes/loci were detected. While for some genes the increase of acetylation levels on H3K27ac and H2A.Zac caused an upregulation of expression of a nearby gene, exemplified by CCL5 and FST, other genes such as ZNF19 or B3GALT2 remained unchanged (Figure 3.19). This observation is in line with previous findings that NuRD is more likely involved in balancing acetylation states thereby fine-tuning gene expression [72, 322]. Consistently, an emerging model proposes that NuRD promotes turnover of acetyl groups primarily at enhancers but likely also at promoters, resulting in fine-tuning of transcriptional output [72]. Moreover, recently it was shown, that first changes in gene expression occur which are consequently followed by changes in H3K27ac levels [274]. Concordantly, it had already been proposed earlier that not the acetylation mark itself, but the dynamic turnover and hence the dynamic interplay of proteins involved in acetylation and deacetylation is most important in the regulation and activation of transcription [320]. Conclusively, PWWP2A not only binds to TSSs but also to regulatory regions, both of which are also co-occupied by H2A.Z, and presumably functions as a M1HR-specific recruiter to H2A.Z-containing thereby contributing to balancing chromatin acetylation levels of H3K27ac and H2A.Zac at a subset of genomic sites and finetuning of specific gene expression (Figure 4.3). Depletion of PWWP2A may lead to improper recruitment of M1HR and the histone deacetylase activity encoded by the HDAC. In agreement with the hypothesis of PWWP2A serving as recruiter of M1HR to H2A.Z-enriched chromatin is the finding that H2A.Z is involved in activation and repression of transcription recruitment of activating and repressive complexes, to keep genomic regions accessible [323]. For example, H2A.Z promotes binding of PRC complexes during mESCs differentiation and NuRD-mediated deacetylation of H3K27ac has been identified as prerequisite for trimethylation of H3K27 by PRC2 [144, 166, 273].

4. DISCUSSION AND FUTURE PERSEPECTIVES

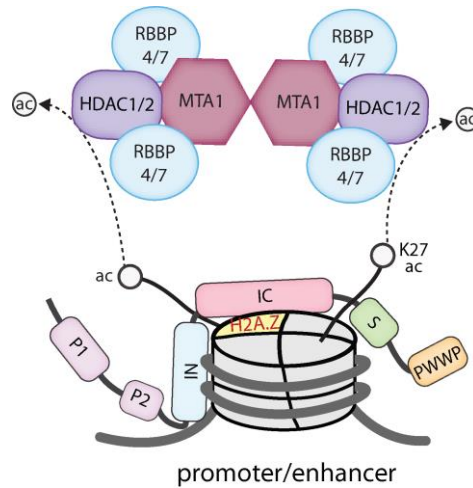


Figure 4.3 Schematic depiction of M1HR-NuRD mediated deacetylation of H3K27 and H2A.Zac at enhancers and promoters. M1HR is recruited to H2A.Z-containing enhancer and promoter regions via PWWP2A. HDAC1/2 proteins within M1HR mediate deacetylation of H3K27ac and H2A.Z ac at these sites. Possibly, H3K27ac and H2A.Zac may also be found at two adjacent nucleosomes.

So far, it is not clear, what other additional features contribute to gene activation or regulation, but it is likely that some genes are more prone to changes in histone acetylation than others. Possibly the genomic location of the regulatory region has an influence, or, alternatively, acetylation changes regulate other more distant genes. More future work on chromatin architecture changes upon PWWP2A depletion will aid in understanding PWWP2A's role in transcriptional regulation. Chromatin conformation capture (Hi-C) experiments upon PWWP2A knockdown can provide answers to the question on which enhancer regulates which gene by mapping the spatial genome organization [324, 325]. Besides solely Hi-C, also Chromatin Interaction Analysis with Paired-End Tag sequencing (ChIA-PET), a combination of Hi-C and ChIP-seq, could be applied to identify long-range interactions of PWWP2A with DNA [326]. Enhancers are frequently transcribed to ncRNAs and eRNAs which are both able to influence transcription. Application of specialized RNA-seq techniques such as random displacement amplification sequencing (RamDA-seq) after PWWP2A depletion may identify misexpression of ncRNAs or eRNAs which are not detected by conventional RNA-seq techniques [327]. Moreover, H2A.Z and DNA methylation is anti-correlated at TSS and gene bodies [149, 150]. This is in line with the observation that enhancers are hypomethylated but display elevated levels of hmC and its oxidized derivatives [214, 215, 328, 329]. Hence, it would be of interest to investigate a potential correlation of PWWP2A with DNA modifications.

ATAC-seq revealed only a slight increase in chromatin accessibility at differentially acetylated loci upon PWWP2A depletion, indicating that a change in acetylation levels is not sufficient to cause a change in chromatin accessibility. Hence, it is likely that chromatin remodeling activity, e.g. executed

4. DISCUSSION AND FUTURE PERSPECTIVES

by a CHD-containing NuRD subcomplex, is relevant for such a change [274]. In agreement with this finding, genome-wide H2A.Z occupancy exhibited only subtle changes after knockdown of PWWP2A, apparent at PWWP2A-bound as well as -unbound sites, underlining the result that chromatin accessibility is not altered and the minimal changes observed are due to the defects in cellular progresses. These data moreover show, that PWWP2A is not involved in H2A.Z deposition. As also the overexpression of PWWP2A did not affect H2A.Z levels, PWWP2A is not required for proper H2A.Z targeting.

Future perspectives regarding the PWWP2A-MTA1-connection

Different combinatorial assembly of the NuRD subunits enables the formation of mutually exclusive NuRD subcomplexes resulting in versatile and diverse specialized functions of the NuRD [65, 330-334]. Moreover, several proteins, e.g. ZMYND8 and SALL4, are known to associate with NuRD with some, such as DOC1 and LSD1, being considered as bona fide NuRD subunits contributing to the diverse flavors of NuRD [69, 335-337]. In this context, these proteins recruit NuRD to genome-wide targets thus regulating NuRD's functions. Although, due to its deacetylase function, NuRD was originally defined as transcriptional co-repressor complex, several studies hint towards a wide functional spectrum of the NuRD including transcriptional activation or balancing and fine-tuning transcriptional output [72, 274, 322, 330, 338, 339]. It is thus likely that various NuRD complexes are targeted by multiple mechanisms to chromatin, with PWWP2A being one recruitment factor specific for M1HR. While MTA1 acts as the scaffold protein during NuRD assembly, PWWP2A presumably serves as recruiter for M1HR to H2A.Z-containing chromatin. MTA proteins are found solely in and have been reported to form mutually exclusive distinct NuRD complexes [340-343]. To test the hypothesis, whether PWWP2A is indeed crucial for recruitment of M1HR, genome-wide occupancy of MTA1 but also HDAC1 and RBBP4/7 upon PWWP2A knockdown should be determined via CHIP-seq. Due to the lack of a good CHIP-applicable antibody for MTA1, GFP-tagged MTA1 needs to be cloned and stable HK cells generated. Such stable transfectants can also be used for FRAP experiments, assessing whether MTA1's chromatin association changes when PWWP2A is depleted.

To gain deeper insights into the PWWP2A-MTA1 connection, preliminary experiments were performed with focus on MTA1 function. Similar to PWWP2A, MTA1 does not execute any enzymatic activity and its functional role is still largely elusive. Most studies focus only on MTA1's role in cancer as the upregulation of MTA1 is associated with metastasis and poor cancer prognosis [344]. First, it was validated, whether siRNAs faithfully decreased expression levels of MTA1. Indeed, knockdown

4. DISCUSSION AND FUTURE PERSPECTIVES

of MTA1 in HK cells using two different siRNAs (MTA1#1, MTA1#2) downregulated expression of MTA1 on mRNA as well as on protein level (Figure 4.4).

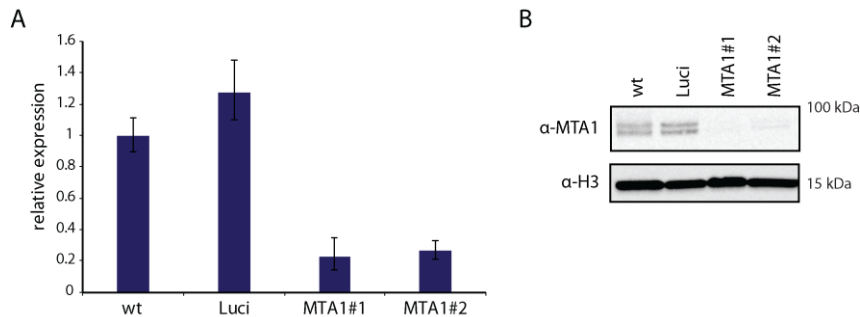


Figure 4.4 RNAi-mediated knockdown of MTA1 is efficient. **A.** RT-qPCR showing relative expression of MTA1 two days after control (wt, Luci) or MTA1 (MTA1#1, MTA1#2) siRNA-mediated knockdown. Shown is the fold-change of three replicates normalized to HPRT expression. Error bars depict SEM (n=3). **B.** Representative immunoblot of HK cell extracts two days after control (wt, Luci) or MTA1 (MTA1#1, MTA1#2) knockdown with antibodies against MTA1 and H3, as loading control.

Investigation of changes in expression levels upon MTA1 knockdown via RNA-seq and the comparison to the RNA-seq data after PWWP2A knockdown may identify commonly regulated genes.

Depletion of PWWP2A increased the acetylation of H3K27ac and H2A.Zac at 566 loci but did not affect global acetylation levels (Figure 3.15, 3.17). Preliminary experiments showed that also loss of MTA1 did not influence global H3K27ac and H2A.Zac levels (Figure 4.5). Accordingly, it will be interesting to determine whether the knockdown of MTA1 features a phenotype similarly to that of PWWP2A at the 566 differentially acetylated sites. Therefore, respective H3K27ac and H2A.Zac nChIPs upon MTA1 knockdown followed by qPCR need to be executed. Interestingly, MTA1-NuRD has also been shown to be involved in non-histone deacetylation [345-347], indicating that histones may be not the only or the incorrect target. For example, the acetylation status of transcription factors may influence their gene regulatory activities [348, 349], therefore, loss of PWWP2A and consequent delocalization of a fraction of HDAC1/2 might lead to changes in transcription factor acetylation and explain the observed upregulation as well as downregulation of genes. Hence, validation and identification of PWWP2A-M1HR deacetylation targets need to be ascertained. To this end, protein acetylation levels before and after PWWP2A depletion could be assessed using mass spectrometry-based approaches [350-352].

4. DISCUSSION AND FUTURE PERSPECTIVES

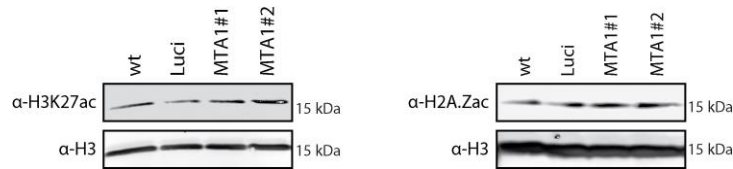


Figure 4.5 Depletion of MTA1 does not influence global H3K27ac or H2A.Zac levels. Representative immunoblots of extracted histones from HK cells two days after control (wt, Luci) or MTA1 (MTA1#1, MTA1#2) knockdown with antibodies against H3K27ac (left) or H2A.Zac (right), and H3 respectively. H3 served as loading control.

Surprisingly, preliminary data from MTA1 knockdowns indicated that the depletion of MTA1 slightly increased PWWP2A's mobility, indicating that MTA1 influences PWWP2A's association with chromatin (Figure 4.6). Hypothetically, MTA1 might be involved in maintaining PWWP2A's stability by so far unknown mechanisms. MTA1 was found to control the stability p53 and HIF-1 α by inhibiting its ubiquitination or recruiting HDAC1, respectively [346, 353].

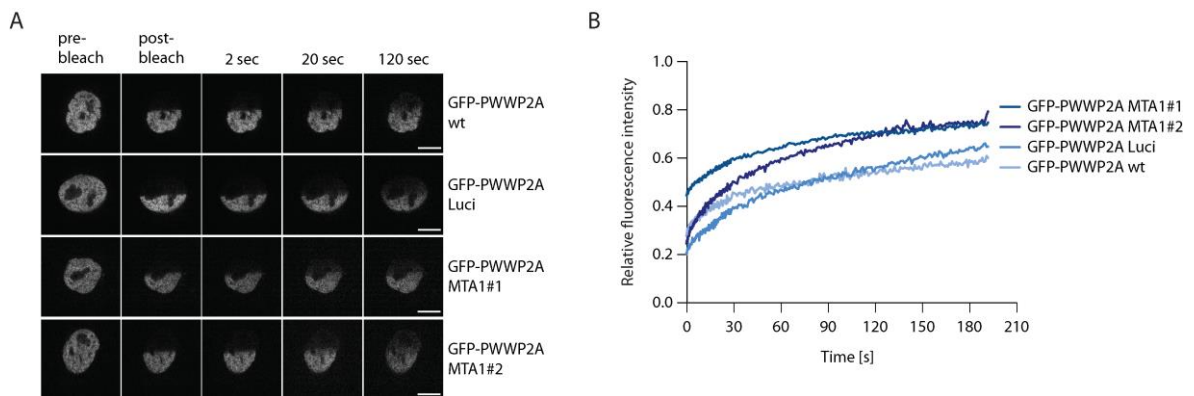


Figure 4.6 MTA1 slightly influences PWWP2A's chromatin binding ability. (A) Confocal microscopy images before and after half-nucleus photobleaching and (B) FRAP quantification curves of average GFP signal relative to fluorescence signal prior to bleaching from HK cells stably expressing GFP-PWWP2A two days after control (wt, Luci) or MTA1 (MTA1#1, MTA1#2) knockdown (n=6-11). Scale bar = 5 μ m.

Eponymous, MTA expression is upregulated in several cancer cell lines and tissues and is well correlated with metastasis potential [342, 354]. Depletion of MTA1 or MTA3 does not affect the viability or fertility of mice, while mice lacking MTA2 exhibit immune defects and are partially embryonic lethal [355, 356]. mESCs devoid of one of the MTA paralogues or all three MTA's exhibit normal morphology although MTA triple knockout cells are unable to maintain lineage and gene expression in a lineage-appropriate manner during differentiation [233]. In somatic cells, MTA proteins have been described to be mutually exclusive [340], while in mESCs they perform redundant

4. DISCUSSION AND FUTURE PERSEPCTIVES

functions [233]. If all three MTA proteins are knocked out, the NuRD is unable to assemble and mESCs are unable to undergo neuroectoderm differentiation although MTA1 ko mice are viable [233]. As neuroectoderm gives rise to the neural tube and neural crest, it is tempting to speculate, that the defects in neural crest differentiation and migration observed in *Xenopus* upon PWWP2A depletion are due to unfaithful MTA recruitment. Studies deciphering functional aspects of NuRD are mostly conducted in mESCs and make use of differentiation techniques. The advantage of this system includes that developmental changes in chromatin can be easily followed. Given the significance of NuRD in mESCs as well as the defect in neural crest cell differentiation in *Xenopus* upon PWWP2A loss, the effect of PWWP2A depletion in mESCs and during differentiation should be assessed. Moreover, also H2A.Z is implicated in developmental processes and is present for example at poised enhancers in mESCs to regulate pluripotency and lineage differentiation [144, 209, 216]. Thus, loss-of-function studies of H2A.Z and PWWP2A in mESCs and during differentiation into different lineages, with special focus on neuronal lineage would aid in better understanding the function of PWWP2A as well as the H2A.Z-PWWP2A-M1HR connectivity. With the help of inducible PWWP2A knockout cell lines one could monitor in which stage of differentiation PWWP2A is crucial. Differentiation into different lineages with the help of specialized protocols, with a special focus on the neuronal ectoderm lineage, in combination with MTA1 and H2A.Z ChIP-seq to test for proper recruitment of M1HR to H2A.Z, may contribute to understand a potential PWWP2A-driven NuRD role in developmental processes. It is tempting to speculate that PWWP2A recruits M1HR-NuRD, to transcriptionally active or bivalent H2A.Z-containing regions in mESCs and during differentiation in order to balance transcriptional output at these sites.

4.3 Multivalent chromatin binder PWWP2A localizes to different chromatin features genome-wide

PWWP2A is a multivalent chromatin binding protein, exerting its exceptional strong binding by means of its different domains. These binding modes have been determined by *in vitro* approaches rendering its functions enigmatic [121, 228]. Novel genome-wide enrichments of PWWP2A at enhancers as well as at gene bodies were identified by reanalysis of ChIP-seq data (Figure 4.7). Colocalization of PWWP2A with H3K27ac and H2A.Zac at regulatory regions is presumably conceived through interaction of PWWP2A with H2A.Z which is likewise found at these regions (Figure 3.12). Binding of PWWP2A to enhancers and promoters is thus highly dependent on its strong interaction with H2A.Z likely through PWWP2A's IC region. At H3K36me3-containing, actively transcribed gene bodies, which lack H2A.Z by definition, weak binding of PWWP2A was observed (Figure 3.11). *In vitro*,

4. DISCUSSION AND FUTURE PERSEPECTIVES

only a construct containing S and PWWP domains but not full-length PWWP2A was able to precipitate H3K36me3 (data from Ramona Spitzer, [228]). PWWP2A interaction with H2A.Z seems to be dominating over binding to H3K36me3. When deleting the H2A.Z-binding domain within PWWP2A, FRAP experiments indicated PWWP2A is less strong associated with chromatin (Figure 3.10), arguing that although binding of PWWP2A to chromatin is dependent on H2A.Z, it is not its only determinant. Further, in an *in vitro* binding assay deletion of the IC domain led to a reduction in H2A.Z interaction, while binding to H3K36me3 is enhanced (data from Ramona Spitzer, [228]). Performing ChIP-seq using the Δ IC deletion construct may be used to address whether PWWP2A's binding to H3K36me3 sites on a genome-wide basis indeed increases. Moreover, when binding of PWWP2A to H2A.Z is impeded, it is tempting to speculate, that so far unknown binding sites may be unraveled. The different binding modes of PWWP2A may be explained by conformational changes that PWWP2A undergoes. Obtaining structural data on PWWP2A will shed further light on PWWP2A's differential binding modes and its possible conformations.

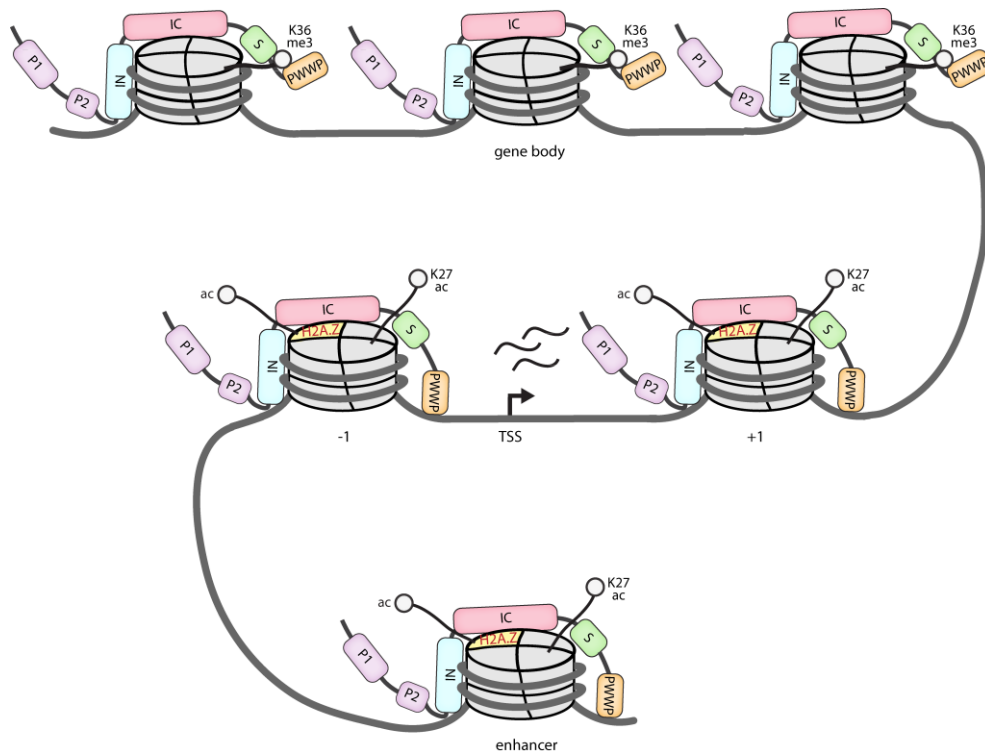


Figure 4.7 Model of PWWP2A binding to different chromatin states. PWWP2A binds to different chromatin states via distinct domains. It binds to H2A.Z-containing enhancer regions which may also be enriched in H2A.Zac and H3K27ac. At promoter regions, PWWP2A localizes at the -1 and the +1 nucleosome, where also H2A.Z resides, around the TSS of actively transcribed genes. Further PWWP2A weakly interacts with H3K36me3-containing gene bodies.

4. DISCUSSION AND FUTURE PERSPECTIVES

Consistently, PWWP2A's localization so far correlates only with rather active chromatin states. Using MNase-digested chromatin for ChIP may cause a bias towards nucleosomal regions associated with active transcription and an open chromatin conformation which are more accessible for MNase. Hence, regions that are nucleosome-free or densely packed nucleosomal regions such as heterochromatin might not be unveiled. Therefore, testing other ChIP approaches such as crosslinked ChIP may reveal additional PWWP2A binding sites across the genome. Whether histone variant H3.3, which is found at active regulatory regions together with H2A.Z, colocalizes with PWWP2A on a genome-wide basis, still needs to be determined by utilizing H3.3 ChIP-seq [144-146, 156, 166]. A possible preference for this variant over canonical H3 or the other variant may be determined using *in vitro* approaches. ChIP-seq in synchronously growing cells as well as in other cell types may contribute to understand whether PWWP2A binds different chromatin modes in a cell cycle or cell specific dependent manner, respectively.

4.4 Consensus and discrepancy between different PWWP2A studies

In the final stages of writing this thesis, a new study on PWWP2A was published [357]. The efforts from the Brockdorff lab largely confirm the findings regarding PWWP2A presented in this thesis and previously shown by our lab [121, 228]. All studies characterize PWWP2A as an H3K36me3-interactor, exerting binding by means of its PWWP domain. Consistent with Zhang et al., we have also identified PWWP2B as an interactor of PWWP2A but did not investigate the protein further. Also, the interaction of PWWP2A with a specific M1HR module as well as an increase in acetylation levels and a deregulation of gene expression when PWWP2A is depleted was uncovered. The main difference exists in the genome wide binding pattern of PWWP2A: In the study by Zhang et al., PWWP2A was predominantly enriched at H3K36me3-containing gene bodies and a small population of PWWP2A was additionally found at poised enhancers. In our hands, only a small fraction of PWWP2A is binding to H3K36me3-containing and H2A.Z-depleted gene bodies, while the vast majority of PWWP2A is found colocalizing with H2A.Z at the TSS and regulatory regions. Interestingly, the ChIP-seq profiles of PWWP2B featuring promoter and enhancer enrichment instead match the PWWP2A ChIP-seq profiles from our group. The obvious discrepancy concerning the ChIP-seq data from the two studies can be due to several reasons. Firstly, Zhang et al. employed mESCs as their model system, although stably expressing FLAG-tagged human PWWP2A, while our lab made use of HK cells. Secondly, and most certainly fundamentally different, the experimental procedures of ChIP vary. Zhang et al. used double-crosslinked ChIP, in which proteins are chemically crosslinked onto DNA followed by sonication to fragment chromatin. In contrast, our lab applied nChIP and so far, I

4. DISCUSSION AND FUTURE PERSPECTIVES

was unable to ChIP PWWP2A from formaldehyde-crosslinked material as PWWP2A was degraded in the course of sonication. It seems reasonable that, by utilizing crosslinked ChIP, also transient binding events are captured. Presumably, PWWP2A binds only weakly to H3K36me3-enriched genomic regions which may be overrepresented after double-crosslinked ChIP. Still, it remains to be elucidated, why PWWP2A promoter binding is absent in this experimental setting. It is thus tempting to speculate, that binding of PWWP2A to H2A.Z-containing promoters and enhancers is superior to gene body binding. Notably, PWWP2A/B DKO mESCs displayed an increase in RNAPII binding at promoter-proximal regions, indicating enhanced RNAPII pausing, as well as an increase in elongating RNAPII. In general, nucleosomes act as barriers for transcriptional elongation and cause stalling of RNAPII [155, 358]. Incorporation of H2A.Z particularly at the +1-nucleosome position relieves the strong nucleosomal barrier and enhances RNAPII efficiency [109]. As H2A.Z has been shown to be involved in the recruitment of RNAPII, and PWWP2A possibly serves as recruiter for transcription factors to H2A.Z sites, the observed phenotype by Zhang et al may possibly be mainly regulated by H2A.Z [157]. The connection between RNAPII and PWWP2A still needs to be further elucidated.

Although not entirely congruent in all aspects, all in all, recent studies on PWWP2A agree in important findings and underline the importance of PWWP2A in chromatin-related processes. Future studies will shed light on the correlation of the paralogues PWWP2A and PWWP2B and will aid to understand how PWWP2A-M1HR functions in terms of transcriptional regulation.

REFERENCES

REFERENCES

1. Kornberg, R.D., *Chromatin structure: a repeating unit of histones and DNA*. Science, 1974. **184**(4139): p. 868-71.
2. Luger, K., et al., *Crystal structure of the nucleosome core particle at 2.8 Å resolution*. Nature, 1997. **389**(6648): p. 251-60.
3. Jenuwein, T. and C.D. Allis, *Translating the histone code*. Science, 2001. **293**(5532): p. 1074-80.
4. Kouzarides, T., *Chromatin modifications and their function*. Cell, 2007. **128**(4): p. 693-705.
5. Hergeth, S.P. and R. Schneider, *The H1 linker histones: multifunctional proteins beyond the nucleosomal core particle*. EMBO Rep, 2015. **16**(11): p. 1439-53.
6. Hammond, C.M., et al., *Histone chaperone networks shaping chromatin function*. Nat Rev Mol Cell Biol, 2017. **18**(3): p. 141-158.
7. Deal, R.B., J.G. Henikoff, and S. Henikoff, *Genome-wide kinetics of nucleosome turnover determined by metabolic labeling of histones*. Science, 2010. **328**(5982): p. 1161-4.
8. Bird, A., *DNA methylation patterns and epigenetic memory*. Genes Dev, 2002. **16**(1): p. 6-21.
9. Korber, P. and P.B. Becker, *Nucleosome dynamics and epigenetic stability*. Essays Biochem, 2010. **48**(1): p. 63-74.
10. Holoch, D. and D. Moazed, *RNA-mediated epigenetic regulation of gene expression*. Nat Rev Genet, 2015. **16**(2): p. 71-84.
11. Li, G. and D. Reinberg, *Chromatin higher-order structures and gene regulation*. Curr Opin Genet Dev, 2011. **21**(2): p. 175-86.
12. Bell, O., et al., *Determinants and dynamics of genome accessibility*. Nat Rev Genet, 2011. **12**(8): p. 554-64.
13. Martin, C. and Y. Zhang, *The diverse functions of histone lysine methylation*. Nat Rev Mol Cell Biol, 2005. **6**(11): p. 838-49.
14. Bartova, E., et al., *Histone modifications and nuclear architecture: a review*. J Histochem Cytochem, 2008. **56**(8): p. 711-21.
15. Chadwick, B.P. and H.F. Willard, *Multiple spatially distinct types of facultative heterochromatin on the human inactive X chromosome*. Proc Natl Acad Sci U S A, 2004. **101**(50): p. 17450-5.
16. Guenatri, M., et al., *Mouse centric and pericentric satellite repeats form distinct functional heterochromatin*. J Cell Biol, 2004. **166**(4): p. 493-505.
17. Ernst, J., et al., *Mapping and analysis of chromatin state dynamics in nine human cell types*. Nature, 2011. **473**(7345): p. 43-9.

REFERENCES

18. Ernst, J. and M. Kellis, *ChromHMM: automating chromatin-state discovery and characterization*. Nat Methods, 2012. **9**(3): p. 215-6.
19. Ernst, J. and M. Kellis, *Chromatin-state discovery and genome annotation with ChromHMM*. Nat Protoc, 2017. **12**(12): p. 2478-2492.
20. Bestor, T.H., J.R. Edwards, and M. Boulard, *Notes on the role of dynamic DNA methylation in mammalian development*. Proc Natl Acad Sci U S A, 2015. **112**(22): p. 6796-9.
21. Schubeler, D., *Function and information content of DNA methylation*. Nature, 2015. **517**(7534): p. 321-6.
22. Sharif, J., et al., *The SRA protein Np95 mediates epigenetic inheritance by recruiting Dnmt1 to methylated DNA*. Nature, 2007. **450**(7171): p. 908-12.
23. Bashtrykov, P., et al., *The UHRF1 protein stimulates the activity and specificity of the maintenance DNA methyltransferase DNMT1 by an allosteric mechanism*. J Biol Chem, 2014. **289**(7): p. 4106-15.
24. Qin, W., et al., *DNA methylation requires a DNMT1 ubiquitin interacting motif (UIM) and histone ubiquitination*. Cell Res, 2015. **25**(8): p. 911-29.
25. Margot, J.B., et al., *Structure and function of the mouse DNA methyltransferase gene: Dnmt1 shows a tripartite structure*. J Mol Biol, 2000. **297**(2): p. 293-300.
26. Fatemi, M., et al., *The activity of the murine DNA methyltransferase Dnmt1 is controlled by interaction of the catalytic domain with the N-terminal part of the enzyme leading to an allosteric activation of the enzyme after binding to methylated DNA*. J Mol Biol, 2001. **309**(5): p. 1189-99.
27. Ito, S., et al., *Tet proteins can convert 5-methylcytosine to 5-formylcytosine and 5-carboxylcytosine*. Science, 2011. **333**(6047): p. 1300-3.
28. He, Y.F., et al., *Tet-mediated formation of 5-carboxylcytosine and its excision by TDG in mammalian DNA*. Science, 2011. **333**(6047): p. 1303-7.
29. Pfaffeneder, T., et al., *The discovery of 5-formylcytosine in embryonic stem cell DNA*. Angew Chem Int Ed Engl, 2011. **50**(31): p. 7008-12.
30. Frias-Lasserre, D. and C.A. Villagra, *The Importance of ncRNAs as Epigenetic Mechanisms in Phenotypic Variation and Organic Evolution*. Front Microbiol, 2017. **8**: p. 2483.
31. Strahl, B.D. and C.D. Allis, *The language of covalent histone modifications*. Nature, 2000. **403**(6765): p. 41-5.
32. Henikoff, S. and A. Shilatifard, *Histone modification: cause or cog?* Trends Genet, 2011. **27**(10): p. 389-96.
33. Rando, O.J., *Combinatorial complexity in chromatin structure and function: revisiting the histone code*. Curr Opin Genet Dev, 2012. **22**(2): p. 148-55.
34. Bannister, A.J. and T. Kouzarides, *Regulation of chromatin by histone modifications*. Cell Res, 2011. **21**(3): p. 381-95.

REFERENCES

35. Rothbart, S.B. and B.D. Strahl, *Interpreting the language of histone and DNA modifications*. Biochim Biophys Acta, 2014. **1839**(8): p. 627-43.
36. Clarke, S., *Protein methylation*. Curr Opin Cell Biol, 1993. **5**(6): p. 977-83.
37. Tachibana, M., et al., *G9a histone methyltransferase plays a dominant role in euchromatic histone H3 lysine 9 methylation and is essential for early embryogenesis*. Genes Dev, 2002. **16**(14): p. 1779-91.
38. Cao, R., et al., *Role of histone H3 lysine 27 methylation in Polycomb-group silencing*. Science, 2002. **298**(5595): p. 1039-43.
39. Rea, S., et al., *Regulation of chromatin structure by site-specific histone H3 methyltransferases*. Nature, 2000. **406**(6796): p. 593-9.
40. Tsukada, Y., et al., *Histone demethylation by a family of JmjC domain-containing proteins*. Nature, 2006. **439**(7078): p. 811-6.
41. Black, J.C., C. Van Rechem, and J.R. Whetstine, *Histone lysine methylation dynamics: establishment, regulation, and biological impact*. Mol Cell, 2012. **48**(4): p. 491-507.
42. Vastenhouw, N.L. and A.F. Schier, *Bivalent histone modifications in early embryogenesis*. Curr Opin Cell Biol, 2012. **24**(3): p. 374-86.
43. Li, F., et al., *Bivalent Histone Modifications and Development*. Curr Stem Cell Res Ther, 2018. **13**(2): p. 83-90.
44. Bannister, A.J., et al., *Spatial distribution of di- and tri-methyl lysine 36 of histone H3 at active genes*. J Biol Chem, 2005. **280**(18): p. 17732-6.
45. Musselman, C.A., et al., *Perceiving the epigenetic landscape through histone readers*. Nat Struct Mol Biol, 2012. **19**(12): p. 1218-27.
46. Grunstein, M., *Histone acetylation in chromatin structure and transcription*. Nature, 1997. **389**(6649): p. 349-52.
47. Roth, S.Y., J.M. Denu, and C.D. Allis, *Histone acetyltransferases*. Annu Rev Biochem, 2001. **70**: p. 81-120.
48. Shogren-Knaak, M., et al., *Histone H4-K16 acetylation controls chromatin structure and protein interactions*. Science, 2006. **311**(5762): p. 844-7.
49. Shahbazian, M.D. and M. Grunstein, *Functions of site-specific histone acetylation and deacetylation*. Annu Rev Biochem, 2007. **76**: p. 75-100.
50. Dhalluin, C., et al., *Structure and ligand of a histone acetyltransferase bromodomain*. Nature, 1999. **399**(6735): p. 491-6.
51. Taylor, G.C., et al., *H4K16 acetylation marks active genes and enhancers of embryonic stem cells, but does not alter chromatin compaction*. Genome Res, 2013. **23**(12): p. 2053-65.
52. Zeng, L. and M.M. Zhou, *Bromodomain: an acetyl-lysine binding domain*. FEBS Lett, 2002. **513**(1): p. 124-8.

REFERENCES

53. Johnson, L.N. and R.J. Lewis, *Structural basis for control by phosphorylation*. Chem Rev, 2001. **101**(8): p. 2209-42.
54. Hendzel, M.J., et al., *Mitosis-specific phosphorylation of histone H3 initiates primarily within pericentromeric heterochromatin during G2 and spreads in an ordered fashion coincident with mitotic chromosome condensation*. Chromosoma, 1997. **106**(6): p. 348-60.
55. Zippo, A., et al., *Histone crosstalk between H3S10ph and H4K16ac generates a histone code that mediates transcription elongation*. Cell, 2009. **138**(6): p. 1122-36.
56. Kawashima, S.A., et al., *Phosphorylation of H2A by Bub1 prevents chromosomal instability through localizing shugoshin*. Science, 2010. **327**(5962): p. 172-7.
57. Polioudaki, H., et al., *Mitotic phosphorylation of histone H3 at threonine 3*. FEBS Lett, 2004. **560**(1-3): p. 39-44.
58. Clapier, C.R., et al., *Mechanisms of action and regulation of ATP-dependent chromatin-remodelling complexes*. Nat Rev Mol Cell Biol, 2017. **18**(7): p. 407-422.
59. Hota, S.K. and B.G. Bruneau, *ATP-dependent chromatin remodeling during mammalian development*. Development, 2016. **143**(16): p. 2882-97.
60. Tong, J.K., et al., *Chromatin deacetylation by an ATP-dependent nucleosome remodelling complex*. Nature, 1998. **395**(6705): p. 917-21.
61. Wade, P.A., et al., *A multiple subunit Mi-2 histone deacetylase from Xenopus laevis cofractionates with an associated Snf2 superfamily ATPase*. Curr Biol, 1998. **8**(14): p. 843-6.
62. Xue, Y., et al., *NURD, a novel complex with both ATP-dependent chromatin-remodeling and histone deacetylase activities*. Mol Cell, 1998. **2**(6): p. 851-61.
63. Zhang, Y., et al., *The dermatomyositis-specific autoantigen Mi2 is a component of a complex containing histone deacetylase and nucleosome remodeling activities*. Cell, 1998. **95**(2): p. 279-89.
64. Denslow, S.A. and P.A. Wade, *The human Mi-2/NuRD complex and gene regulation*. Oncogene, 2007. **26**(37): p. 5433-8.
65. Lai, A.Y. and P.A. Wade, *Cancer biology and NuRD: a multifaceted chromatin remodelling complex*. Nat Rev Cancer, 2011. **11**(8): p. 588-96.
66. Li, D.Q. and R. Kumar, *Mi-2/NuRD complex making inroads into DNA-damage response pathway*. Cell Cycle, 2010. **9**(11): p. 2071-9.
67. Allen, H.F., P.A. Wade, and T.G. Kutateladze, *The NuRD architecture*. Cell Mol Life Sci, 2013. **70**(19): p. 3513-24.
68. de Dieuleveult, M., et al., *Genome-wide nucleosome specificity and function of chromatin remodellers in ES cells*. Nature, 2016. **530**(7588): p. 113-6.
69. Miller, A., et al., *Sall4 controls differentiation of pluripotent cells independently of the Nucleosome Remodelling and Deacetylation (NuRD) complex*. Development, 2016. **143**(17): p. 3074-84.

REFERENCES

70. Shimbo, T., et al., *MBD3 localizes at promoters, gene bodies and enhancers of active genes*. PLoS Genet, 2013. **9**(12): p. e1004028.
71. Stevens, T.J., et al., *3D structures of individual mammalian genomes studied by single-cell Hi-C*. Nature, 2017. **544**(7648): p. 59-64.
72. Hu, G. and P.A. Wade, *NuRD and pluripotency: a complex balancing act*. Cell Stem Cell, 2012. **10**(5): p. 497-503.
73. Keenen, B. and I.L. de la Serna, *Chromatin remodeling in embryonic stem cells: regulating the balance between pluripotency and differentiation*. J Cell Physiol, 2009. **219**(1): p. 1-7.
74. Marzluff, W.F., E.J. Wagner, and R.J. Duronio, *Metabolism and regulation of canonical histone mRNAs: life without a poly(A) tail*. Nat Rev Genet, 2008. **9**(11): p. 843-54.
75. Maze, I., et al., *Every amino acid matters: essential contributions of histone variants to mammalian development and disease*. Nat Rev Genet, 2014. **15**(4): p. 259-71.
76. Henikoff, S., T. Furuyama, and K. Ahmad, *Histone variants, nucleosome assembly and epigenetic inheritance*. Trends Genet, 2004. **20**(7): p. 320-6.
77. Talbert, P.B., et al., *A unified phylogeny-based nomenclature for histone variants*. Epigenetics Chromatin, 2012. **5**: p. 7.
78. Goldberg, A.D., et al., *Distinct factors control histone variant H3.3 localization at specific genomic regions*. Cell, 2010. **140**(5): p. 678-91.
79. Wiedemann, S.M., et al., *Identification and characterization of two novel primate-specific histone H3 variants, H3.X and H3.Y*. J Cell Biol, 2010. **190**(5): p. 777-91.
80. Tachiwana, H., et al., *Nucleosome formation with the testis-specific histone H3 variant, H3t, by human nucleosome assembly proteins in vitro*. Nucleic Acids Res, 2008. **36**(7): p. 2208-18.
81. Urahama, T., et al., *Histone H3.5 forms an unstable nucleosome and accumulates around transcription start sites in human testis*. Epigenetics Chromatin, 2016. **9**: p. 2.
82. Black, B.E. and D.W. Cleveland, *Epigenetic centromere propagation and the nature of CENP-a nucleosomes*. Cell, 2011. **144**(4): p. 471-9.
83. Urahama, T., et al., *Structure of human nucleosome containing the testis-specific histone variant TSH2B*. Acta Crystallogr F Struct Biol Commun, 2014. **70**(Pt 4): p. 444-9.
84. Montellier, E., et al., *Chromatin-to-nucleoprotamine transition is controlled by the histone H2B variant TH2B*. Genes Dev, 2013. **27**(15): p. 1680-92.
85. Shinagawa, T., et al., *Histone variants enriched in oocytes enhance reprogramming to induced pluripotent stem cells*. Cell Stem Cell, 2014. **14**(2): p. 217-27.
86. Boulard, M., et al., *The NH2 tail of the novel histone variant H2BFWT exhibits properties distinct from conventional H2B with respect to the assembly of mitotic chromosomes*. Mol Cell Biol, 2006. **26**(4): p. 1518-26.

REFERENCES

87. Chadwick, B.P. and H.F. Willard, *A novel chromatin protein, distantly related to histone H2A, is largely excluded from the inactive X chromosome*. J Cell Biol, 2001. **152**(2): p. 375-84.
88. Bao, Y., et al., *Nucleosomes containing the histone variant H2A.Bbd organize only 118 base pairs of DNA*. EMBO J, 2004. **23**(16): p. 3314-24.
89. Doyen, C.M., et al., *Dissection of the unusual structural and functional properties of the variant H2A.Bbd nucleosome*. EMBO J, 2006. **25**(18): p. 4234-44.
90. Tolstorukov, M.Y., et al., *Histone variant H2A.Bbd is associated with active transcription and mRNA processing in human cells*. Mol Cell, 2012. **47**(4): p. 596-607.
91. Fernandez-Capetillo, O., et al., *H2AX: the histone guardian of the genome*. DNA Repair (Amst), 2004. **3**(8-9): p. 959-67.
92. Bao, Y., *Chromatin response to DNA double-strand break damage*. Epigenomics, 2011. **3**(3): p. 307-21.
93. Turinetto, V. and C. Giachino, *Multiple facets of histone variant H2AX: a DNA double-strand-break marker with several biological functions*. Nucleic Acids Res, 2015. **43**(5): p. 2489-98.
94. Singh, I., et al., *High mobility group protein-mediated transcription requires DNA damage marker gamma-H2AX*. Cell Res, 2015. **25**(7): p. 837-50.
95. Chakravarthy, S., et al., *Structural characterization of the histone variant macroH2A*. Mol Cell Biol, 2005. **25**(17): p. 7616-24.
96. Buschbeck, M., et al., *The histone variant macroH2A is an epigenetic regulator of key developmental genes*. Nat Struct Mol Biol, 2009. **16**(10): p. 1074-9.
97. Doyen, C.M., et al., *Mechanism of polymerase II transcription repression by the histone variant macroH2A*. Mol Cell Biol, 2006. **26**(3): p. 1156-64.
98. Changolkar, L.N., G. Singh, and J.R. Pehrson, *macroH2A1-dependent silencing of endogenous murine leukemia viruses*. Mol Cell Biol, 2008. **28**(6): p. 2059-65.
99. Costanzi, C. and J.R. Pehrson, *Histone macroH2A1 is concentrated in the inactive X chromosome of female mammals*. Nature, 1998. **393**(6685): p. 599-601.
100. Angelov, D., et al., *The histone variant macroH2A interferes with transcription factor binding and SWI/SNF nucleosome remodeling*. Mol Cell, 2003. **11**(4): p. 1033-41.
101. Changolkar, L.N., et al., *Developmental changes in histone macroH2A1-mediated gene regulation*. Mol Cell Biol, 2007. **27**(7): p. 2758-64.
102. Fan, J.Y., et al., *H2A.Z alters the nucleosome surface to promote HP1alpha-mediated chromatin fiber folding*. Mol Cell, 2004. **16**(4): p. 655-61.
103. Suto, R.K., et al., *Crystal structure of a nucleosome core particle containing the variant histone H2A.Z*. Nat Struct Biol, 2000. **7**(12): p. 1121-4.
104. Thambirajah, A.A., et al., *H2A.Z stabilizes chromatin in a way that is dependent on core histone acetylation*. J Biol Chem, 2006. **281**(29): p. 20036-44.

REFERENCES

105. Placek, B.J., et al., *The H2A.Z/H2B dimer is unstable compared to the dimer containing the major H2A isoform*. Protein Sci, 2005. **14**(2): p. 514-22.
106. Park, Y.J., et al., *A new fluorescence resonance energy transfer approach demonstrates that the histone variant H2AZ stabilizes the histone octamer within the nucleosome*. J Biol Chem, 2004. **279**(23): p. 24274-82.
107. Henikoff, S., et al., *Genome-wide profiling of salt fractions maps physical properties of chromatin*. Genome Res, 2009. **19**(3): p. 460-9.
108. Zhang, H., D.N. Roberts, and B.R. Cairns, *Genome-wide dynamics of Htz1, a histone H2A variant that poises repressed/basal promoters for activation through histone loss*. Cell, 2005. **123**(2): p. 219-31.
109. Rudnizky, S., et al., *H2A.Z controls the stability and mobility of nucleosomes to regulate expression of the LH genes*. Nat Commun, 2016. **7**: p. 12958.
110. Zlatanova, J. and A. Thakar, *H2A.Z: view from the top*. Structure, 2008. **16**(2): p. 166-79.
111. Bonisch, C. and S.B. Hake, *Histone H2A variants in nucleosomes and chromatin: more or less stable?* Nucleic Acids Res, 2012. **40**(21): p. 10719-41.
112. Chakravarthy, S., et al., *Structural characterization of histone H2A variants*. Cold Spring Harb Symp Quant Biol, 2004. **69**: p. 227-34.
113. Horikoshi, N., et al., *Crystal structures of heterotypic nucleosomes containing histones H2A.Z and H2A*. Open Biol, 2016. **6**(6).
114. Nekrasov, M., et al., *Histone variant selectivity at the transcription start site: H2A.Z or H2A.Lap1*. Nucleus, 2013. **4**(6): p. 431-8.
115. Dryhurst, D., et al., *Characterization of the histone H2A.Z-1 and H2A.Z-2 isoforms in vertebrates*. BMC Biol, 2009. **7**: p. 86.
116. Eirin-Lopez, J.M., et al., *The evolutionary differentiation of two histone H2A.Z variants in chordates (H2A.Z-1 and H2A.Z-2) is mediated by a stepwise mutation process that affects three amino acid residues*. BMC Evol Biol, 2009. **9**: p. 31.
117. Matsuda, R., et al., *Identification and characterization of the two isoforms of the vertebrate H2A.Z histone variant*. Nucleic Acids Res, 2010. **38**(13): p. 4263-73.
118. Bonisch, C., et al., *H2A.Z.2.2 is an alternatively spliced histone H2A.Z variant that causes severe nucleosome destabilization*. Nucleic Acids Res, 2012. **40**(13): p. 5951-64.
119. Horikoshi, N., et al., *Structural polymorphism in the L1 loop regions of human H2A.Z.1 and H2A.Z.2*. Acta Crystallogr D Biol Crystallogr, 2013. **69**(Pt 12): p. 2431-9.
120. Vardabasso, C., et al., *Histone Variant H2A.Z.2 Mediates Proliferation and Drug Sensitivity of Malignant Melanoma*. Mol Cell, 2015. **59**(1): p. 75-88.
121. Punzeler, S., et al., *Multivalent binding of PWWP2A to H2A.Z regulates mitosis and neural crest differentiation*. EMBO J, 2017.

REFERENCES

122. Luk, E., et al., *Chz1, a nuclear chaperone for histone H2AZ*. Mol Cell, 2007. **25**(3): p. 357-68.
123. Straube, K., J.S. Blackwell, Jr., and L.F. Pemberton, *Nap1 and Chz1 have separate Htz1 nuclear import and assembly functions*. Traffic, 2010. **11**(2): p. 185-97.
124. Latrick, C.M., et al., *Molecular basis and specificity of H2A.Z-H2B recognition and deposition by the histone chaperone YL1*. Nat Struct Mol Biol, 2016. **23**(4): p. 309-16.
125. Liang, X., et al., *Structural basis of H2A.Z recognition by SRCAP chromatin-remodeling subunit YL1*. Nat Struct Mol Biol, 2016. **23**(4): p. 317-23.
126. Mao, Z., et al., *Anp32e, a higher eukaryotic histone chaperone directs preferential recognition for H2A.Z*. Cell Res, 2014. **24**(4): p. 389-99.
127. Obri, A., et al., *ANP32E is a histone chaperone that removes H2A.Z from chromatin*. Nature, 2014. **505**(7485): p. 648-53.
128. Cai, Y., et al., *The mammalian YL1 protein is a shared subunit of the TRRAP/TIP60 histone acetyltransferase and SRCAP complexes*. J Biol Chem, 2005. **280**(14): p. 13665-70.
129. Ruhl, D.D., et al., *Purification of a human SRCAP complex that remodels chromatin by incorporating the histone variant H2A.Z into nucleosomes*. Biochemistry, 2006. **45**(17): p. 5671-7.
130. Gevry, N., et al., *p21 transcription is regulated by differential localization of histone H2A.Z*. Genes Dev, 2007. **21**(15): p. 1869-81.
131. Hsu, C.C., et al., *Recognition of histone acetylation by the GAS41 YEATS domain promotes H2A.Z deposition in non-small cell lung cancer*. Genes Dev, 2018. **32**(1): p. 58-69.
132. Carr, A.M., et al., *Analysis of a histone H2A variant from fission yeast: evidence for a role in chromosome stability*. Mol Gen Genet, 1994. **245**(5): p. 628-35.
133. Jackson, J.D. and M.A. Gorovsky, *Histone H2A.Z has a conserved function that is distinct from that of the major H2A sequence variants*. Nucleic Acids Res, 2000. **28**(19): p. 3811-6.
134. van Daal, A. and S.C. Elgin, *A histone variant, H2AvD, is essential in Drosophila melanogaster*. Mol Biol Cell, 1992. **3**(6): p. 593-602.
135. Clarkson, M.J., et al., *Regions of variant histone His2AvD required for Drosophila development*. Nature, 1999. **399**(6737): p. 694-7.
136. Iouzalén, N., J. Moreau, and M. Mechali, *H2A.ZI, a new variant histone expressed during Xenopus early development exhibits several distinct features from the core histone H2A*. Nucleic Acids Res, 1996. **24**(20): p. 3947-52.
137. Ridgway, P., et al., *Unique residues on the H2A.Z containing nucleosome surface are important for Xenopus laevis development*. J Biol Chem, 2004. **279**(42): p. 43815-20.
138. Faast, R., et al., *Histone variant H2A.Z is required for early mammalian development*. Curr Biol, 2001. **11**(15): p. 1183-7.

REFERENCES

139. Dunn, C.J., et al., *Histone Hypervariants H2A.Z.1 and H2A.Z.2 Play Independent and Context-Specific Roles in Neuronal Activity-Induced Transcription of Arc/Arg3.1 and Other Immediate Early Genes*. eNeuro, 2017. **4**(4).
140. Maruyama, E.O., et al., *The actin family member Arp6 and the histone variant H2A.Z are required for spatial positioning of chromatin in chicken cell nuclei*. J Cell Sci, 2012. **125**(Pt 16): p. 3739-43.
141. Kusakabe, M., et al., *Genetic complementation analysis showed distinct contributions of the N-terminal tail of H2A.Z to epigenetic regulations*. Genes Cells, 2016. **21**(2): p. 122-35.
142. Raisner, R.M., et al., *Histone variant H2A.Z marks the 5' ends of both active and inactive genes in euchromatin*. Cell, 2005. **123**(2): p. 233-48.
143. Hardy, S., et al., *The euchromatic and heterochromatic landscapes are shaped by antagonizing effects of transcription on H2A.Z deposition*. PLoS Genet, 2009. **5**(10): p. e1000687.
144. Hu, G., et al., *H2A.Z facilitates access of active and repressive complexes to chromatin in embryonic stem cell self-renewal and differentiation*. Cell Stem Cell, 2013. **12**(2): p. 180-92.
145. Jin, C., et al., *H3.3/H2A.Z double variant-containing nucleosomes mark 'nucleosome-free regions' of active promoters and other regulatory regions*. Nat Genet, 2009. **41**(8): p. 941-5.
146. Barski, A., et al., *High-resolution profiling of histone methylations in the human genome*. Cell, 2007. **129**(4): p. 823-37.
147. Guillemette, B., et al., *Variant histone H2A.Z is globally localized to the promoters of inactive yeast genes and regulates nucleosome positioning*. PLoS Biol, 2005. **3**(12): p. e384.
148. Soboleva, T.A., et al., *Histone variants at the transcription start-site*. Trends Genet, 2014. **30**(5): p. 199-209.
149. Zilberman, D., et al., *Histone H2A.Z and DNA methylation are mutually antagonistic chromatin marks*. Nature, 2008. **456**(7218): p. 125-9.
150. Conerly, M.L., et al., *Changes in H2A.Z occupancy and DNA methylation during B-cell lymphomagenesis*. Genome Res, 2010. **20**(10): p. 1383-90.
151. Murphy, P.J., et al., *Placeholder Nucleosomes Underlie Germline-to-Embryo DNA Methylation Reprogramming*. Cell, 2018. **172**(5): p. 993-1006 e13.
152. Sarcinella, E., et al., *Monoubiquitylation of H2A.Z distinguishes its association with euchromatin or facultative heterochromatin*. Mol Cell Biol, 2007. **27**(18): p. 6457-68.
153. Kim, K., et al., *Gene dysregulation by histone variant H2A.Z in bladder cancer*. Epigenetics Chromatin, 2013. **6**(1): p. 34.
154. Bargaje, R., et al., *Proximity of H2A.Z containing nucleosome to the transcription start site influences gene expression levels in the mammalian liver and brain*. Nucleic Acids Res, 2012. **40**(18): p. 8965-78.

REFERENCES

155. Weber, C.M., S. Ramachandran, and S. Henikoff, *Nucleosomes are context-specific, H2A.Z-modulated barriers to RNA polymerase*. *Mol Cell*, 2014. **53**(5): p. 819-30.
156. Ku, M., et al., *H2A.Z landscapes and dual modifications in pluripotent and multipotent stem cells underlie complex genome regulatory functions*. *Genome Biol*, 2012. **13**(10): p. R85.
157. Brunelle, M., et al., *The histone variant H2A.Z is an important regulator of enhancer activity*. *Nucleic Acids Res*, 2015. **43**(20): p. 9742-56.
158. Guillemette, B. and L. Gaudreau, *Reuniting the contrasting functions of H2A.Z*. *Biochem Cell Biol*, 2006. **84**(4): p. 528-35.
159. Marques, M., et al., *Reconciling the positive and negative roles of histone H2A.Z in gene transcription*. *Epigenetics*, 2010. **5**(4): p. 267-72.
160. Rangasamy, D., et al., *Pericentric heterochromatin becomes enriched with H2A.Z during early mammalian development*. *EMBO J*, 2003. **22**(7): p. 1599-607.
161. Greaves, I.K., et al., *H2A.Z contributes to the unique 3D structure of the centromere*. *Proc Natl Acad Sci U S A*, 2007. **104**(2): p. 525-30.
162. Boyarchuk, E., et al., *The histone variant composition of centromeres is controlled by the pericentric heterochromatin state during the cell cycle*. *J Cell Sci*, 2014. **127**(Pt 15): p. 3347-59.
163. Ryan, D.P. and D.J. Tremethick, *The interplay between H2A.Z and H3K9 methylation in regulating HP1alpha binding to linker histone-containing chromatin*. *Nucleic Acids Res*, 2018.
164. Kelly, T.K., et al., *H2A.Z maintenance during mitosis reveals nucleosome shifting on mitotically silenced genes*. *Mol Cell*, 2010. **39**(6): p. 901-11.
165. Gallant-Behm, C.L., et al., *DeltaNp63alpha represses anti-proliferative genes via H2A.Z deposition*. *Genes Dev*, 2012. **26**(20): p. 2325-36.
166. Creighton, M.P., et al., *H2AZ is enriched at polycomb complex target genes in ES cells and is necessary for lineage commitment*. *Cell*, 2008. **135**(4): p. 649-61.
167. Illingworth, R.S., et al., *PRC1 and PRC2 are not required for targeting of H2A.Z to developmental genes in embryonic stem cells*. *PLoS One*, 2012. **7**(4): p. e34848.
168. Wang, J., et al., *Pluripotency Activity of Nanog Requires Biochemical Stabilization by Variant Histone Protein H2A.Z*. *Stem Cells*, 2015. **33**(7): p. 2126-34.
169. Li, Z., et al., *Foxa2 and H2A.Z mediate nucleosome depletion during embryonic stem cell differentiation*. *Cell*, 2012. **151**(7): p. 1608-16.
170. Wang, Y., et al., *Histone variants H2A.Z and H3.3 coordinately regulate PRC2-dependent H3K27me3 deposition and gene expression regulation in mES cells*. *BMC Biol*, 2018. **16**(1): p. 107.
171. Domaschenz, R., et al., *The Histone Variant H2A.Z Is a Master Regulator of the Epithelial-Mesenchymal Transition*. *Cell Rep*, 2017. **21**(4): p. 943-952.

REFERENCES

172. Yang, S.S., et al., *Eukaryotic initiation factor 6 modulates myofibroblast differentiation at transforming growth factor-beta1 transcription level via H2A.Z occupancy and Sp1 recruitment*. J Cell Sci, 2015. **128**(21): p. 3977-89.
173. Zovkic, I.B., et al., *Histone H2A.Z subunit exchange controls consolidation of recent and remote memory*. Nature, 2014. **515**(7528): p. 582-6.
174. Stefanelli, G., et al., *Learning and Age-Related Changes in Genome-wide H2A.Z Binding in the Mouse Hippocampus*. Cell Rep, 2018. **22**(5): p. 1124-1131.
175. Shen, T., et al., *Brain-specific deletion of histone variant H2A.z results in cortical neurogenesis defects and neurodevelopmental disorder*. Nucleic Acids Res, 2018. **46**(5): p. 2290-2307.
176. Chang, M., et al., *Association of common variants in H2AFZ gene with schizophrenia and cognitive function in patients with schizophrenia*. J Hum Genet, 2015. **60**(10): p. 619-24.
177. Nekrasov, M., et al., *Histone H2A.Z inheritance during the cell cycle and its impact on promoter organization and dynamics*. Nat Struct Mol Biol, 2012. **19**(11): p. 1076-83.
178. Rangasamy, D., I. Greaves, and D.J. Tremethick, *RNA interference demonstrates a novel role for H2A.Z in chromosome segregation*. Nat Struct Mol Biol, 2004. **11**(7): p. 650-5.
179. Alatwi, H.E. and J.A. Downs, *Removal of H2A.Z by INO80 promotes homologous recombination*. EMBO Rep, 2015. **16**(8): p. 986-94.
180. Gursoy-Yuzugullu, O., M.K. Ayrapetov, and B.D. Price, *Histone chaperone Anp32e removes H2A.Z from DNA double-strand breaks and promotes nucleosome reorganization and DNA repair*. Proc Natl Acad Sci U S A, 2015. **112**(24): p. 7507-12.
181. Xu, Y., et al., *Histone H2A.Z controls a critical chromatin remodeling step required for DNA double-strand break repair*. Mol Cell, 2012. **48**(5): p. 723-33.
182. Brahma, S., et al., *INO80 exchanges H2A.Z for H2A by translocating on DNA proximal to histone dimers*. Nat Commun, 2017. **8**: p. 15616.
183. Papamichos-Chronakis, M., et al., *Global regulation of H2A.Z localization by the INO80 chromatin-remodeling enzyme is essential for genome integrity*. Cell, 2011. **144**(2): p. 200-13.
184. Yang, H.D., et al., *Oncogenic potential of histone-variant H2A.Z.1 and its regulatory role in cell cycle and epithelial-mesenchymal transition in liver cancer*. Oncotarget, 2016. **7**(10): p. 11412-23.
185. Hua, S., et al., *Genomic analysis of estrogen cascade reveals histone variant H2A.Z associated with breast cancer progression*. Mol Syst Biol, 2008. **4**: p. 188.
186. Dryhurst, D., et al., *Histone H2A.Z prepares the prostate specific antigen (PSA) gene for androgen receptor-mediated transcription and is upregulated in a model of prostate cancer progression*. Cancer Lett, 2012. **315**(1): p. 38-47.
187. Sevilla, A. and O. Binda, *Post-translational modifications of the histone variant H2AZ*. Stem Cell Res, 2014. **12**(1): p. 289-95.

REFERENCES

188. Corujo, D. and M. Buschbeck, *Post-Translational Modifications of H2A Histone Variants and Their Role in Cancer*. *Cancers (Basel)*, 2018. **10**(3).
189. Draker, R., E. Sarcinella, and P. Cheung, *USP10 deubiquitylates the histone variant H2A.Z and both are required for androgen receptor-mediated gene activation*. *Nucleic Acids Res*, 2011. **39**(9): p. 3529-42.
190. Binda, O., et al., *SETD6 monomethylates H2AZ on lysine 7 and is required for the maintenance of embryonic stem cell self-renewal*. *Epigenetics*, 2013. **8**(2): p. 177-83.
191. Tsai, C.H., et al., *SMYD3-Mediated H2A.Z.1 Methylation Promotes Cell Cycle and Cancer Proliferation*. *Cancer Res*, 2016. **76**(20): p. 6043-6053.
192. Fukuto, A., et al., *SUMO modification system facilitates the exchange of histone variant H2A.Z-2 at DNA damage sites*. *Nucleus*, 2018. **9**(1): p. 87-94.
193. Ishibashi, T., et al., *Acetylation of vertebrate H2A.Z and its effect on the structure of the nucleosome*. *Biochemistry*, 2009. **48**(22): p. 5007-17.
194. Keogh, M.C., et al., *The Saccharomyces cerevisiae histone H2A variant Htz1 is acetylated by NuA4*. *Genes Dev*, 2006. **20**(6): p. 660-5.
195. Millar, C.B., et al., *Acetylation of H2AZ Lys 14 is associated with genome-wide gene activity in yeast*. *Genes Dev*, 2006. **20**(6): p. 711-22.
196. Giaimo, B.D., et al., *Histone variant H2A.Z deposition and acetylation directs the canonical Notch signaling response*. *Nucleic Acids Res*, 2018.
197. Perell, G.T., et al., *Specific Acetylation Patterns of H2A.Z Form Transient Interactions with the BPTF Bromodomain*. *Biochemistry*, 2017. **56**(35): p. 4607-4615.
198. Bruce, K., et al., *The replacement histone H2A.Z in a hyperacetylated form is a feature of active genes in the chicken*. *Nucleic Acids Res*, 2005. **33**(17): p. 5633-9.
199. Valdes-Mora, F., et al., *Acetylation of H2A.Z is a key epigenetic modification associated with gene deregulation and epigenetic remodeling in cancer*. *Genome Res*, 2012. **22**(2): p. 307-21.
200. Valdes-Mora, F., et al., *Acetylated histone variant H2A.Z is involved in the activation of neo-enhancers in prostate cancer*. *Nat Commun*, 2017. **8**(1): p. 1346.
201. Colino-Sanguino, Y., S.J. Clark, and F. Valdes-Mora, *H2A.Z acetylation and transcription: ready, steady, go!* *Epigenomics*, 2016. **8**(5): p. 583-6.
202. Law, C. and P. Cheung, *Expression of Non-acetylatable H2A.Z in Myoblast Cells Blocks Myoblast Differentiation through Disruption of MyoD Expression*. *J Biol Chem*, 2015. **290**(21): p. 13234-49.
203. Atkinson, T.J. and M.S. Halfon, *Regulation of gene expression in the genomic context*. *Comput Struct Biotechnol J*, 2014. **9**: p. e201401001.
204. Nolis, I.K., et al., *Transcription factors mediate long-range enhancer-promoter interactions*. *Proc Natl Acad Sci U S A*, 2009. **106**(48): p. 20222-7.

REFERENCES

205. Consortium, E.P., *An integrated encyclopedia of DNA elements in the human genome*. Nature, 2012. **489**(7414): p. 57-74.
206. Chen, H., et al., *Non-coding Transcripts from Enhancers: New Insights into Enhancer Activity and Gene Expression Regulation*. Genomics Proteomics Bioinformatics, 2017. **15**(3): p. 201-207.
207. Gibcus, J.H. and J. Dekker, *The hierarchy of the 3D genome*. Mol Cell, 2013. **49**(5): p. 773-82.
208. Kim, S., N.K. Yu, and B.K. Kaang, *CTCF as a multifunctional protein in genome regulation and gene expression*. Exp Mol Med, 2015. **47**: p. e166.
209. Heintzman, N.D., et al., *Distinct and predictive chromatin signatures of transcriptional promoters and enhancers in the human genome*. Nat Genet, 2007. **39**(3): p. 311-8.
210. Creighton, M.P., et al., *Histone H3K27ac separates active from poised enhancers and predicts developmental state*. Proc Natl Acad Sci U S A, 2010. **107**(50): p. 21931-6.
211. Skalska, L., et al., *Chromatin signatures at Notch-regulated enhancers reveal large-scale changes in H3K56ac upon activation*. EMBO J, 2015. **34**(14): p. 1889-904.
212. Heintzman, N.D., et al., *Histone modifications at human enhancers reflect global cell-type-specific gene expression*. Nature, 2009. **459**(7243): p. 108-12.
213. Dorschner, M.O., et al., *High-throughput localization of functional elements by quantitative chromatin profiling*. Nat Methods, 2004. **1**(3): p. 219-25.
214. Shen, L., et al., *Genome-wide analysis reveals TET- and TDG-dependent 5-methylcytosine oxidation dynamics*. Cell, 2013. **153**(3): p. 692-706.
215. Song, C.X., et al., *Genome-wide profiling of 5-formylcytosine reveals its roles in epigenetic priming*. Cell, 2013. **153**(3): p. 678-91.
216. Zentner, G.E., P.J. Tesar, and P.C. Scacheri, *Epigenetic signatures distinguish multiple classes of enhancers with distinct cellular functions*. Genome Res, 2011. **21**(8): p. 1273-83.
217. Deaton, A.M. and A. Bird, *CpG islands and the regulation of transcription*. Genes Dev, 2011. **25**(10): p. 1010-22.
218. Liang, G., et al., *Distinct localization of histone H3 acetylation and H3-K4 methylation to the transcription start sites in the human genome*. Proc Natl Acad Sci U S A, 2004. **101**(19): p. 7357-62.
219. Barrera, L.O., et al., *Genome-wide mapping and analysis of active promoters in mouse embryonic stem cells and adult organs*. Genome Res, 2008. **18**(1): p. 46-59.
220. Myers, F.A., et al., *Targeted and extended acetylation of histones H4 and H3 at active and inactive genes in chicken embryo erythrocytes*. J Biol Chem, 2001. **276**(23): p. 20197-205.
221. Batta, K., et al., *Genome-wide function of H2B ubiquitylation in promoter and genic regions*. Genes Dev, 2011. **25**(21): p. 2254-65.

REFERENCES

222. Ng, H.H., et al., *Lysine-79 of histone H3 is hypomethylated at silenced loci in yeast and mammalian cells: a potential mechanism for position-effect variegation*. Proc Natl Acad Sci U S A, 2003. **100**(4): p. 1820-5.
223. Minsky, N., et al., *Monoubiquitinated H2B is associated with the transcribed region of highly expressed genes in human cells*. Nat Cell Biol, 2008. **10**(4): p. 483-8.
224. Wagner, E.J. and P.B. Carpenter, *Understanding the language of Lys36 methylation at histone H3*. Nat Rev Mol Cell Biol, 2012. **13**(2): p. 115-26.
225. Zhang, T., S. Cooper, and N. Brockdorff, *The interplay of histone modifications - writers that read*. EMBO Rep, 2015. **16**(11): p. 1467-81.
226. Draker, R., et al., *A combination of H2A.Z and H4 acetylation recruits Brd2 to chromatin during transcriptional activation*. PLoS Genet, 2012. **8**(11): p. e1003047.
227. Stec, I., et al., *WHSC1, a 90 kb SET domain-containing gene, expressed in early development and homologous to a Drosophila dysmorphia gene maps in the Wolf-Hirschhorn syndrome critical region and is fused to IgH in t(4;14) multiple myeloma*. Hum Mol Genet, 1998. **7**(7): p. 1071-82.
228. Link, S., et al., *PWWP2A binds distinct chromatin moieties and interacts with an MTA1-specific core NuRD complex*. Nat Commun, 2018. **9**(1): p. 4300.
229. Wen, H., et al., *ZMYND11 links histone H3.3K36me3 to transcription elongation and tumour suppression*. Nature, 2014. **508**(7495): p. 263-8.
230. Vezzoli, A., et al., *Molecular basis of histone H3K36me3 recognition by the PWWP domain of Brpf1*. Nat Struct Mol Biol, 2010. **17**(5): p. 617-9.
231. Rona, G.B., E.C.A. Eleutherio, and A.S. Pinheiro, *PWWP domains and their modes of sensing DNA and histone methylated lysines*. Biophys Rev, 2016. **8**(1): p. 63-74.
232. Kaji, K., et al., *The NuRD component Mbd3 is required for pluripotency of embryonic stem cells*. Nat Cell Biol, 2006. **8**(3): p. 285-92.
233. Burgold, T., et al., *Subunit redundancy within the NuRD complex ensures fidelity of ES cell lineage commitment*. bioRxiv, 2018.
234. Jeppesen, P. and B.M. Turner, *The inactive X chromosome in female mammals is distinguished by a lack of histone H4 acetylation, a cytogenetic marker for gene expression*. Cell, 1993. **74**(2): p. 281-9.
235. Schneider, K., et al., *Dissection of cell cycle-dependent dynamics of Dnmt1 by FRAP and diffusion-coupled modeling*. Nucleic Acids Res, 2013. **41**(9): p. 4860-76.
236. Sansoni, V., et al., *The histone variant H2A.Bbd is enriched at sites of DNA synthesis*. Nucleic Acids Res, 2014. **42**(10): p. 6405-20.
237. Kloet, S.L., et al., *Towards elucidating the stability, dynamics and architecture of the nucleosome remodeling and deacetylase complex by using quantitative interaction proteomics*. FEBS J, 2015. **282**(9): p. 1774-85.

REFERENCES

238. Corces, M.R., et al., *Lineage-specific and single-cell chromatin accessibility charts human hematopoiesis and leukemia evolution*. Nat Genet, 2016. **48**(10): p. 1193-203.
239. Ramirez, F., et al., *deepTools: a flexible platform for exploring deep-sequencing data*. Nucleic Acids Res, 2014. **42**(Web Server issue): p. W187-91.
240. Stielow, C., et al., *SUMOylation of the polycomb group protein L3MBTL2 facilitates repression of its target genes*. Nucleic Acids Res, 2014. **42**(5): p. 3044-58.
241. Love, M.I., W. Huber, and S. Anders, *Moderated estimation of fold change and dispersion for RNA-seq data with DESeq2*. Genome Biol, 2014. **15**(12): p. 550.
242. Gentleman, R.C., et al., *Bioconductor: open software development for computational biology and bioinformatics*. Genome Biol, 2004. **5**(10): p. R80.
243. Hahne, F. and R. Ivanek, *Visualizing Genomic Data Using Gviz and Bioconductor*. Methods Mol Biol, 2016. **1418**: p. 335-51.
244. Lawrence, M., et al., *Software for computing and annotating genomic ranges*. PLoS Comput Biol, 2013. **9**(8): p. e1003118.
245. Yu, G., L.G. Wang, and Q.Y. He, *ChIPseeker: an R/Bioconductor package for ChIP peak annotation, comparison and visualization*. Bioinformatics, 2015. **31**(14): p. 2382-3.
246. Cox, J. and M. Mann, *MaxQuant enables high peptide identification rates, individualized p.p.b.-range mass accuracies and proteome-wide protein quantification*. Nat Biotechnol, 2008. **26**(12): p. 1367-72.
247. Cox, J., et al., *Accurate proteome-wide label-free quantification by delayed normalization and maximal peptide ratio extraction, termed MaxLFQ*. Mol Cell Proteomics, 2014. **13**(9): p. 2513-26.
248. Tyanova, S., et al., *The Perseus computational platform for comprehensive analysis of (prote)omics data*. Nat Methods, 2016. **13**(9): p. 731-40.
249. Langmead, B., *Aligning short sequencing reads with Bowtie*. Curr Protoc Bioinformatics, 2010. **Chapter 11**: p. Unit 11 7.
250. Li, H., et al., *The Sequence Alignment/Map format and SAMtools*. Bioinformatics, 2009. **25**(16): p. 2078-9.
251. Lun, A.T. and G.K. Smyth, *csaw: a Bioconductor package for differential binding analysis of ChIP-seq data using sliding windows*. Nucleic Acids Res, 2016. **44**(5): p. e45.
252. Kitagawa, M. and S.H. Lee, *The chromosomal passenger complex (CPC) as a key orchestrator of orderly mitotic exit and cytokinesis*. Front Cell Dev Biol, 2015. **3**: p. 14.
253. Lischetti, T. and J. Nilsson, *Regulation of mitotic progression by the spindle assembly checkpoint*. Mol Cell Oncol, 2015. **2**(1): p. e970484.
254. Primorac, I. and A. Musacchio, *Panta rhei: the APC/C at steady state*. J Cell Biol, 2013. **201**(2): p. 177-89.

REFERENCES

255. Wood, K.W., et al., *CENP-E is a plus end-directed kinetochore motor required for metaphase chromosome alignment*. *Cell*, 1997. **91**(3): p. 357-66.
256. Woolner, S., et al., *Myosin-10 and actin filaments are essential for mitotic spindle function*. *J Cell Biol*, 2008. **182**(1): p. 77-88.
257. Heng, Y.W. and C.G. Koh, *Actin cytoskeleton dynamics and the cell division cycle*. *Int J Biochem Cell Biol*, 2010. **42**(10): p. 1622-33.
258. Sandquist, J.C., A.M. Kita, and W.M. Bement, *And the dead shall rise: actin and myosin return to the spindle*. *Dev Cell*, 2011. **21**(3): p. 410-9.
259. Cooper, J.A. and T.D. Pollard, *Effect of capping protein on the kinetics of actin polymerization*. *Biochemistry*, 1985. **24**(3): p. 793-9.
260. Janke, C., et al., *Tubulin polyglutamylase enzymes are members of the TTL domain protein family*. *Science*, 2005. **308**(5729): p. 1758-62.
261. Abal, M., G. Keryer, and M. Bornens, *Centrioles resist forces applied on centrosomes during G2/M transition*. *Biol Cell*, 2005. **97**(6): p. 425-34.
262. Waters, J.E., et al., *P-Rex1 - a multidomain protein that regulates neurite differentiation*. *J Cell Sci*, 2008. **121**(Pt 17): p. 2892-903.
263. Yoshizawa, M., et al., *Involvement of a Rac activator, P-Rex1, in neurotrophin-derived signaling and neuronal migration*. *J Neurosci*, 2005. **25**(17): p. 4406-19.
264. Krause, M., et al., *Ena/VASP proteins: regulators of the actin cytoskeleton and cell migration*. *Annu Rev Cell Dev Biol*, 2003. **19**: p. 541-64.
265. Sechi, A.S. and J. Wehland, *ENA/VASP proteins: multifunctional regulators of actin cytoskeleton dynamics*. *Front Biosci*, 2004. **9**: p. 1294-310.
266. Bear, J.E. and F.B. Gertler, *Ena/VASP: towards resolving a pointed controversy at the barbed end*. *J Cell Sci*, 2009. **122**(Pt 12): p. 1947-53.
267. Werner, E., A.P. Kowalczyk, and V. Faundez, *Anthrax toxin receptor 1/tumor endothelium marker 8 mediates cell spreading by coupling extracellular ligands to the actin cytoskeleton*. *J Biol Chem*, 2006. **281**(32): p. 23227-36.
268. Hotchkiss, K.A., et al., *TEM8 expression stimulates endothelial cell adhesion and migration by regulating cell-matrix interactions on collagen*. *Exp Cell Res*, 2005. **305**(1): p. 133-44.
269. Joshi, P., et al., *The functional interactome landscape of the human histone deacetylase family*. *Mol Syst Biol*, 2013. **9**: p. 672.
270. Hein, M.Y., et al., *A human interactome in three quantitative dimensions organized by stoichiometries and abundances*. *Cell*, 2015. **163**(3): p. 712-23.
271. Torchy, M.P., A. Hamiche, and B.P. Klaholz, *Structure and function insights into the NuRD chromatin remodeling complex*. *Cell Mol Life Sci*, 2015. **72**(13): p. 2491-507.

REFERENCES

272. Zhang, W., et al., *The Nucleosome Remodeling and Deacetylase Complex NuRD Is Built from Preformed Catalytically Active Sub-modules*. J Mol Biol, 2016. **428**(14): p. 2931-42.
273. Reynolds, N., et al., *NuRD-mediated deacetylation of H3K27 facilitates recruitment of Polycomb Repressive Complex 2 to direct gene repression*. EMBO J, 2012. **31**(3): p. 593-605.
274. Bornelov, S., et al., *The Nucleosome Remodeling and Deacetylation Complex Modulates Chromatin Structure at Sites of Active Transcription to Fine-Tune Gene Expression*. Mol Cell, 2018. **71**(1): p. 56-72 e4.
275. Berger, S.L., *The complex language of chromatin regulation during transcription*. Nature, 2007. **447**(7143): p. 407-12.
276. Li, B., M. Carey, and J.L. Workman, *The role of chromatin during transcription*. Cell, 2007. **128**(4): p. 707-19.
277. Wang, Z., et al., *Genome-wide mapping of HATs and HDACs reveals distinct functions in active and inactive genes*. Cell, 2009. **138**(5): p. 1019-31.
278. Kelly, R.D. and S.M. Cowley, *The physiological roles of histone deacetylase (HDAC) 1 and 2: complex co-stars with multiple leading parts*. Biochem Soc Trans, 2013. **41**(3): p. 741-9.
279. Kim, T.K. and R. Shiekhhattar, *Architectural and Functional Commonalities between Enhancers and Promoters*. Cell, 2015. **162**(5): p. 948-59.
280. Link, S. and S.B. Hake, *PWWP2A: A novel mitosis link?* Cell Cycle, 2017. **16**(20): p. 1849-1850.
281. Maiato, H., et al., *Mechanisms of Chromosome Congression during Mitosis*. Biology (Basel), 2017. **6**(1).
282. Sanchez, I. and B.D. Dynlacht, *New insights into cyclins, CDKs, and cell cycle control*. Semin Cell Dev Biol, 2005. **16**(3): p. 311-21.
283. Weaver, B.A., et al., *Centromere-associated protein-E is essential for the mammalian mitotic checkpoint to prevent aneuploidy due to single chromosome loss*. J Cell Biol, 2003. **162**(4): p. 551-63.
284. Putkey, F.R., et al., *Unstable kinetochore-microtubule capture and chromosomal instability following deletion of CENP-E*. Dev Cell, 2002. **3**(3): p. 351-65.
285. Plohl, M., N. Mestrovic, and B. Mravinac, *Centromere identity from the DNA point of view*. Chromosoma, 2014. **123**(4): p. 313-25.
286. Rosenblatt, J., et al., *Myosin II-dependent cortical movement is required for centrosome separation and positioning during mitotic spindle assembly*. Cell, 2004. **117**(3): p. 361-72.
287. Bear, J.E., et al., *Antagonism between Ena/VASP proteins and actin filament capping regulates fibroblast motility*. Cell, 2002. **109**(4): p. 509-21.
288. Edwards, M., et al., *Capping protein regulators fine-tune actin assembly dynamics*. Nat Rev Mol Cell Biol, 2014. **15**(10): p. 677-89.

REFERENCES

289. Bartolini, F., N. Ramalingam, and G.G. Gundersen, *Actin-capping protein promotes microtubule stability by antagonizing the actin activity of mDia1*. *Mol Biol Cell*, 2012. **23**(20): p. 4032-40.
290. Jonkman, J.E., et al., *An introduction to the wound healing assay using live-cell microscopy*. *Cell Adh Migr*, 2014. **8**(5): p. 440-51.
291. Lee, Y.J., et al., *Prognostic value of CAPZA1 overexpression in gastric cancer*. *Int J Oncol*, 2013. **42**(5): p. 1569-77.
292. Hou, H., et al., *Histone variant H2A.Z regulates centromere silencing and chromosome segregation in fission yeast*. *J Biol Chem*, 2010. **285**(3): p. 1909-18.
293. Aucott, R., et al., *HP1-beta is required for development of the cerebral neocortex and neuromuscular junctions*. *J Cell Biol*, 2008. **183**(4): p. 597-606.
294. Garay, P.M., M.A. Wallner, and S. Iwase, *Yin-yang actions of histone methylation regulatory complexes in the brain*. *Epigenomics*, 2016. **8**(12): p. 1689-1708.
295. Eberl, H.C., et al., *A map of general and specialized chromatin readers in mouse tissues generated by label-free interaction proteomics*. *Mol Cell*, 2013. **49**(2): p. 368-78.
296. Carmona-Mora, P. and K. Walz, *Retinoic Acid Induced 1, RAI1: A Dosage Sensitive Gene Related to Neurobehavioral Alterations Including Autistic Behavior*. *Curr Genomics*, 2010. **11**(8): p. 607-17.
297. Tahir, R., et al., *Retinoic acid induced-1 (Rai1) regulates craniofacial and brain development in Xenopus*. *Mech Dev*, 2014. **133**: p. 91-104.
298. Darvekar, S., et al., *A phylogenetic study of SPBP and RAI1: evolutionary conservation of chromatin binding modules*. *PLoS One*, 2013. **8**(10): p. e78907.
299. Babbs, C., et al., *De novo and rare inherited mutations implicate the transcriptional coregulator TCF20/SPBP in autism spectrum disorder*. *J Med Genet*, 2014. **51**(11): p. 737-47.
300. Adams, M.S., L.S. Gammill, and M. Bronner-Fraser, *Discovery of transcription factors and other candidate regulators of neural crest development*. *Dev Dyn*, 2008. **237**(4): p. 1021-33.
301. Rekdal, C., E. Sjøttem, and T. Johansen, *The nuclear factor SPBP contains different functional domains and stimulates the activity of various transcriptional activators*. *J Biol Chem*, 2000. **275**(51): p. 40288-300.
302. Liao, C., et al., *Prenatal diagnosis and molecular characterization of a novel locus for Dandy-Walker malformation on chromosome 7p21.3*. *Eur J Med Genet*, 2012. **55**(8-9): p. 472-5.
303. Zhang, L., et al., *A novel PHD-finger protein 14/KIF4A complex overexpressed in lung cancer is involved in cell mitosis regulation and tumorigenesis*. *Oncotarget*, 2017. **8**(12): p. 19684-19698.
304. Molli, P.R., et al., *MTA1-mediated transcriptional repression of BRCA1 tumor suppressor gene*. *Oncogene*, 2008. **27**(14): p. 1971-80.

REFERENCES

305. Liu, J., et al., *The subcellular distribution and function of MTA1 in cancer differentiation*. *Oncotarget*, 2014. **5**(13): p. 5153-64.
306. Li, S., et al., *Down-regulation of MTA1 protein leads to the inhibition of migration, invasion, and angiogenesis of non-small-cell lung cancer cell line*. *Acta Biochim Biophys Sin (Shanghai)*, 2013. **45**(2): p. 115-22.
307. Ma, K., et al., *MTA1 promotes epithelial to mesenchymal transition and metastasis in non-small-cell lung cancer*. *Oncotarget*, 2017. **8**(24): p. 38825-38840.
308. Townsend, K., et al., *Mediator of DNA damage checkpoint 1 (MDC1) regulates mitotic progression*. *J Biol Chem*, 2009. **284**(49): p. 33939-48.
309. Coster, G., et al., *The DNA damage response mediator MDC1 directly interacts with the anaphase-promoting complex/cyclosome*. *J Biol Chem*, 2007. **282**(44): p. 32053-64.
310. Ritchie, K., et al., *Loss of ATRX leads to chromosome cohesion and congression defects*. *J Cell Biol*, 2008. **180**(2): p. 315-24.
311. Low, J.K., et al., *CHD4 Is a Peripheral Component of the Nucleosome Remodeling and Deacetylase Complex*. *J Biol Chem*, 2016. **291**(30): p. 15853-66.
312. Millard, C.J., L. Fairall, and J.W. Schwabe, *Towards an understanding of the structure and function of MTA1*. *Cancer Metastasis Rev*, 2014. **33**(4): p. 857-67.
313. Millard, C.J., et al., *The structure of the core NuRD repression complex provides insights into its interaction with chromatin*. *Elife*, 2016. **5**: p. e13941.
314. Schmidberger, J.W., et al., *The MTA1 subunit of the nucleosome remodeling and deacetylase complex can recruit two copies of RBBP4/7*. *Protein Sci*, 2016. **25**(8): p. 1472-82.
315. Millard, C.J., et al., *Class I HDACs share a common mechanism of regulation by inositol phosphates*. *Mol Cell*, 2013. **51**(1): p. 57-67.
316. Smits, A.H., et al., *Stoichiometry of chromatin-associated protein complexes revealed by label-free quantitative mass spectrometry-based proteomics*. *Nucleic Acids Res*, 2013. **41**(1): p. e28.
317. Torrado, M., et al., *Refinement of the subunit interaction network within the nucleosome remodelling and deacetylase (NuRD) complex*. *FEBS J*, 2017. **284**(24): p. 4216-4232.
318. Luo, Y., et al., *Trans-regulation of histone deacetylase activities through acetylation*. *J Biol Chem*, 2009. **284**(50): p. 34901-10.
319. Zupkovitz, G., et al., *Negative and positive regulation of gene expression by mouse histone deacetylase 1*. *Mol Cell Biol*, 2006. **26**(21): p. 7913-28.
320. Clayton, A.L., C.A. Hazzalin, and L.C. Mahadevan, *Enhanced histone acetylation and transcription: a dynamic perspective*. *Mol Cell*, 2006. **23**(3): p. 289-96.
321. Ferrari, K.J., et al., *Polycomb-dependent H3K27me1 and H3K27me2 regulate active transcription and enhancer fidelity*. *Mol Cell*, 2014. **53**(1): p. 49-62.

REFERENCES

322. Reynolds, N., A. O'Shaughnessy, and B. Hendrich, *Transcriptional repressors: multifaceted regulators of gene expression*. Development, 2013. **140**(3): p. 505-12.
323. Weber, C.M. and S. Henikoff, *Histone variants: dynamic punctuation in transcription*. Genes Dev, 2014. **28**(7): p. 672-82.
324. Dekker, J., et al., *Capturing chromosome conformation*. Science, 2002. **295**(5558): p. 1306-11.
325. Denker, A. and W. de Laat, *The second decade of 3C technologies: detailed insights into nuclear organization*. Genes Dev, 2016. **30**(12): p. 1357-82.
326. Fullwood, M.J. and Y. Ruan, *ChIP-based methods for the identification of long-range chromatin interactions*. J Cell Biochem, 2009. **107**(1): p. 30-9.
327. Hayashi, T., et al., *Single-cell full-length total RNA sequencing uncovers dynamics of recursive splicing and enhancer RNAs*. Nat Commun, 2018. **9**(1): p. 619.
328. Stadler, M.B., et al., *DNA-binding factors shape the mouse methylome at distal regulatory regions*. Nature, 2011. **480**(7378): p. 490-5.
329. Varley, K.E., et al., *Dynamic DNA methylation across diverse human cell lines and tissues*. Genome Res, 2013. **23**(3): p. 555-67.
330. Baubec, T., et al., *Methylation-dependent and -independent genomic targeting principles of the MBD protein family*. Cell, 2013. **153**(2): p. 480-92.
331. Bode, D., et al., *Characterization of Two Distinct Nucleosome Remodeling and Deacetylase (NuRD) Complex Assemblies in Embryonic Stem Cells*. Mol Cell Proteomics, 2016. **15**(3): p. 878-91.
332. Hoffmeister, H., et al., *CHD3 and CHD4 form distinct NuRD complexes with different yet overlapping functionality*. Nucleic Acids Res, 2017. **45**(18): p. 10534-10554.
333. Le Guezennec, X., et al., *MBD2/NuRD and MBD3/NuRD, two distinct complexes with different biochemical and functional properties*. Mol Cell Biol, 2006. **26**(3): p. 843-51.
334. O'Shaughnessy-Kirwan, A., et al., *Constraint of gene expression by the chromatin remodelling protein CHD4 facilitates lineage specification*. Development, 2015. **142**(15): p. 2586-97.
335. Spruijt, C.G., et al., *CDK2AP1/DOC-1 is a bona fide subunit of the Mi-2/NuRD complex*. Mol Biosyst, 2010. **6**(9): p. 1700-6.
336. Spruijt, C.G., et al., *ZMYND8 Co-localizes with NuRD on Target Genes and Regulates Poly(ADP-Ribose)-Dependent Recruitment of GATAD2A/NuRD to Sites of DNA Damage*. Cell Rep, 2016. **17**(3): p. 783-798.
337. Wang, Y., et al., *LSD1 is a subunit of the NuRD complex and targets the metastasis programs in breast cancer*. Cell, 2009. **138**(4): p. 660-72.
338. Ahringer, J., *NuRD and SIN3 histone deacetylase complexes in development*. Trends Genet, 2000. **16**(8): p. 351-6.

REFERENCES

339. McDonel, P., I. Costello, and B. Hendrich, *Keeping things quiet: roles of NuRD and Sin3 co-repressor complexes during mammalian development*. *Int J Biochem Cell Biol*, 2009. **41**(1): p. 108-16.
340. Yao, Y.L. and W.M. Yang, *The metastasis-associated proteins 1 and 2 form distinct protein complexes with histone deacetylase activity*. *J Biol Chem*, 2003. **278**(43): p. 42560-8.
341. Zhang, Y., et al., *Analysis of the NuRD subunits reveals a histone deacetylase core complex and a connection with DNA methylation*. *Genes Dev*, 1999. **13**(15): p. 1924-35.
342. Fujita, N., et al., *MTA3, a Mi-2/NuRD complex subunit, regulates an invasive growth pathway in breast cancer*. *Cell*, 2003. **113**(2): p. 207-19.
343. Fujita, N., et al., *MTA3 and the Mi-2/NuRD complex regulate cell fate during B lymphocyte differentiation*. *Cell*, 2004. **119**(1): p. 75-86.
344. Malisetty, V.L., et al., *MTA1 expression in human cancers - Clinical and pharmacological significance*. *Biomed Pharmacother*, 2017. **95**: p. 956-964.
345. Moon, H.E., H. Cheon, and M.S. Lee, *Metastasis-associated protein 1 inhibits p53-induced apoptosis*. *Oncol Rep*, 2007. **18**(5): p. 1311-4.
346. Yoo, Y.G., G. Kong, and M.O. Lee, *Metastasis-associated protein 1 enhances stability of hypoxia-inducible factor-1alpha protein by recruiting histone deacetylase 1*. *EMBO J*, 2006. **25**(6): p. 1231-41.
347. Dhar, S., et al., *Resveratrol regulates PTEN/Akt pathway through inhibition of MTA1/HDAC unit of the NuRD complex in prostate cancer*. *Biochim Biophys Acta*, 2015. **1853**(2): p. 265-75.
348. Park, J.M., et al., *Role of transcription factor acetylation in the regulation of metabolic homeostasis*. *Protein Cell*, 2015. **6**(11): p. 804-13.
349. Bannister, A.J. and E.A. Miska, *Regulation of gene expression by transcription factor acetylation*. *Cell Mol Life Sci*, 2000. **57**(8-9): p. 1184-92.
350. Zee, B.M. and B.A. Garcia, *Validation of protein acetylation by mass spectrometry*. *Methods Mol Biol*, 2013. **981**: p. 1-11.
351. Kori, Y., et al., *Proteome-wide acetylation dynamics in human cells*. *Sci Rep*, 2017. **7**(1): p. 10296.
352. Feller, C., et al., *Global and specific responses of the histone acetylome to systematic perturbation*. *Mol Cell*, 2015. **57**(3): p. 559-71.
353. Li, D.Q., et al., *MTA1 coregulator regulates p53 stability and function*. *J Biol Chem*, 2009. **284**(50): p. 34545-52.
354. Li, D.Q., et al., *Metastasis-associated protein 1/nucleosome remodeling and histone deacetylase complex in cancer*. *Cancer Res*, 2012. **72**(2): p. 387-94.
355. Lu, X., et al., *Inactivation of NuRD component Mta2 causes abnormal T cell activation and lupus-like autoimmune disease in mice*. *J Biol Chem*, 2008. **283**(20): p. 13825-33.

REFERENCES

356. Manavathi, B., et al., *Repression of Six3 by a corepressor regulates rhodopsin expression*. Proc Natl Acad Sci U S A, 2007. **104**(32): p. 13128-33.
357. Zhang, T., et al., *A variant NuRD complex containing PWWP2A/B excludes MBD2/3 to regulate transcription at active genes*. Nat Commun, 2018. **9**(1): p. 3798.
358. Bondarenko, V.A., et al., *Nucleosomes can form a polar barrier to transcript elongation by RNA polymerase II*. Mol Cell, 2006. **24**(3): p. 469-79.

REFERENCES

ACKNOWLEDGMENTS

ACKNOWLEDGMENTS

Thank you

... Sandra for your great enthusiasm and encouragement, trust and discussions at eye level and for many fun toasts with prosecco. For millions of ideas, your scientific advice and support on the protein with this annoying name.

... Peter for giving me the opportunity to work in his scientifically inspiring and extremely well-organized and -equipped department.

... members of my TAC committee Ralph, Andi and Sebastian for scientific input and guidance.

... Elizabeth for being a great graduate school coordinator and for helpful advice.

... Catherine, member of the 'PWWP team', for that your door was always open and for your help in all kinds of concerns.

... Yolanda for introducing me to PWWP2A via the microscope and letting me suffer there for endless hours.

... Ramona for mutual motivation, drama lamas, lunch dates and bird and cat stories.

... the FMPs and especially Ashish for being fun and helpful lab mates.

... Martha, Susi, Michi and Chris for that help was always just a call away.

... collaborations, without which this project would not have been possible: Susi for countless FRAP session and curve modelling options; Gabi, Edith, Barbara and Ralph for the *Xenopus* work; Eva for mass spec; members of the Mackay lab and Thomas and Brian for binding studies; Tobias and Marek for bioinformatic analysis.

... Mom and Dad for believing in me and their constant support.

... Ben for being the best.